

UNCLASSIFIED

AD NUMBER
ADB031629
NEW LIMITATION CHANGE
TO Approved for public release, distribution unlimited
FROM Distribution authorized to U.S. Gov't. agencies only; Test and Evaluation; 10 Jul 1978. Other requests shall be referred to Air Force Flight Dynamics Laboratory, Attn: AFFDL/FXB, Wright-Patterson AFB, OH 45433.
AUTHORITY
AFWAL ltr, 11 Feb 1980

THIS PAGE IS UNCLASSIFIED

DDC FILE COPY AD B031629

AFFDL-TR-78-91
Volume I

Vol 1
12031 555

② LEVEL III

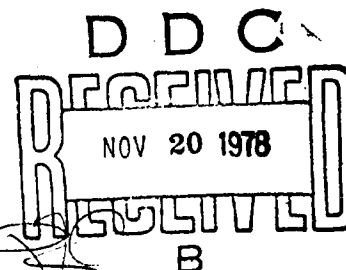
RAPID EVALUATION OF PROPULSION SYSTEM EFFECTS Volume I—Final Report

W.H. Ball and T.E. Hickcox

BOEING AEROSPACE COMPANY
SEATTLE, WASHINGTON 98124

JULY 1978

TECHNICAL REPORT AFFDL-TR-78-91, VOLUME I
Final Report for Period July 1977–July 1978



Distribution limited to U.S. Government agencies only; test and evaluation; statement applied 10 July 1978. Other requests for this document must be referred to the Air Force Flight Dynamics Laboratory (AFFDL/FXB), Wright-Patterson Air Force Base, Ohio 45433.


AIR FORCE FLIGHT DYNAMICS LABORATORY
AIR FORCE WRIGHT AERONAUTICAL LABORATORIES
AIR FORCE SYSTEMS COMMAND
WRIGHT-PATTERSON AIR FORCE BASE, OHIO 45433

78 11 13 040

NOTICE


When Government drawings, specifications, or other data are used for any purpose other than in connection with a definitely related Government procurement operation, the United States Government thereby incurs no responsibility nor any obligation whatsoever; and the fact that the government may have formulated, furnished, or in any way supplied the said drawings, specifications, or other data, is not to be regarded by implication or otherwise as in any manner licensing the holder or any other person or corporation, or conveying any rights or permission to manufacture, use, or sell any patented invention that may in any way be related thereto.

This technical report has been reviewed and is approved for publication.


GORDON C. TAMPLIN
Project Engineer
Vehicle Synthesis Branch


RAYMOND L. HAAS
Chief, Vehicle Synthesis Branch
AF Flight Dynamics Laboratory

FOR THE COMMANDER


MELVIN L. BUCK
Acting Chief
Aeromechanics Division

"If your address has changed, if you wish to be removed from our mailing list, or if the addressee is no longer employed by your organization, please notify AFFDL/FXB, W-PAFB, OH 45433 to help us maintain a current mailing list."

Copies of this report should not be returned unless return is required by security considerations, contractual obligations, or notice on a specific document.

Unclassified

SECURITY CLASSIFICATION OF THIS PAGE (When Data Entered)

19 REPORT DOCUMENTATION PAGE		READ INSTRUCTIONS BEFORE COMPLETING FORM	
1. REPORT NUMBER AFFDL-TR-78-91-Vol-1	2. GOVT ACCESSION NO.	3. RECIPIENT'S CATALOG NUMBER rept.	
4. TITLE (and Subtitle) RAPID EVALUATION OF PROPULSION SYSTEM EFFECTS, VOLUME I, FINAL REPORT		5. TYPE OF REPORT & PERIOD COVERED FINAL JUL 1977-JUL 1978	
6. AUTHOR(s) W. H. Ball T. E. Hickcox		7. PERFORMING ORG. REPORT NUMBER	
8. CONTRACT OR GRANT NUMBER(s) F33615-77-C-3885			
9. PERFORMING ORGANIZATION NAME AND ADDRESS Boeing Aerospace Company A Division of the Boeing Company Seattle, Washington 98124		10. PROGRAM ELEMENT, PROJECT, TASK AREA & WORK UNIT NUMBERS 24040121 01	
11. CONTROLLING OFFICE NAME AND ADDRESS Vehicle Synthesis Branch (AFFDL/FXB) Air Force Flight Dynamics Laboratory Wright-Patterson AFB, Ohio 45433		12. REPORT DATE JUL 1978	
13. NUMBER OF PAGES 114		14. SECURITY CLASS. (of this report) Unclassified	
14. MONITORING AGENCY NAME & ADDRESS (if different from Controlling Office) 12 125p.		15a. DECLASSIFICATION, DOWNGRADING SCHEDULE	
16. DISTRIBUTION STATEMENT (of this Report) Distribution limited to U.S. Government Agencies only; Test and Evaluation; Statement applied 10 July 1978. Other requests for this document must be referred to Air Force Flight Dynamics Laboratory (AFFDL/FXB); Wright-Patterson Air Force Base, Ohio 45433			
17. DISTRIBUTION STATEMENT (of the abstract entered in Block 20, if different from Report)			
18. SUPPLEMENTARY NOTES			
19. KEY WORDS (Continue on reverse side if necessary and identify by block number) Installed engine performance Inlet performance Nozzle performance			
20. ABSTRACT (Continue on reverse side if necessary and identify by block number) This report presents the results of a research program to develop computerized preliminary analysis procedures for calculating propulsion system installation losses. These losses include inlet and nozzle internal losses and external drag losses for a wide variety of subsonic and supersonic aircraft configurations up to Mach 3.5. The calculation procedures used in the computer programs, which were largely developed from existing engineering procedures and experimental data, are suitable for preliminary studies of advanced aircraft configurations. Two interactive computer programs were developed during the			

DDC
RECEIVED
NOV 20 1978
B

DD FORM 1 JAN 73 1473 EDITION OF 1 NOV 65 IS OBSOLETE

Unclassified

SECURITY CLASSIFICATION OF THIS PAGE (When Data Entered)

059 480 11 13 04 08

Unclassified

SECURITY CLASSIFICATION OF THIS PAGE (When Data Entered)

contract; (1) A propulsion installation effects program that calculates installed performance, using input maps of inlet and nozzle/aftbody characteristics for specific configurations; and (2) a "derivative" program that allows the user to generate new sets of input maps by perturbations to the geometries of the basic input maps. The work accomplished during the contract is documented in four separate volumes. Volume I is a Final Report discussing the analysis methods and data used to develop the programs, and major technical observations from the study. Volume II is a PIPSI Users Manual, containing documentation of the interactive propulsion installation program. Volume III is the Derivative Procedure Users Manual, documenting the methods and usage of the derivative procedure. Volume IV is the library of input maps.

Unclassified

SECURITY CLASSIFICATION OF THIS PAGE (When Data Entered)

FOREWORD

This report documents the work accomplished during USAF Contract No. F33615-77-C-3085. The work consisted of developing an interactive PIPSI computer program, developing an interactive derivative computer program, and developing and documenting supporting data libraries. The work was accomplished in three phases. As part of the work accomplished in Phase I of the contract, the interactive PIPSI program was completed and delivered to the Air Force. As part of Phase II work, derivative parameters were selected and development work was completed on the derivative program. During Phase III a library of inlet and nozzle/aftbody characteristics was prepared, test cases were completed, documentation was accomplished, and final programs were delivered to the Air Force. The program was conducted under the direction of the Vehicle Synthesis Branch, Air Force Flight Dynamics Laboratory, Air Force Systems Command. Mr. Gordon Tamplin was the Air Force Program Monitor.

The program was initiated on 17 July 1977 and draft copies of the final reports were submitted for approval on 15 May 1978.

Mr. W. H. Ball was Program Manager for The Boeing Company. The following individuals contributed significantly to the work accomplished during this contract: R. A. Atkins, Jr., computer programming; T. E. Hickcox, inlet derivative procedure development; E. J. Kowalski, inlet configurations and performance; and J. E. Petit and R. M. Trayler, nozzle/aftbody procedure and configurations.

ACCESSION	
NTIS	✓
DDC	
UNCLAS	
DATE	
BY	
DATE	
Dist	SPECIAL
B	

CONTENTS

	<u>PAGE</u>
SUMMARY	xi
NOMENCLATURE AND SYMBOLS	xiii
I INTRODUCTION	1
II PERFORMANCE OF INSTALLED PROPULSION SYSTEMS INTERACTIVE (PIPSI) PROGRAM	5
III LIBRARY MAP CONFIGURATIONS	43
3.1 Inlet Map Configurations	43
3.2 Nozzle/Aftbody Map Configurations	45
IV DERIVATIVE PROGRAM (DERIVP)	51
4.1 Derivative Parameters	51
4.2 Inlet Derivative Procedure	59
4.3 Nozzle/Aftbody Procedure	72
APPENDIX	105
REFERENCES	111

LIST OF ILLUSTRATIONS

<u>FIGURE</u>	<u>PAGE</u>
1. Preliminary Analysis Process Using PIPSI	7
2. PIPSI Data Flow	8
3. PIPSI Program Interactive Input	9
4. Format for Inlet Performance Characteristics	11
5. Format for Nozzle/Aftbody Drag and C_{F_G} Maps	12
6. Typical Uninstalled Engine Data Tables	13
7. Application Spectrum of PIPSI	17
8. Inlet Procedure	18
9. Nozzle/Aftbody Procedure	19
10. PIPSI Performance Calculation for an External-Compression Inlet	22
11. PIPSI Performance Calculation for a Mixed-Compression Inlet	23
12. Definition of Inlet Reference Mass Flow Ratio	26
13. General Flow Chart for Bypass Vs. Spillage Trade Studies	31
14. Calculation Procedure for Effects of Nozzle Static Pressure Ratio on Drag	33
15. Typical Nozzle/Aftbody Drag Data	36
16. Matrix of Inlet Maps	44
17. Representative Spectrum of Inlets	46
18. Nozzle/Aftbody Files	47
19. Sources of Data for Inlet Maps	49
20. Nozzle/Aftbody Drag Map for Twin Round Nozzles	73
21. IMS_T Calculation Procedure	75
22. Nozzle/Aftbody Area Distribution for a Twin Round Nozzle Configuration	76
23. Nozzle/Aftbody Drag Correlations for a Twin C-D Axisymmetric Nozzle Configuration	77

LIST OF ILLUSTRATIONS (cont.)

<u>FIGURE</u>	<u>PAGE</u>
24. Nozzle/Aftbody Drag Correlations for Twin and Single 2-D Wedge Nozzle Configurations	78
25. Pressure Drag Coefficient for Twin-Jet Axisymmetric Plug Nozzles	79
26. Default Nozzle Area Ratio Schedule	81
27. Nozzle/Aftbody Drag Derivative Procedure	82
28. Correction for Radial Orientation of Tail	83
29. Incremental Drag Coefficient Due to Tail Fore-and-Aft Location	84
30. Base Pressure Coefficient	86
31. Flow Chart for Tail Effects and Base Drag Increments	87
32. Gross Thrust Coefficient for a Round C-D Nozzle	89
33. Divergence Angle/Area Ratio Relationship for a Round C-D Nozzle	90
34. Angularity Loss Coefficient for Convergent-Divergent Nozzles	92
35. Gross Thrust Coefficient for Axisymmetric Plug Nozzles	93
36. Internal Area Variation for a Round Plug Nozzle	94
37. Performance Loss Due to Difference Between Cowl Angle and Plug Angle	95
38. Gross Thrust Coefficient for a 2-D/C-D Nozzle	97
39. Optimum Area Ratio for a 2-D/C-D Nozzle	98
40. Optimum Divergence Angle as a Function of 2-D/C-D Nozzle Area Ratio	99
41. Effect of Divergence Angle on C_{F_g} for a 2-D/C-D Nozzle	100
42. Effect of Aspect Ratio on 2-D/C-D Nozzle Performance	101
43. Gross Thrust Coefficient for a 2-D Wedge Nozzle	102
44. Effect of Aspect Ratio on 2-D Plug Nozzle Performance	103
45. Effect of Plug Angle on 2-D Plug Nozzle Performance	104

LIST OF TABLES

<u>TABLE</u>	<u>PAGE</u>
I Thermodynamic Subroutines	35
II Derivative Parameters and Their Definitions	53
III Inlet Derivative Procedure Cross-Reference	57
IV Nozzle/Aftbody Derivative Procedure Reference List	58
V Derivative Parameters for Nozzle C_{F_G} Calculation	88

SUMMARY

An analytical program was conducted to develop and document two computer programs that can be used to correct uninstalled propulsion system performance data for inlet and nozzle/aftbody installation effects.

The program consisted of three phases: (I) Development and delivery of an interactive PIPSI computer program, (II) Development and delivery of an interactive Derivative Procedure computer program and Users Manual, and (III) Preparation of test cases, library maps, and PIPSI Users Manual. During Phase I, an interactive version of the PIPSI computer program was developed and checked out on the WPAFB CDC 6600 computer system. This program permits the rapid calculation of propulsion system performance using a library of inlet and nozzle/aftbody characteristics contained in computer disk files. During Phase II, an interactive derivative procedure was developed and programmed that will allow the user to obtain new PIPSI inlet and nozzle input characteristics by perturbations to the geometric variables represented by the stored library of maps. During Phase III, test cases were completed, library maps of inlet and nozzle/aftbody performance characteristics were developed and documentation was completed.

The computer programs and data input formats were developed in a form that will allow the user to significantly improve the accuracy of the calculated results by adding new data as it becomes available.

LIST OF NOMENCLATURE AND SYMBOLS

A^*	Sonic area, in ²
A	Area, in ²
A_c	Inlet capture area, in ²
A_o	Local stream tube area ahead of the inlet, in ²
A_{oI}	Free-stream tube area of air entering the inlet, in ²
AR	Aspect ratio, W_c/H_c for inlets, W_g/H_g for nozzles, dimensionless
C_D	Drag coefficient, $\frac{D}{q A_{ref.}}$, dimensionless
C	Sonic velocity; ft/sec.
$C-D$	Convergent-divergent
C_{DADD}	Additive drag coefficient, $C_{DADD} = \frac{D_{ADD}}{q A_c}$, dimensionless
C_{DA10}	Afterbody drag coefficient, $\frac{DRAG}{q A_{10}}$, dimensionless
C_{DBase}	Base drag coefficient $\frac{(P_b - P_{\infty}) A_{base}}{q A_{10}}$, dimensionless
$C_{DA10-A9}$	
C_{DPAP}	Drag coefficient, $\frac{D}{q_o (A_{10} - A_9)}$, based on projected area, dimensionless
C_{DS}	Scrubbing drag coefficient, $\frac{DRAG}{q A_{10}}$, dimensionless
C_{fG}	Thrust coefficient, $\frac{F_g}{\frac{W}{g} (V_1)}$ dimensionless
C_v	Nozzle velocity coefficient, dimensionless
Conv.	Convergent

LIST OF NOMENCLATURE AND SYMBOLS (Continued)

D	Drag, lb.; Hydraulic Diameter, $\frac{4A}{P}$, in., diameter, in.
F	Thrust, lb.
F_N	Net thrust, lb.
F_{NA}	Installed net thrust, lb.
F_{g_i}	Ideal gross thrust (fully expanded), lb.
f/a	Fuel/air ratio, dimensionless
g	Gravitational constant, ft/sec ²
h	Enthalpy per unit mass, BTU/lb.; height, in.
h_{fan}	Enthalpy of fan discharge flow, BTU/lb
h_{pri}	Enthalpy of primary exhaust flow after heat addition, BTU/lb
h_t	Throat height, in
IMS_T	Integral mean slope parameter, truncated
	$IMS_T = - \frac{1}{(1 - A_9/A_{10})} \int_{A_9/A_{10}}^{1.0} \frac{d(A/A_{10})}{d(L/D_{eq})} d(A/A_{10})$
L	Length, in.
M	Mach number, dimensionless
P	Static pressure, lb/in ² , perimeter, in.
P_r	Relative pressure,; the ratio of the pressures p_a and p_b corresponding to the temperatures T_a and T_b , respectively, along a given isentrope, dimensionless
P.S.	Power setting
P_T	Total pressure, lb/in ²
Q	Effective heating value of fuel, BTU/lb.

LIST OF NOMENCLATURE AND SYMBOLS (Continued)

q	Dynamic pressure, lb/in ²
R	Gas constant
R, r	Radius, in.
R _F	Total pressure recovery
SFC	Specific fuel consumption
SFC _A	Installed specific fuel consumption
T	Temperature, °R
V	Velocity, ft/sec
W	Mass flow, lb/sec
W _{BX}	Bleed air removed from engine, lb/sec.
W _C	Corrected airflow, lb/sec. $\frac{W\sqrt{\theta}}{.6}$
W _f	Weight flow rate of fuel, lb/sec.
W ₂	Weight flow rate of air, primary plus secondary, lb/sec.
W ₈	Primary nozzle airflow rate, lb/sec.
x	Length, in.
α	Angle of attack; convergence angle of nozzle, degrees
γ	Ratio of specific heats, dimensionless
δ _{T₂}	Pressure correction factor, P _{T₂} /P _{STD.}
ε	Diffuser loss coefficient, $\frac{\Delta P_T}{q_1}$, dimensionless
θ _{T₂}	Temperature correction factor, T _{T₂} /T _{STN.}

LIST OF NOMENCLATURE AND SYMBOLS (Concluded)

θ_N	2-D Nozzle wedge half-angle
θ_P	Round Plug nozzle half-angle
η_B	Burner efficiency, dimensionless
ν	Kinematic viscosity, ft ² /sec.
ρ	Density, lb/ft ³

SUBSCRIPTS

amb	Ambient
AB	Afterbody
B	Burner
B _x	Bleed airflow extracted from the engine
b, base	Base flow region
BP	Bypass
BLC	Boundary layer bleed
btail	Boattail
2CT	Temporary inlet data table 2C
2A, 2B, 2C, 3, 3A, 6A	Inlet data tables
6AT	Temporary inlet data table 6A
3T	Temporary inlet data table 3

SECTION I

INTRODUCTION

During the preliminary design phase of military aircraft development, it is necessary to evaluate many potential engine/airframe combinations to determine the best solution to a given set of mission/payload requirements.

The evaluation process must be thorough enough not to eliminate, at an early point in the preliminary design process, any configurations that might ultimately prove to be viable candidates if time were available to study them in detail.

At the same time, speed in evaluating the configurations is also important because it permits many more configurations to be analyzed on the basis of actual data rather than subjective judgment or experience.

In addition, manpower and money are often limited, especially in the typical preliminary design study group. This means that calculation procedures employed during these studies must be simple to use and require a minimum of input data preparation and setup time. Also, output data must be easily understood and the results presented in a format that is readily usable in comparing competing configurations. This report describes the results of a study to develop an advanced computerized, interactive propulsion system installation calculation procedure that meets these objectives. The calculation procedure consists of two main parts:

- (1) An interactive computerized procedure for calculating installed propulsion system performance using computer-stored files of inlet, nozzle/aftbody characteristics, and uninstalled engine data. The inlet and nozzle/aftbody characteristics used in this procedure are obtained from a library of maps representing specific configurations.

- (2) An interactive derivative procedure to generate new maps of inlet and nozzle/aftbody characteristics for configurations that are different from those represented in the library. The characteristics of the new configurations are obtained by first order perturbations to the configurations in the library.

The development of the interactive PIPSI program has taken full advantage of the existing Batch-Job version PIPS computer program and PITAP procedure developed for AFFDL under Contract F33615-72-C-1580 (Reference 1). The capability of the existing procedure was improved by developing interactive procedures for automatically utilizing inlet and nozzle/aftbody performance characteristics obtained from computerized files. These computerized files represent maps of standardized format which provide the internal losses and drag characteristics for a variety of specific inlet and nozzle/aftbody configurations. These configurations are designed to cover a wide spectrum of Mach numbers from subsonic to Mach 3.5.

The expansion of the computer library of inlet and nozzle/aftbody characteristics was a significant part of the contract effort because it enables the user to find in the available files (for instant retrieval) an inlet or nozzle/aftbody configuration that is a fairly close match to the configuration under investigation. Inlet maps for a total of 18 configurations and nozzle/aftbody maps for 8 configurations are available for use with the interactive procedure. The configurations to which these maps correspond are described in Section III of this report. The complete documentation of input maps is provided in Volume IV.

Another significant improvement that was made to the interactive calculation procedure is the incorporation of a procedure that allows the program user to make trade studies between bypass and spillage airflow. The purpose of this procedure is to provide the user with maximum visibility of the effects on performance of various design options that may be available for handling excess inlet airflow. The bypass vs. spillage trade study analysis procedure is discussed in Subsection 2.2.5 of this report.

The derivative procedure was also developed during the contract period, to determine the effect on inlet and nozzle/aftbody performance of perturbations in the inlet and nozzle/aftbody geometries. This derivative procedure was designed to calculate the performance characteristics for configurations that are different from those specific configurations for which complete maps are stored in computer files. This work included selection of the derivative parameters that were used during the development of the derivative procedure. These derivative parameters are discussed in Subsection 4.1 of this report and the derivative procedure is discussed in Section IV.

SECTION II

PERFORMANCE OF INSTALLED PROPULSION SYSTEMS-INTERACTIVE (PIPSI) PROGRAM

The contract effort was divided into two major parts. The first part consisted of the development of an interactive propulsion system performance computer program and a supporting library of inlet and nozzle/aftbody maps for specific configurations that can be used as input data. This computer program was given the designation PIPSI, for "Performance of Installed Propulsion Systems - Interactive". The second major part of the contract was the development of an interactive derivative procedure program that will enable the user to rapidly create new inlet and nozzle/aftbody input maps for use in the PIPSI program. This was accomplished by accounting for the first order effects due to differences between the desired configuration and a selected library configuration. This computer program has been designated DERIVP, for "Derivative Processor". The PIPSI program development is discussed in this section and the DERIVP program development is discussed in Section IV. In addition to the material contained in this document, additional details of the computer programs are contained in the users manuals for the two computer programs. The users manual for the PIPSI program is Volume II and the users manual for the DERIVP program is Volume III.

2.1 STRUCTURE AND USAGE

The PIPSI program was designed to meet the objective of speeding up the process of calculating installed propulsion system performance data while including realistic effects of inlet and nozzle losses due to drag and internal performance. The program was also designed to satisfy two additional criteria: (1) the accuracy of the data generated by the calculation procedure must be suitable for use in preliminary design studies (when detailed knowledge of all geometric features of the design are not known) and (2) the method must reflect the effects of throttle-sensitive changes in inlet and nozzle/aftbody losses.

To achieve the desired capability, a previously-developed batch-job propulsion installation correction program (P.I.P.S., Reference 1), was improved and made interactive for use on the AFFDL CDC 6600 computer system. This program utilizes a computer-stored library of inlet and nozzle performance characteristics and uninstalled engine data as input to interactively calculate installed propulsion system performance. A chart showing how this computer program is used in a typical preliminary analysis process is presented in Figure 1. The calculation of installed propulsion system performance is almost instantaneous if the tabulated performance characteristics of the desired inlet and nozzle/aftbody configurations are available as previously-stored computer files. To provide a readily-available source of inlet and nozzle/aftbody data, a library of inlet and nozzle/aftbody performance characteristics was created, covering a wide variety of possible configurations. The computer files that are required to be attached prior to executing the PIPSI program are shown in Figure 1, as well as the internally-stored propulsion calculation options that are built into the program. Figure 2 shows the data flow from operation of the PIPSI program. Required and optional files are attached externally prior to execution of the program. The user then enters the interactive input commands. The output from the program can be displayed on a scope or stored on an output disk file for disposition to an off-line printer. The interactive commands that can be entered as input by the user are shown in the schematic diagram presented in Figure 3.

The single most important factor that made it possible to reduce the time required to perform installed propulsion system performance calculations was the extensive use of computerized files. These files contain tables of data representing the non-dimensionalized performance characteristics of inlets and nozzle aftbodies. These files allow instant retrieval of inlet and nozzle/aftbody data that can be matched with the uninstalled engine performance data (also contained in a computer file) during the execution of the program, which produces the installed propulsion data.

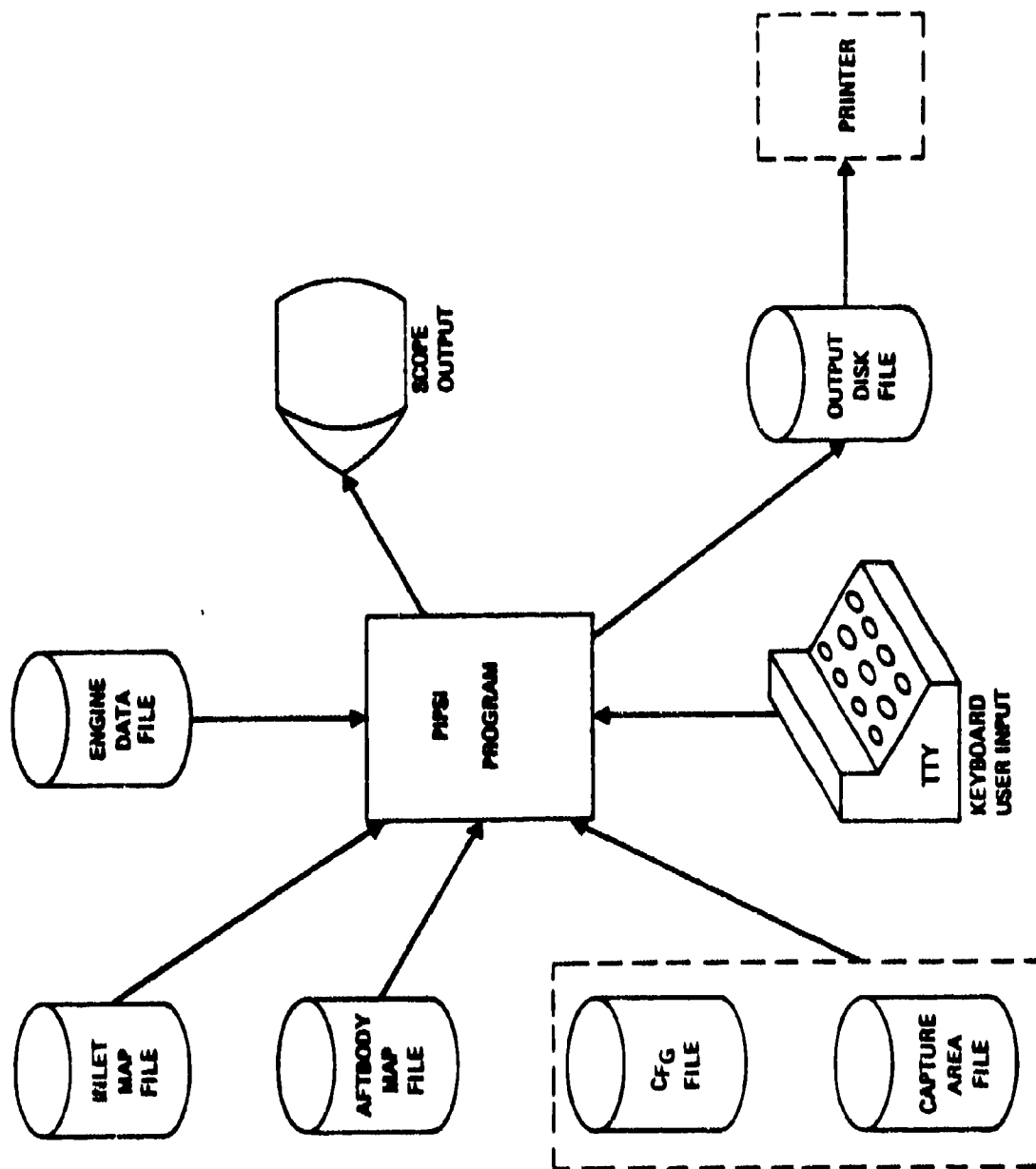


Figure 2. PIPSI Data Flow

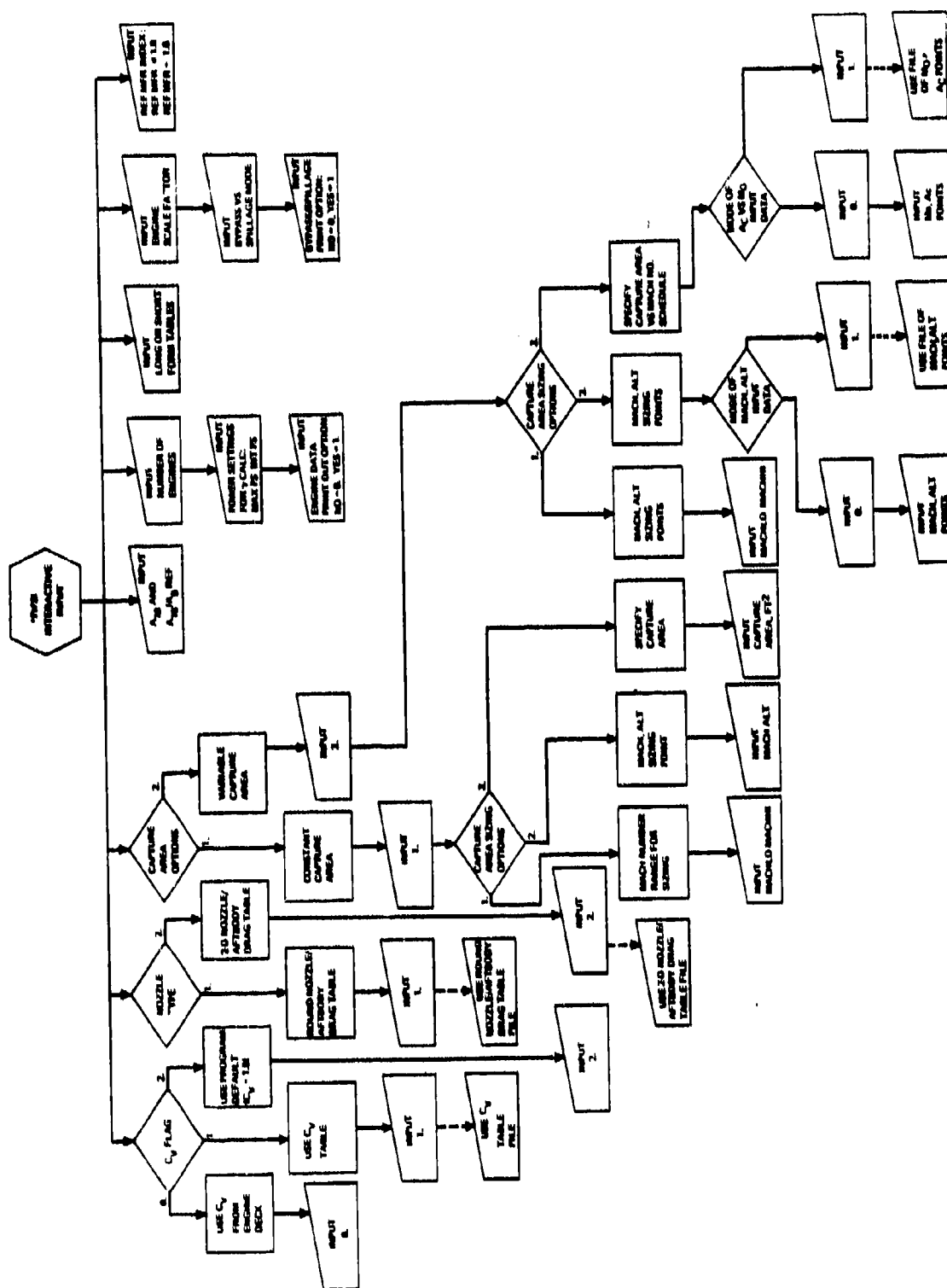


Figure 3. PIPSI Program Interactive Input

The inlet and nozzle/aftbody computerized files and the uninstalled engine data are shown in the typical examples of Figures 4, 5, and 6. The format of the data was selected to provide a standardized framework in which either experimental data or the results of analytical calculations can be used. The input format for the data remains constant, but the data that goes into the tables can come from various sources depending on the amount of time available for preparing the data and/or the amount of experimental data available. Because of the fact that data in the input tables can be changed as better data become available, it is possible to improve the accuracy of the installed propulsion system performance calculations as the aircraft development cycle progresses from preliminary design (level I) through full-scale flight test. The use of the PIPSI program throughout the development cycle is illustrated in Figure 7.

The basic structure of the main calculation procedures of the PIPSI computer program is shown by the flow charts in Figures 8 and 9. Figure 8 shows the inlet procedure. This procedure handles the functions of sizing the inlet, matching the inlet input data with the engine airflow demand, and obtaining the matched inlet performance parameters from the inlet data tables. Engine corrected airflow demand is the matching parameter between engine data and inlet data. Figure 9 shows the nozzle/aftbody procedure. Nozzle total-to-ambient pressure ratio is used as the matching parameter for matching nozzle performance data to engine data.

2.2 INLET SUBPROGRAM

The inlet performance subprogram of the PIPSI procedure involves considerably more procedural steps than the nozzle/aftbody drag and gross thrust coefficient subprograms. This is due to the fact that the individual inlet component drags that contribute to the total inlet drag must be calculated separately. Each of these drags (spillage, bleed, and bypass) must be determined individually as a function of mass flow ratio, which adds to the complexity of the computer program.

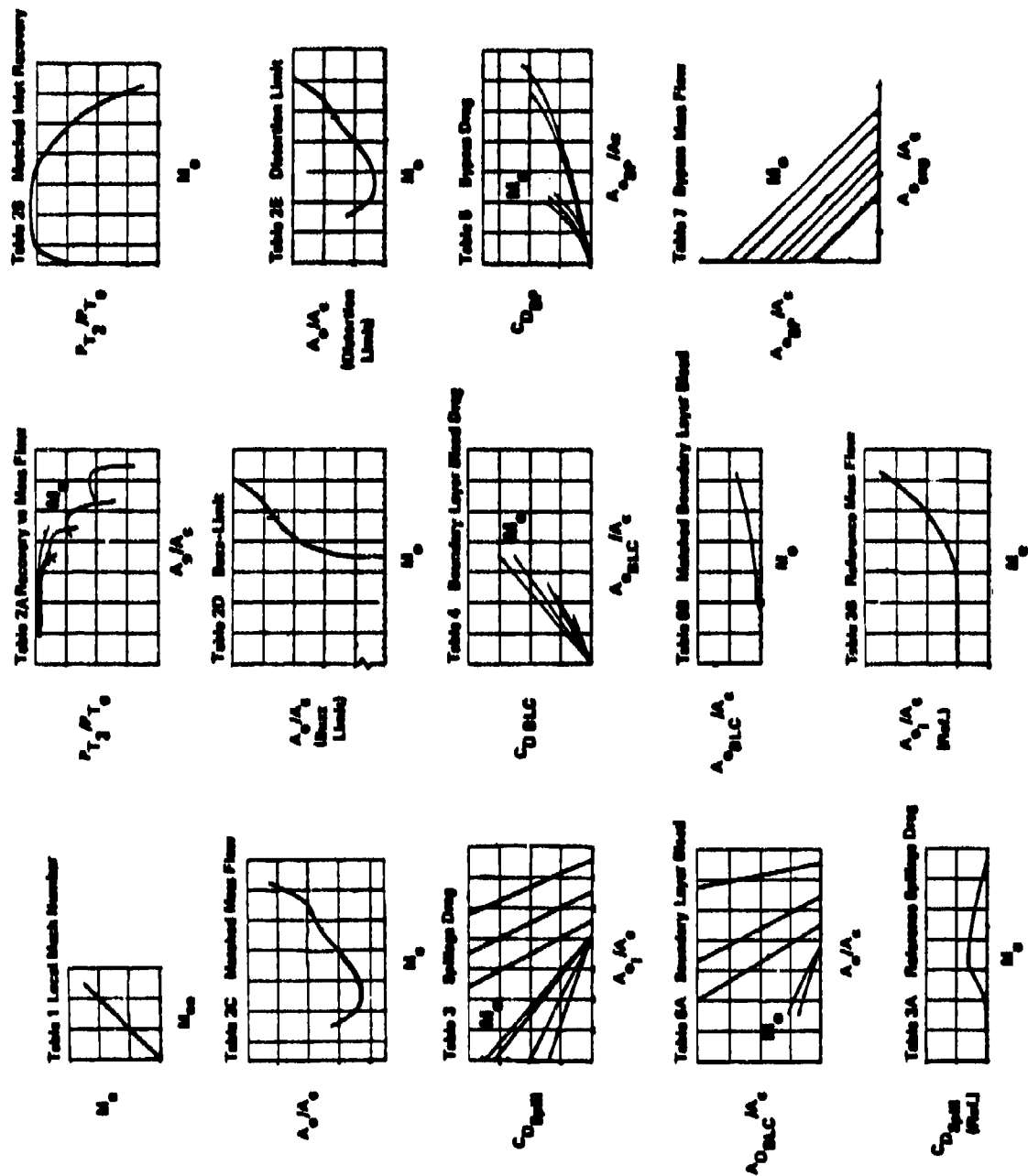
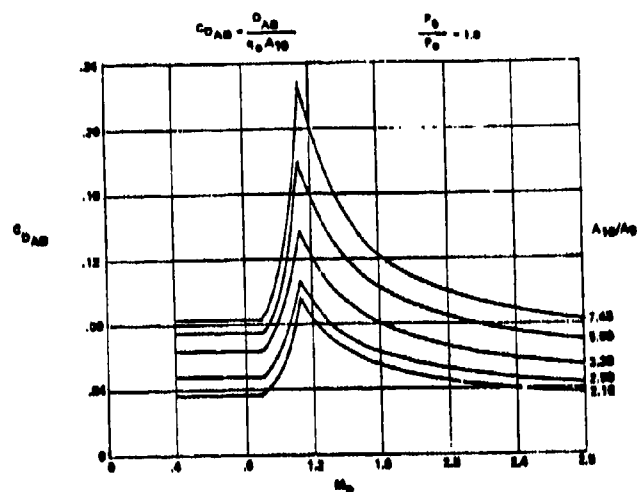
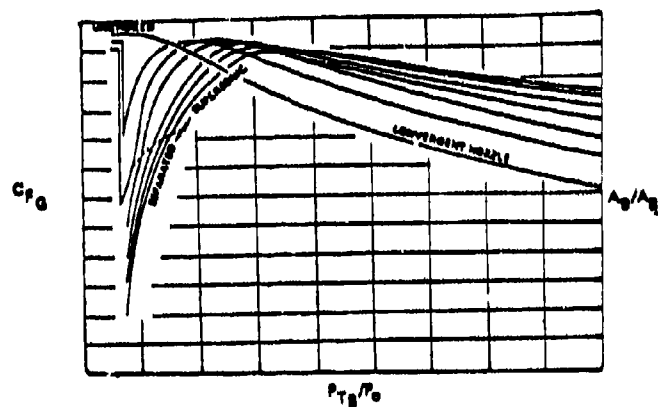


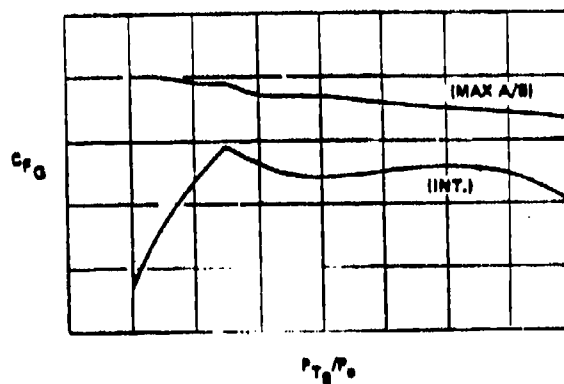
Figure 4. Format for Inlet Performance Characteristics



(a) Data format for nozzle / aftbody drag



(b) Data format for round nozzle Gross Thrust Coefficient



(c) Data format for nozzle gross thrust coefficient for two-dimensional nozzles

Figure 5. Format for Nozzle/Aftbody Drag and C_{FG} Maps

M ₀	ALT.	P.S.	FN	W _F	$\frac{W_2 \sqrt{\theta} T_2}{\delta T_2}$	PTB/P ₀	A _B	A _g	C _{FG}
AIR FORCE TEST CASE									
0.00	0.	1.00	18326.	36462.	182.68	2.767	3.753	3.842	.9856
.20	0.	1.00	19225.	39433.	182.68	2.982	3.752	3.962	.9859
.50	0.	1.00	21396.	43304.	182.68	3.471	3.754	4.184	.9865
.85	0.	1.00	24134.	53700.	167.86	4.129	3.715	4.576	.9863
1.00	0.	1.00	25337.	56386.	158.66	4.491	3.726	4.944	.9860
1.20	0.	1.00	28031.	66436.	146.70	5.121	3.738	5.448	.9854
1.60	0.	1.00	35537.	86437.	121.41	6.624	3.807	6.608	.9848
1.78	0.	1.00	40482.	94250.	112.92	7.613	3.830	6.960	.9845
1.95	0.	1.00	46398.	114689.	106.69	8.846	3.835	7.272	.9849
2.12	0.	1.00	53272.	132392.	101.03	10.285	3.837	7.815	.9827
2.30	0.	1.00	60994.	153687.	95.80	12.063	3.831	8.004	.9814
0.00	10000.	1.00	12973.	25956.	182.68	2.762	3.863	3.963	.9856
.20	10000.	1.00	13623.	28054.	182.68	2.971	3.869	4.091	.9859
.50	10000.	1.00	15202.	32239.	182.68	3.455	3.822	4.322	.9869
.85	10000.	1.00	19544.	41435.	181.25	4.625	3.700	4.825	.9868
1.00	10000.	1.00	20699.	45137.	171.72	5.040	3.712	5.146	.9867
1.20	10000.	1.00	22776.	51048.	157.96	5.716	3.724	6.066	.9829
1.60	10000.	4.00	29635.	67608.	132.73	7.604	3.750	6.813	.9845
1.60	10000.	4.00	21277.	38290.	132.73	7.735	3.096	6.219	.9785
1.60	10000.	4.00	12942.	19181.	132.73	7.842	2.484	4.816	.9786
1.78	10000.	4.00	32293.	75388.	120.07	8.388	3.814	6.995	.9850
1.78	10000.	4.00	22942.	42696.	120.07	8.538	3.157	6.352	.9817
1.78	10000.	4.00	12629.	19625.	120.07	8.668	2.485	5.242	.9769
1.95	10000.	4.00	36560.	86206.	112.36	9.597	3.837	7.475	.9840
1.95	10000.	4.00	25833.	48823.	112.36	9.768	3.189	6.639	.9823
1.95	10000.	4.00	13325.	21278.	112.36	9.924	2.487	5.410	.9797
2.12	10000.	4.00	41981.	94021.	105.87	11.123	3.831	7.983	.9821
2.12	10000.	4.00	29210.	56087.	105.87	11.318	3.190	7.119	.9815
2.12	10000.	4.00	14273.	23424.	105.87	11.501	2.481	5.982	.9782
2.30	10000.	4.00	47845.	114606.	100.10	12.954	3.837	8.216	.9804
2.30	10000.	4.00	33025.	64907.	100.10	13.178	3.208	7.191	.9819
2.30	10000.	4.00	15111.	25769.	100.10	13.396	2.484	6.072	.9810
0.00	22500.	1.00	8107.	16323.	182.68	2.755	4.014	4.131	.9856
.20	22500.	1.00	8933.	17646.	182.68	2.961	4.025	4.264	.9859
.50	22500.	1.00	9957.	20289.	182.68	3.443	3.981	4.530	.9864
.85	22500.	1.00	12513.	26303.	182.68	4.665	3.839	5.044	.9868
1.00	22500.	1.00	14473.	30346.	182.68	5.527	3.755	5.593	.9870
1.20	22500.	1.00	17143.	38920.	175.51	6.669	3.706	6.386	.9846
1.60	22500.	4.00	21945.	47096.	146.17	8.776	3.736	7.030	.9849
1.60	22500.	4.00	15970.	26673.	146.17	8.929	3.075	6.190	.9827
1.60	22500.	4.00	10157.	13940.	146.17	9.047	2.484	5.159	.9795
1.78	22500.	4.00	24630.	53538.	134.49	10.017	3.748	7.394	.9837
1.78	22500.	4.00	17769.	30321.	134.49	10.190	3.090	6.532	.9823
1.78	22500.	4.00	10660.	15320.	134.49	10.329	2.482	5.515	.9797
1.95	22500.	4.00	26839.	59583.	122.63	11.062	3.795	7.915	.9821
1.95	22500.	4.00	14228.	33745.	122.63	11.257	3.140	7.169	.9805
1.95	22500.	4.00	10916.	19405.	122.63	11.424	2.485	5.713	.9803
2.12	22500.	4.00	29636.	67119.	113.50	12.418	3.833	8.056	.9816
2.12	22500.	4.00	21099.	38013.	113.50	12.639	3.180	7.238	.9815
2.12	22500.	4.00	11152.	16743.	113.50	12.840	2.485	6.059	.9804
2.30	22500.	4.00	33535.	77237.	106.70	14.386	3.835	8.258	.9784
2.30	22500.	4.00	23674.	43743.	106.70	14.639	3.194	7.582	.9798
2.30	22500.	4.00	11318.	18405.	106.70	14.877	2.484	6.274	.9806
0.00	35000.	1.00	4788.	9743.	182.68	2.757	4.146	4.284	.9856
.20	35000.	1.00	5061.	10538.	182.68	2.963	4.166	4.436	.9859
.50	35000.	1.00	5706.	12123.	182.68	3.441	4.140	4.725	.9864
.85	35000.	1.00	7527.	15740.	182.68	4.657	4.035	5.275	.9869
1.00	35000.	1.00	8733.	18164.	182.68	5.513	3.921	5.746	.9869
1.20	35000.	1.00	11041.	22449.	182.68	7.081	3.797	6.815	.9837
1.60	35000.	4.00	1951.	31618.	182.68	10.321	3.717	7.543	.9830

Figure 6. Typical Uninstalled Engine Data Tables

THIS PAGE IS BEST QUALITY PRACTICABLE
FROM COPY FURNISHED TO DDG

1.60	35000.	4.00	11474.	17907.	162.97	10.501	3.051	6.150	.9845
1.60	35000.	4.00	7667.	9789.	162.97	10.634	2.444	5.355	.9821
1.78	35000.	4.00	17419.	35821.	149.53	11.713	3.731	7.736	.9814
1.78	35000.	4.00	12741.	20298.	149.53	11.917	3.070	7.006	.9815
1.78	35000.	4.00	8181.	10721.	149.53	12.074	2.484	5.634	.9819
1.95	35000.	4.00	14375.	40433.	138.00	13.255	3.743	8.083	.9803
1.95	35000.	4.00	14066.	22899.	138.00	13.484	3.087	7.103	.9815
1.95	35000.	4.00	8726.	11713.	139.00	13.667	2.484	6.025	.9815
2.12	35000.	4.00	21239.	49227.	126.74	14.827	3.765	8.263	.9779
2.12	35000.	4.00	15307.	25614.	126.74	15.084	3.114	7.497	.9797
2.12	35000.	4.00	9036.	12510.	126.74	15.298	2.484	6.060	.9822
2.30	35000.	4.00	22899.	50176.	115.17	16.273	3.930	8.673	.9755
2.30	35000.	4.00	16360.	28417.	115.17	16.563	3.177	7.745	.9785
2.30	35000.	4.00	8819.	12682.	115.17	16.825	2.486	6.423	.9805
0.00	47500.	1.00	2566.	5306.	182.68	2.857	3.872	4.025	.9857
.20	47500.	1.00	2719.	5746.	182.68	3.066	3.914	4.197	.9860
.50	47500.	1.00	3080.	6620.	182.68	3.545	3.939	4.516	.9865
.85	47500.	1.00	4108.	8614.	182.68	4.770	3.881	5.181	.9869
1.00	47500.	1.00	4783.	9450.	182.68	5.623	3.831	5.648	.9867
1.20	47500.	1.00	6069.	12313.	182.68	7.206	3.731	6.697	.9841
1.60	47500.	4.00	8174.	16749.	157.43	9.947	3.720	7.312	.9839
1.60	47500.	4.00	6015.	9486.	157.43	10.121	3.056	6.467	.9822
1.60	47500.	4.00	3986.	5174.	157.43	10.250	2.485	5.327	.9816
1.78	47500.	4.00	9207.	19101.	145.25	11.366	3.733	7.334	.9821
1.78	47500.	4.00	6732.	10818.	145.25	11.563	3.074	6.334	.9826
1.78	47500.	4.00	4299.	5712.	145.25	11.716	2.484	5.642	.9814
1.95	47500.	4.00	10295.	21648.	134.56	12.914	3.744	8.015	.9807
1.95	47500.	4.00	7480.	12261.	134.56	13.137	3.392	7.111	.9816
1.95	47500.	4.00	4595.	6270.	134.56	13.316	2.485	5.563	.9830
2.12	47500.	4.00	11413.	24426.	124.60	14.595	3.760	8.260	.9783
2.12	47500.	4.00	8237.	13834.	124.60	14.846	3.114	7.439	.9800
2.12	47500.	4.00	4863.	6789.	124.60	15.057	2.485	6.265	.9808
2.30	47500.	4.00	12290.	27084.	113.16	15.979	3.832	8.629	.9759
2.30	47500.	4.00	8796.	15339.	113.16	16.263	3.182	7.725	.9787
2.30	47500.	4.00	4711.	6839.	113.16	16.522	2.487	6.349	.9808
0.00	60000.	1.00	1317.	2876.	182.68	3.040	3.364	3.330	.9863
.20	60000.	1.00	1386.	3109.	182.68	3.253	3.412	3.696	.9863
.50	60000.	1.00	1591.	3574.	182.68	3.743	3.516	4.034	.9867
.85	60000.	1.00	2159.	4660.	182.68	4.980	3.583	4.833	.9866
1.00	60000.	1.00	2404.	5214.	177.07	5.591	3.611	5.193	.9859
1.20	60000.	1.00	2804.	6069.	166.87	6.512	3.656	5.311	.9839
1.60	60000.	4.00	3894.	8325.	144.42	8.959	3.725	7.088	.9849
1.60	60000.	4.00	2855.	4715.	144.42	9.114	3.067	6.216	.9827
1.60	60000.	4.00	1950.	2526.	144.42	9.232	2.487	5.293	.9789
1.78	60000.	4.00	4492.	9618.	134.73	10.391	3.740	7.637	.9828
1.78	60000.	4.00	3269.	5447.	134.73	10.570	3.086	6.256	.9843
1.78	60000.	4.00	2043.	2834.	134.73	10.713	2.485	5.515	.9806
1.95	60000.	4.00	5112.	11023.	126.07	11.946	3.754	7.830	.9817
1.95	60000.	4.00	3704.	8243.	126.07	12.152	3.105	6.871	.9823
1.95	60000.	4.00	2230.	3149.	126.07	12.321	2.486	5.999	.9800
2.12	60000.	4.00	5782.	12609.	118.27	13.686	3.774	9.187	.9795
2.12	60000.	4.00	4166.	7141.	118.27	13.922	3.130	7.101	.9817
2.12	60000.	4.00	2395.	3451.	118.27	14.125	2.486	6.059	.9817
2.30	60000.	4.00	6286.	14093.	108.13	15.118	3.842	8.511	.9771
2.30	60000.	4.00	4495.	7982.	108.13	15.386	3.196	7.678	.9795
2.30	60000.	4.00	2346.	3513.	108.13	15.636	2.488	6.292	.9809
400000.									
.25	0.	5.00	12051.	11294.	182.68	3.151	2.415	2.481	.9862
.25	0.	6.67	6242.	5690.	135.51	2.144	2.416	2.135	.9841
.25	0.	8.34	2217.	2384.	90.17	1.415	2.416	1.992	.9850
.25	0.	10.00	713.	1344.	54.70	1.163	2.415	1.936	.9850

Figure 8 (cont.)

THIS PAGE IS BEST QUALITY PRACTICABLE
FROM COPY FURNISHED TO DDQ

.50	0.	5.00	12719.	13116.	142.64	3.582	2.415	2.631	.9867
.50	0.	6.67	7105.	7238.	141.64	2.549	2.416	2.262	.9853
.50	0.	8.34	2924.	3372.	104.10	1.729	2.415	2.090	.9850
.40	0.	10.00	939.	1698.	74.70	1.321	2.416	1.972	.9855
.40	0.	5.00	13017.	14878.	170.74	4.148	2.416	2.750	.9862
.40	0.	6.67	7942.	8832.	137.64	3.072	2.415	2.474	.9860
.40	0.	8.34	3586.	4740.	109.02	2.244	2.416	2.173	.9844
.40	0.	10.00	1366.	2444.	97.25	1.682	2.417	2.044	.9850
.90	0.	5.00	12937.	15467.	164.82	4.372	2.416	3.124	.9830
.90	0.	6.67	7589.	9472.	135.14	3.248	2.415	2.640	.9854
.90	0.	8.34	3579.	5324.	109.58	2.472	2.415	2.338	.9831
.90	0.	10.00	900.	2452.	89.72	1.481	2.416	2.119	.9809
1.00	0.	5.00	12256.	16130.	158.66	4.632	2.416	3.381	.9808
1.00	0.	6.67	6703.	9969.	131.27	3.919	2.416	2.894	.9799
1.00	0.	8.34	2666.	5748.	108.34	2.681	2.415	2.532	.9795
1.00	0.	10.00	-98.	3150.	84.93	2.072	2.416	2.232	.9789
.25	20000.	5.00	5955.	4804.	182.68	3.154	2.416	2.476	.9862
.25	20000.	6.67	2910.	2441.	135.36	2.150	2.416	2.135	.9841
.25	20000.	8.34	1034.	1127.	89.79	1.419	2.416	1.994	.9850
.25	20000.	10.00	354.	718.	58.75	1.171	2.416	1.928	.9850
.50	20000.	5.00	5862.	5982.	182.68	3.586	2.415	2.623	.9867
.50	20000.	6.67	3271.	3115.	141.24	2.548	2.416	2.258	.9853
.50	20000.	8.34	1352.	1521.	103.67	1.730	2.417	2.053	.9850
.50	20000.	10.00	406.	869.	74.39	1.326	2.418	1.976	.9850
.80	20000.	5.00	7036.	7438.	182.68	4.590	2.415	2.950	.9853
.80	20000.	6.67	4081.	4355.	145.73	3.324	2.416	2.569	.9863
.80	20000.	8.34	1848.	2251.	111.86	2.332	2.416	2.202	.9847
.80	20000.	10.00	513.	1166.	86.88	1.687	2.418	2.047	.9850
.90	20000.	5.00	7654.	8424.	182.68	5.095	2.415	3.258	.9852
.90	20000.	6.67	4432.	4985.	146.95	3.710	2.416	2.743	.9856
.90	20000.	8.34	1968.	2607.	114.03	2.614	2.417	2.343	.9835
.90	20000.	10.00	439.	1327.	89.29	1.883	2.417	2.121	.9809
1.00	20000.	5.00	8160.	9617.	182.68	5.704	2.416	3.630	.9831
1.00	20000.	6.67	4440.	5646.	145.74	4.134	2.416	3.272	.9775
1.00	20000.	8.34	1692.	2918.	114.17	2.990	2.416	2.589	.9814
1.00	20000.	10.00	-28.	1448.	89.49	2.071	2.416	2.231	.9789
.25	30000.	5.00	3613.	3020.	182.68	3.165	2.416	2.477	.9863
.25	30000.	6.67	2161.	1790.	143.13	2.317	2.415	2.178	.9847
.25	30000.	8.34	1024.	976.	105.54	1.624	2.416	2.033	.9850
.25	30000.	10.00	346.	608.	70.37	1.259	2.418	1.960	.9850
.50	30000.	5.00	3808.	3496.	182.68	3.594	2.416	2.623	.9867
.50	30000.	6.67	2370.	2181.	147.62	2.707	2.416	2.307	.9856
.50	30000.	8.34	1212.	1242.	114.22	1.957	2.416	2.090	.9832
.50	30000.	10.00	471.	745.	85.21	1.461	2.415	2.002	.9850
.80	30000.	5.00	4565.	4645.	182.68	4.599	2.415	2.945	.9853
.80	30000.	6.67	2417.	2986.	151.16	3.507	2.416	3.594	.9866
.80	30000.	8.34	1561.	1745.	120.42	2.587	2.415	2.285	.9853
.80	30000.	10.00	627.	1003.	95.55	1.910	2.416	2.082	.9829
.90	30000.	5.00	4967.	5239.	182.68	5.103	2.415	3.260	.9852
.90	30000.	6.67	3141.	3377.	151.76	3.895	2.416	2.808	.9852
.90	30000.	8.34	1649.	1982.	121.76	2.872	2.416	2.502	.9839
.90	30000.	10.00	405.	1123.	97.18	2.125	2.415	2.209	.9816
1.00	30000.	5.00	5294.	5973.	182.68	5.715	2.415	3.623	.9832
1.00	30000.	6.67	3211.	3816.	151.43	4.340	2.416	3.303	.9790
1.00	30000.	8.34	1504.	2204.	121.61	3.172	2.416	2.685	.9824
1.00	30000.	10.00	336.	1225.	97.29	2.336	2.416	2.344	.9797
.25	45000.	5.00	1827.	1564.	182.68	3.231	2.415	2.499	.9863
.25	45000.	6.67	1134.	962.	142.70	2.371	2.416	2.195	.9848
.25	45000.	8.34	541.	563.	134.68	1.668	2.416	2.042	.9850
.25	45000.	10.00	224.	360.	71.34	1.249	2.417	1.964	.9850
.50	45000.	5.00	1428.	1797.	182.68	5.566	2.416	2.646	.9868

THIS PAGE IS BEST QUALITY PRACTICABLE
FROM COPY FURNISHED TO DDG

14122
Atlantic Railroad Bureau, Inc.

.50	45000.	6.67	1209.	1146.	147.22	2.763	2.415	2.333	.9857
.50	45000.	8.34	633.	695.	113.15	2.003	2.416	2.094	.9834
.50	45000.	10.00	272.	439.	84.72	1.504	2.416	2.010	.9850
.80	45000.	5.00	2305.	2357.	192.68	4.676	2.415	2.969	.9853
.80	45000.	6.67	1481.	1938.	130.76	3.565	2.415	2.606	.9867
.90	45000.	8.34	806.	927.	119.63	2.630	2.416	2.301	.9854
.90	45000.	10.00	344.	575.	94.19	1.947	2.416	2.091	.9831
.90	45000.	5.00	2506.	2645.	182.68	5.184	2.416	3.252	.9854
.90	45000.	6.67	1593.	1728.	151.33	3.954	2.415	2.837	.9849
.90	45000.	8.34	851.	1038.	121.00	2.916	2.417	2.513	.9841
.90	45000.	10.00	332.	630.	95.86	2.157	2.416	2.227	.9815
1.00	45000.	5.00	2670.	3001.	182.68	5.798	2.416	3.642	.9832
1.00	45000.	6.67	1624.	1940.	150.96	4.398	2.416	3.313	.9794
1.00	45000.	8.34	780.	1148.	120.84	3.215	2.416	2.674	.9834
1.00	45000.	10.00	198.	675.	95.98	2.363	2.416	2.366	.9793
.25	60000.	5.00	956.	943.	182.68	3.395	2.416	2.557	.9865
.25	60000.	6.67	586.	614.	140.68	2.490	2.415	2.236	.9851
.25	60000.	8.34	302.	384.	101.24	1.762	2.416	2.057	.9850
.25	60000.	10.00	150.	291.	68.58	1.382	2.416	1.986	.9856
.50	60000.	5.00	1008.	1060.	182.68	3.838	2.416	2.664	.9866
.50	60000.	6.67	642.	713.	145.80	2.890	2.417	2.383	.9859
.50	60000.	8.34	352.	438.	109.97	2.107	2.415	2.108	.9838
.50	60000.	10.00	178.	317.	82.35	1.505	2.417	2.031	.9850
.80	60000.	5.00	1200.	1339.	182.68	4.863	2.416	3.178	.9848
.80	60000.	6.67	775.	910.	149.34	3.698	2.416	2.658	.9868
.80	60000.	8.34	441.	590.	117.33	2.739	2.415	2.344	.9856
.80	60000.	10.00	218.	385.	91.38	2.056	2.417	2.103	.9836
.90	60000.	5.00	1294.	1670.	182.09	5.362	2.416	3.267	.9859
.90	60000.	6.67	829.	999.	149.50	4.077	2.415	2.927	.9841
.90	60000.	8.34	464.	649.	118.75	3.024	2.416	2.570	.9841
.90	60000.	10.00	213.	416.	93.17	2.264	2.415	2.266	.9820
1.00	60000.	5.00	1294.	1566.	177.07	5.747	2.417	3.641	.9831
1.00	60000.	6.67	802.	1053.	146.03	4.384	2.416	3.319	.9794
1.00	60000.	8.34	415.	689.	117.32	3.273	2.416	2.732	.9820
1.00	60000.	10.00	151.	442.	93.50	2.471	2.415	2.417	.9796

-1.

Figure 8 (Concluded)

Standard version of PIPSI with inlet maps obtained from full-scale tests or flight tests	Level IV	Flight or engine rig data-hardware needed
Standard version of PIPSI with inlet input maps obtained from scale model tests of exact configuration	Level III	Scale model or component data full details needed
Standard version of PIPSI with detailed inlet maps obtained from detailed analysis or tests of similar configurations	Level II	Empirical correlations, analysis of similar configurations-some geometric details needed
Limited input version of PIPSI (default values)	Level I	Historical trends-little geometric definition needed

Figure 7. Application Spectrum of PIPSI

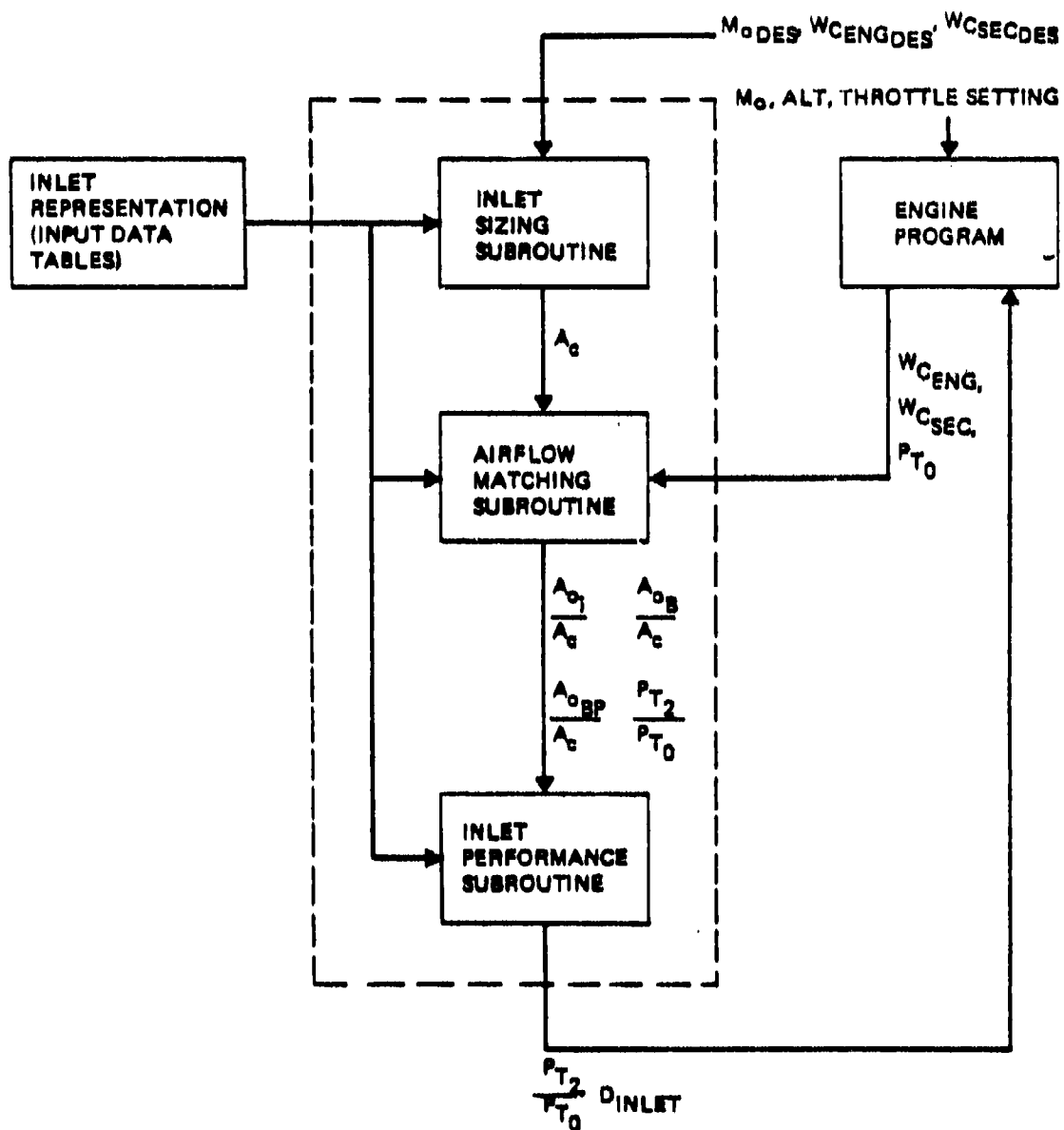


Figure 8. Inlet Procedure

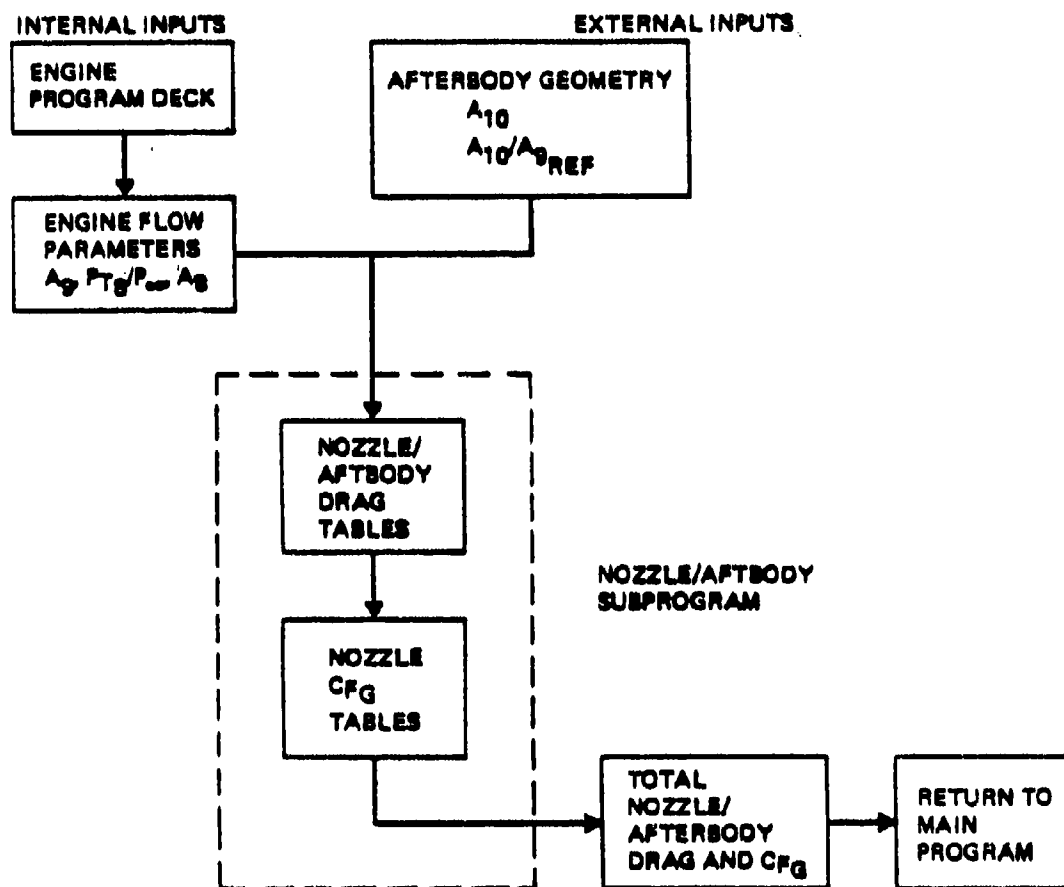


Figure 9. Nozzle/Aftbody Procedure

2.2.1 Inlet Performance

Inlet performance maps are input data to the inlet subprogram. This subprogram sizes the inlet capture area (if it is required) and converts the inlet performance maps into total pressure recovery and inlet drags that are matched to the corrected airflow demand of the engine.

The operation of the inlet procedure is shown schematically in Figure 8. The connecting link between the engine data and the inlet procedure is engine-plus-secondary corrected airflow. The sizing routine permits the inlet to be sized for operation at a desired inlet mass flow ratio and recovery using the design engine airflow demand. A specified capture area size can also be input, if desired, instead of requiring the program to calculate the size.

The inlet input requires fourteen tables of input data which describe the performance characteristics of the inlet. Engineering data obtained from wind tunnel tests and theoretical calculations are used to obtain the inlet performance characteristics. The format for the inlet data was shown in Figure 4. Data taken from these engineering plots are punched on cards as part of the inlet library for input into PIPSI.

The inlet procedure recognizes three modes of inlet operation: low-speed, external compression, and mixed compression. The low-speed mode is used only at very low Mach numbers, e.g., takeoff conditions, when only high engine power settings are likely to be of interest and inlet drag is negligible. The external-compression mode is used over the remaining Mach number regime for external-compression inlets. It is also used for the remaining subsonic regime and supersonic Mach numbers up to the starting Mach number for mixed-compression inlets. The mixed-compression mode is used at or above the starting Mach number for mixed-compression inlets.

- a) External-Compression Inlets. The PIPSI calculation of recovery and drag for an external-compression inlet is illustrated in Figure 10. The required performance maps are input as tables, as indicated. Table 1 is used to represent the effect of the airplane flow field on the local Mach number seen by the inlet. Table 2A gives the basic recovery/mass-flow-ratio characteristics of the inlet. The minimum Mach number for which data is input in Table 2A is taken by the program to be $M_{0_{min}}$, below which only the lowspeed mode is used.

In the low-speed mode, recovery is read directly out of Table 2B as a function of local Mach number only, and inlet drag is neglected.

If the local Mach number exceeds $M_{0_{min}}$, the recovery and mass flow ratio are determined using Table 2A, Table 7 (which gives the schedules bypass flow, if any, as a function of engine mass flow ratio), and the engine corrected airflow demand.

PIPSI iterates to solve simultaneously for the matchpoint recovery and inlet mass flow ratio, as well as the engine mass flow ratio and scheduled bypass flow. If the indicated buzz (Table 2D) or distortion (Table 2E) limits are exceeded, an appropriate warning message will appear, but no fatal error will result. The bleed mass flow associated with the calculated inlet mass flow ratio is determined from Table 6A.

After the required mass flow ratios are determined, spillage, bleed, and bypass drags are found from Tables 3, 4, and 5, respectively. Spillage drag is the incremental change in additive drag and pressure drag on the airplane due to inlet operations at mass flow ratios less than a reference mass flow ratio. The bleed and bypass drags include door drags as well as momentum loss of the airflow.

- b) Mixed-Compression Inlets. The performance calculation for a mixed-compression inlet is illustrated in Figure 11. Below the starting Mach number M_S , the low-speed mode and external compression mode

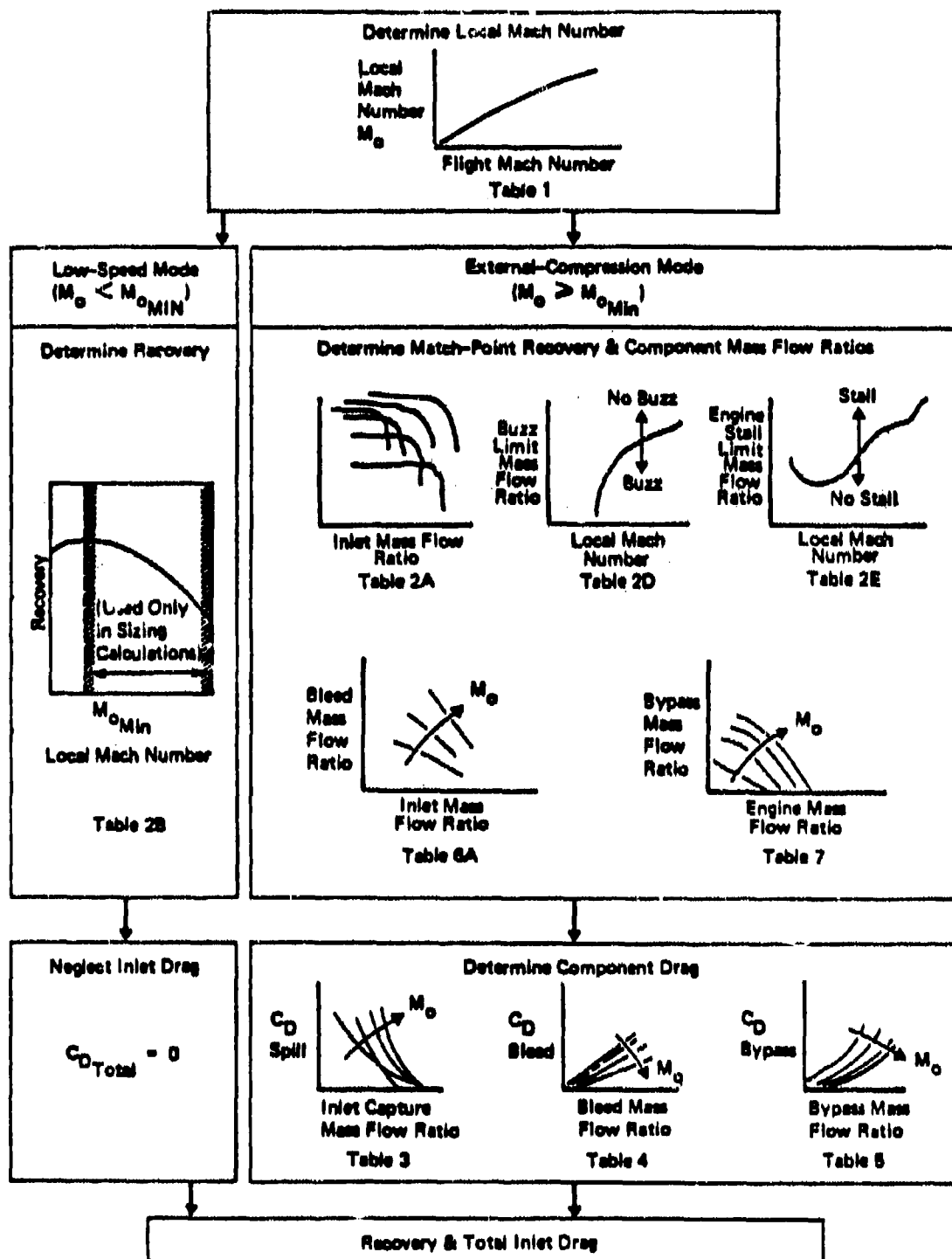


Figure 10. PIPSI Performance Calculation for an External-Compression Inlet

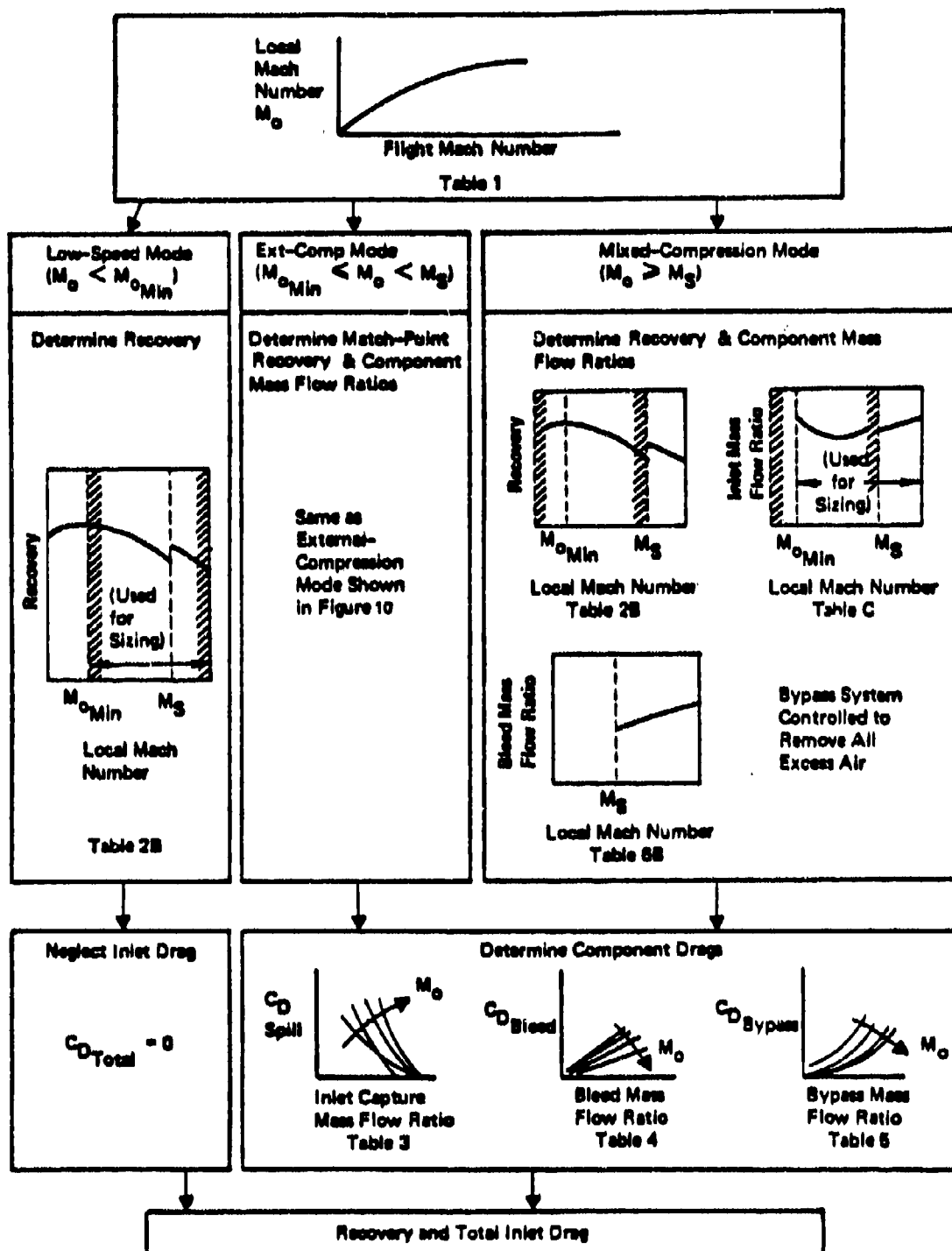


Figure 11. PIPSI Performance Calculation for a Mixed-Compression Inlet

are used in the same way as in the case of an external-compression inlet. The mixed-compression mode, used at or above M_S , is based on the assumption that a closed-loop bypass system is available to remove all excess air. Thus, except for the case of excessive engine airflow demand, the inlet mass flow ratio, bleed flow, and recovery may all be scheduled as a function of local Mach number only; the bypass system compensates for changes in engine airflow demand.

If the corrected airflow delivered by the inlet is inadequate to meet the engine demand at the scheduled recovery, the program will permit the inlet to operate at an excessive supercritical margin. The recovery will be lowered sufficiently to match the engine corrected airflow demand, and an appropriate message will warn the user of an undersized inlet.

Inlet spillage, bleed, and bypass drag are found using Tables 3, 4, and 5, as in the external-compression mode. The data in these tables for Mach numbers equal to or greater than M_S apply only for started inlet operation.

2.2.2 Inlet Sizing

The inlet sizing procedure in the computer program determines the inlet capture area required to match the largest engine airflow demand at each Mach number. From these calculated inlet sizes, the largest required size is selected as the inlet capture area. For sizing calculations, an input curve (Table 2C) of recommended (matched) inlet airflow variations (A_O/A_C) vs. M_O and an input curve (Table 2B) of recommended (matched) inlet total pressure recovery vs. M_O are used to determine the required capture area variation with Mach number. These parameters are used in the following equations to calculate capture area, A_C :

$$A_{C, \text{in.}^2} = \frac{A_{O \text{ ENG}}}{(A_O/A_C)_{\text{MATCHED}}} = \frac{\left(\frac{W\sqrt{\theta}}{\delta} \right) \left(\frac{P_{T2}}{P_{T0}} \right)_{\text{MATCHED}} \left(\frac{A}{A^*} \right)_O}{.343 (A_O/A_C)_{\text{MATCHED}}}$$

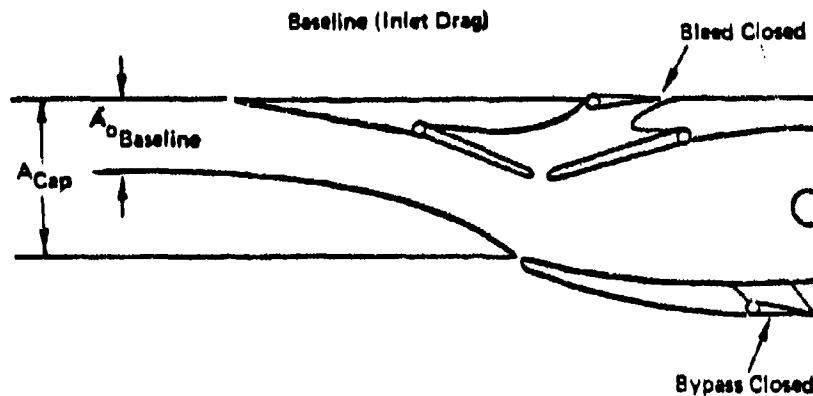
2.2.3 Inlet Reference Conditions

For purposes of aero-propulsion thrust/drag bookkeeping, a reference mass flow ratio is employed. This reference mass flow ratio is always shown in inlet input Table 3B. It represents the inlet mass flow ratio, A_{O_I}/A_C , at which the spillage drag is defined as zero. This reference provides the zero drag reference base for the input spillage drag variations vs. A_{O_I}/A_C at each Mach number input as Table 3. The reference mass flow ratio is selected to be a mass flow ratio at or near the point of maximum inlet mass flow ratio at each M_O . At this point, no further throttle-dependent inlet airflow variations would be expected. Therefore, at this mass flow ratio it is logical to include the drag of the spilled airflow in the airplane drag polar. The inlet drag reference mass flow ratio concept is illustrated in Figure 12.

For users who prefer to use a mass flow ratio of 1.0, an option is included in the computer program to add the incremental reference spillage drag to the spillage drag input data of Table 3, thereby creating a reference mass flow ratio equal to 1.0.

2.2.4 Inlet Recovery Correction

The engine input provides the required data for inlet drag, inlet recovery, nozzle afterbody drag and nozzle coefficient calculations. The engine section of the PIPSI program calculates only the changes in internal performance due to changes in inlet recovery. Changes in inlet recovery produce a directly proportional change in nozzle pressure ratio, airflow, and fuel flow because the nozzle throat area does not change. Furthermore; it is assumed that engine data is calculated with MIL STD 5008B recovery and all inlet recovery changes are made relative to that value unless the user inputs a different reference recovery. Thermodynamic data from Keenan and Kaye tables has been "curve-fitted" and subroutines are provided to calculate the thermodynamic properties of the exhaust gases.



The inlet baseline reference condition for spillage drag is defined at each Mach number as shown below. This condition was chosen because:

- a) it corresponds to an accurate reference and measurable condition for the real inlet,
- b) it corresponds to a condition when inlet spillage drag is minimum (i.e., minimum lip separation and therefore less error in scaling),
- c) it is near the operating condition of the inlet (airplane reference model therefore contains major inlet interference effects).

Figure 12. Definition of Inlet Reference Mass Flow Ratio

The calculation procedure is as follows: for each altitude, Mach number, and power setting, the net thrust (F_N), fuel flow (W_F), corrected airflow ($W\sqrt{\theta_2}/\delta_2$), nozzle throat area (A_g), nozzle exit area (A_9), and nozzle thrust coefficient (C_{F_G}) are given.

Standard atmosphere and MIL Standard 5008B inlet recovery are used to calculate the airflow at the engine face and gross thrust is calculated for the given engine data before any changes in inlet recovery by the following equation:

$$F_{G\text{ OLD}} = F_N + \frac{W_2 V_\infty}{g}$$

The desired inlet recovery is obtained from the inlet subprogram and the engine gross thrust is first calculated with MIL Standard recovery and then with the calculated recovery. To calculate engine gross thrust, the engine corrected airflow remains constant for any change in inlet recovery, and at any given power setting, the nozzle exhaust areas and burner fuel-air ratio remain constant. The engine performance for any change in inlet recovery is calculated by the following relations:

$$(W_8)_{RF} = W_8 \left[\frac{(P_{T_2}/P_{T_0})}{(P_{T_2}/P_{T_0})_{\text{MIL 5008B}}} \right]$$

$$(W_F)_{RF} = W_F \left[\frac{(P_{T2}/P_{T0})}{(P_{T2}/P_{T0})_{MIL\ 5008B}} \right]$$

$$(W_2)_{RF} = W_2 \left[\frac{(P_{T2}/P_{T0})}{(P_{T2}/P_{T0})_{MIL\ 5008B}} \right]$$

$$(P_{T8}/P_0)_{RF} = P_{T8}/P_0 \left[\frac{(P_{T2}/P_{T0})}{(P_{T2}/P_{T0})_{MIL\ 5008B}} \right]$$

After the above quantities are computed, the corrected quantities $(W_B)_{RF}$, $(W_F)_{RF}$, $(W_2)_{RF}$ and $(P_{T8}/P_0)_{RF}$ are used to compute a new gross thrust, F_{G2} . This new gross thrust and the gross thrust, F_{G1} , calculated using the same subroutines and the uncorrected (MIL 5008B) quantities $(W_B, W_F, W_2, P_{T8}/P_0)$ are used to compute a ratio, F_{G2}/F_{G1} . This ratio is then used to obtain the new value of gross thrust, $F_{G_{NEW}}$. The new value of gross thrust is then found by ratio

$$F_{G_{NEW}} = F_{G_{OLD}} \frac{F_{G2}}{F_{G1}}$$

The ratio procedure is used to minimize any inaccuracies that may be caused by assuming burner efficiency (η_B) is constant for all engine operating conditions.

The net thrust and fuel flow after correction for inlet recovery are:

$$F_{NR} = F_{G_{NEW}} - \frac{WV_{\infty}}{g} \frac{R_F}{R_{F_{MIL}}}$$

$$W_{FR} = W_F \frac{R_F}{R_{F_{MIL}}}$$

and the installed propulsion system thrust and SFC:

$$F_{NA} = F_{NR} - D_{INLET} - D_{NOZ} + D_{NOZ_{REF}}$$

$$SFC_A = \frac{W_{FR}}{F_{NA}}$$

2.2.5 Bypass Vs. Spillage Trade Calculation

A calculation procedure has been developed and programmed that provides the capability to automatically perform trade studies between bypass and spillage airflow. The purpose of this procedure is to provide the program user with maximum visibility of the effects of various design options that may be available for handling excess inlet airflow.

The trade study procedure provides the user with the option to select any of the following modes for disposing of excess airflow:

Mode

- 1 All excess airflow spilled
- 2 All excess airflow bypassed above a specified Mach number
- 3 Scheduled bypass with rest of excess airflow spilled
- 4 Optimum combination of bypass and spillage for minimum drag
- 5 Optimum combination of bypass and spillage for minimum installed SFC (includes effect of bypass on total pressure recovery)

For visibility, an optional printout can be specified by the user that will display the complete results of the spillage/bypass trade studies.

The bypass vs. spillage trade study procedure was developed by modifying and adding to the existing program calculation routines. For Options 1, 2 and 3 existing program calculation routines are used to allow the user to simply select the mode. For Options 4 and 5 which involve optimization, standard methods are used to find the minimum C_D and SFC_A values.

Figure 13 presents a general flow chart of the bypass vs. spillage trade study procedure. Complete flow charts of the PIPSI program are contained in Volume II.

2.3 NOZZLE SUBPROGRAM

The purpose of the nozzle/afterbody drag and C_F input data and calculation subprograms is to calculate nozzle internal losses (ΔC_{F_G}) and nozzle/afterbody drag.

2.3.1 Nozzle/Afterbody Drag

The nozzle/afterbody drag is computed using maps which represent the afterbody drag characteristics (Figure 5) as a function of A_{10}/A_9 and M_0 , external input geometry and engine data. Engine data obtained internally from the engine subprogram include nozzle throat area, nozzle pressure ratio, freestream conditions, and ideal gross thrust. An essential geometry input is the nozzle exit area, A_9 , which is required for boattail drag computation. This parameter is obtained in either of two ways:

1. From the engine subprogram when the existing nozzle data are used;
2. From a calculation of fully-expanded A_9 as a function of nozzle total pressure ratio for wedge and plug nozzles.

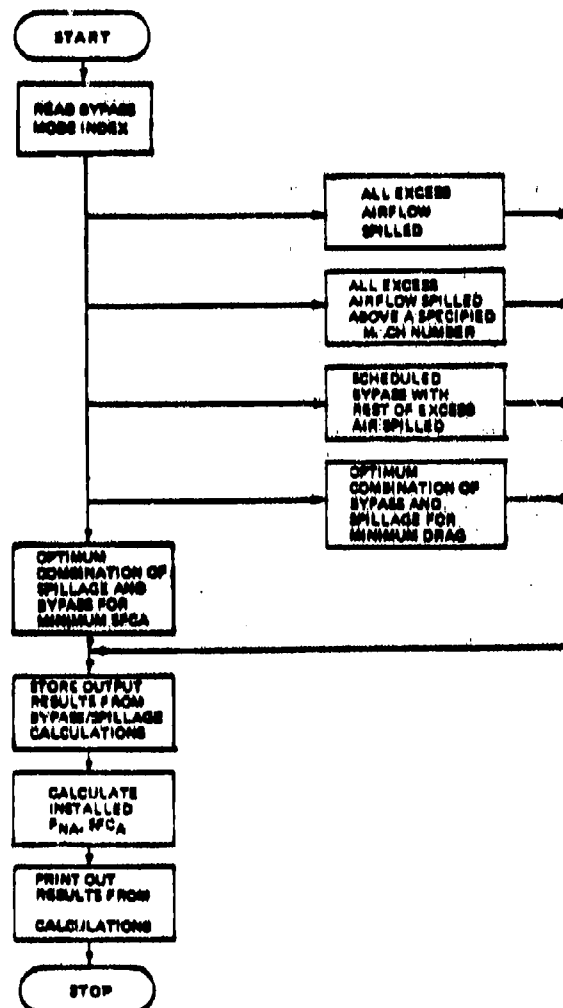


Figure 13. General Flow Chart for Bypass Vs. Spillage Trade Studies

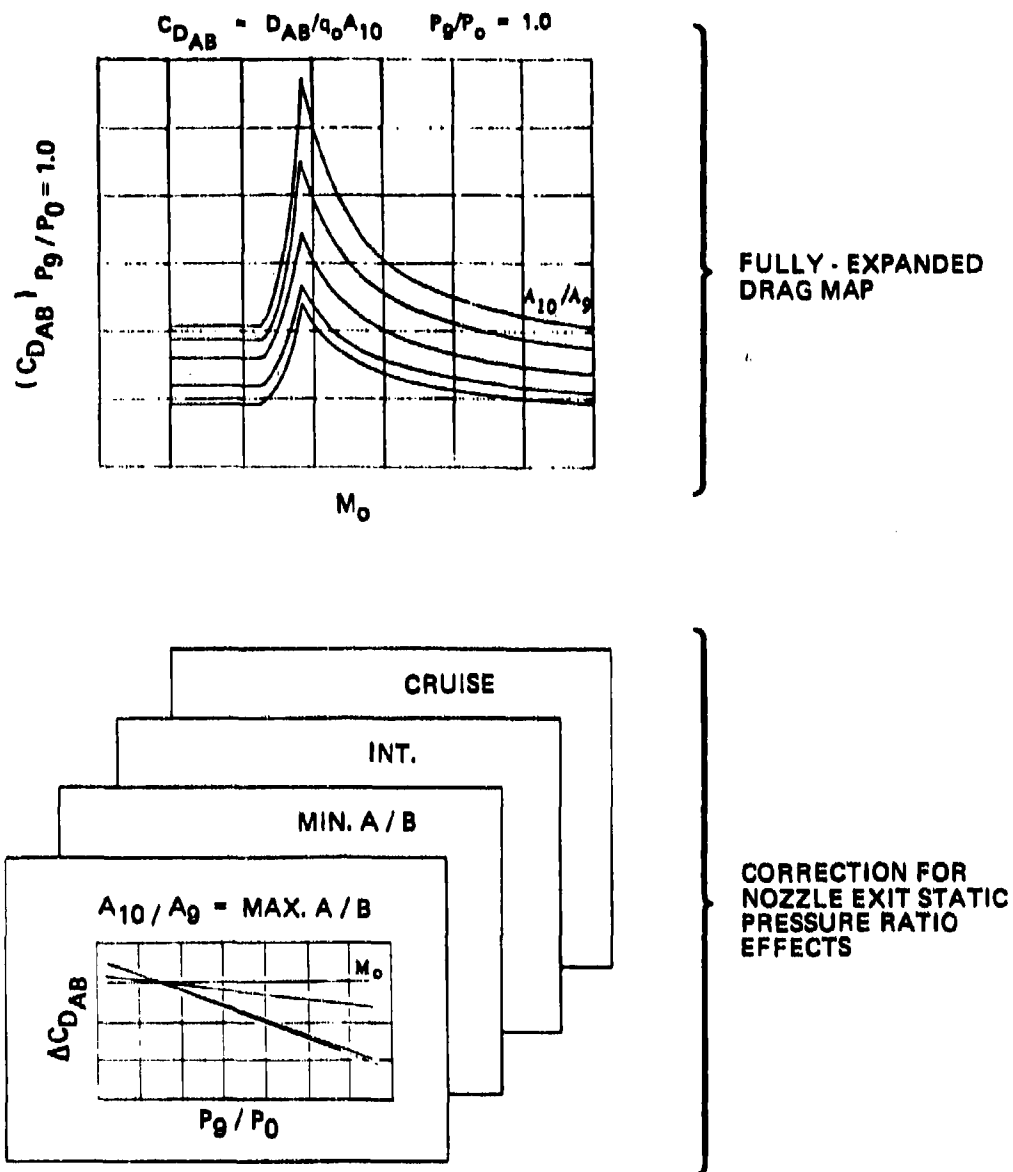
The program currently has built in the variation of base pressure, P_b/P_o , as a function of freestream Mach number. This is then used to calculate $C_{D_{Base}}$.

Fully-expanded nozzle/-aftbody drag coefficient is obtained from tables such as those illustrated in Figure 5a. The drag coefficient is obtained as a function of the ratio of nozzle exit area to maximum cross-sectional area, A_9/A_{10} , and free-stream Mach number.

A procedure has been programmed that allows the program to account for effects of varying nozzle exit static pressure ratio. This procedure determines an incremental drag coefficient, $\Delta C_{D_{AB}}$, to be added to the fully-expanded nozzle/aftbody drag coefficient. The incremental drag coefficient is a function of nozzle exit static pressure ratio (P_9/P_o) and free-stream Mach number (M_o) and is available for a range of nozzle/aftbody area ratios (A_{10}/A_9) from max A/B to subsonic cruise. The incremental drag coefficient maps allow the user to input the pressure ratio effects data if it is available. If the user does not have such data available, a set of dummy maps are used that sets $\Delta C_{D_{AB}} = 0$ for all P_9/P_o , M_o , and A_{10}/A_9 . A three-dimensional table look-up procedure is used to obtain the $\Delta C_{D_{AB}}$ values during the program operation. A maximum of four maps are used representing different nozzle/aftbody area ratios. An illustration showing the nozzle/aftbody drag procedure is presented in Figure 14.

2.3.2 Nozzle Gross Thrust Coefficient

The nozzle gross thrust coefficient input data maps are used to provide a means for correcting uninstalled engine data for the effects of nozzle internal performance that are different from the nozzle internal performance used in generating the uninstalled engine data.



$$C_{DAB} = (C_{DAB})_{P_9/P_0 = 1.0} + (\Delta C_{DAB})_{P_9/P_0, M_0, A_{10}/A_9}$$

Figure 14. Calculation Procedure for Effects of Nozzle Static Pressure Ratio on Drag

Two different types of nozzle C_F maps are provided, as shown in Figure 5. Figure 5b shows the data input format for a round nozzle and Figure 5c shows the data input format for two-dimensional nozzles. For round nozzles, the nozzle area ratio, A_9/A_8 is calculated from tabulated input values provided along with nozzle pressure ratio, P_{T_8}/P_0 , as part of the engine data.

For use with the two-dimensional nozzle C_F input, the engine power setting and nozzle pressure ratio are obtained from the engine input data by procedures programmed into the engine performance subprogram.

The data input table format for the round nozzle (Figure 5b) provides nozzle gross thrust coefficient as a function of nozzle total pressure ratio and area ratio. In the case of two-dimensional nozzles, however, the nozzle gross thrust coefficient (Figure 5c) is input as a function of nozzle total pressure ratio for maximum afterburning and intermediate (dry) power settings. This input data format is based on the assumption that a variable area nozzle will be used which will be scheduled to provide an optimum variation of area ratio as a function of nozzle pressure ratio.

The calculated installed propulsion system performance data include the throttle-dependent inlet and nozzle/aftbody losses. To determine the throttle-dependent portion of the nozzle/aftbody drag to be included as a loss to the propulsion system performance, a reference condition has been established for the nozzle/aftbody drag as follows:

The nozzle/aftbody drag increment to be included in propulsion system installed net thrust will be defined as zero when the nozzle is at its maximum (full-open) geometry and operating at a nozzle static pressure ratio, P_9/P_0 , equal to 1.0 (fully-expanded). The nozzle/aftbody drag at this condition will be included in the aerodynamic drag. Incremental changes in nozzle aftbody drag due to changes in nozzle/aftbody geometry and/or nozzle static pressure

ratio different from this condition will be included as propulsion system drag. This reference condition is illustrated in Figure 15 for a typical set of nozzle/aftbody drag data from Reference 2.

2.3.3 Thermodynamic Properties

Thermodynamic properties required for throat calculations are obtained using the functions shown in Table I. The functions listed in Table I are "curve-fits" of Keenan and Kaye data (Reference 29). The gas tables are primarily used to calculate exhaust nozzle static pressures and jet velocities.

TABLE I

THERMODYNAMIC SUBROUTINES	
H = HOFT (T,FOA)	Enthalpy as a function of temperature (degrees R) and fuel-air ratio
T = TOFH (H,FOA)	Temperature as a function of enthalpy and fuel-air ratio
PR = PROFH (H,FOA)	Relative pressure, (P_r) as a function of enthalpy and fuel/air ratio
H = HOFPR (PR,FOA)	Enthalpy as a function of relative pressure and fuel-air ratio
C = COFH (H,FOA)	Sonic velocity as a function of total enthalpy and fuel-air ratio
C = COFHS (H,FOA)	Sonic velocity as a function of static enthalpy and fuel-air ratio

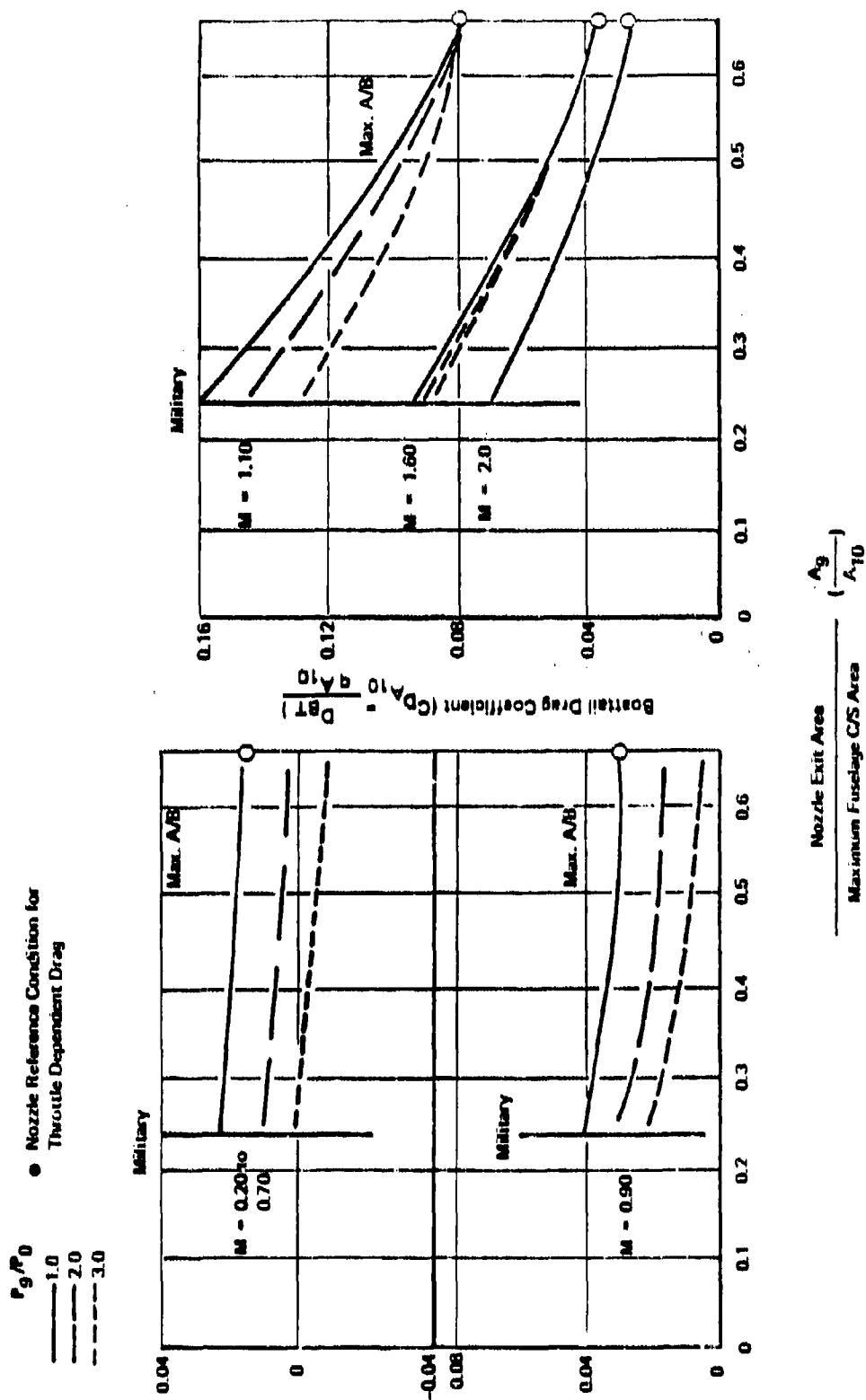


Figure 15. Typical Nozzle/Mftbody Drag Data

2.3.4 Energy Balance for Exhaust Gas Calculations

If the temperature at the engine compressor face, airflow, pressure ratio and fuel flow are known, the exhaust gas enthalpy (h) and relative pressure (p_r) can be calculated from the energy balance:

$$W_2 h_{T_2} + W_f Q \eta_B = W_{18} h_{T_{18}} + W_8 h_{T_8} + W_{BX} h_{T_{BX}}$$

(for either mixed or non-mixed flow engines)

For mixed flow fans or a turbojet:

$$W_8 = W_2 - W_{BX} + W_f$$

$$(f/a)_8 = W_f / (W_2 - W_{BX})$$

$$h_{T_8} = (W_2 h_{T_2} + W_f Q \eta_B) / W_8 \quad (W_{BX} h_{T_{BX}} \text{ is considered negligible})$$

$$P_{rT_8} = f(h_{T_8}, (f/a)_8)$$

For a separate flow ducted fan (fan nozzle and primary nozzle):

$$h_{T_2} = f(T_{T_2}, (f/a)_2) ; \text{ where } f/a = 0$$

$$(P_{rT})_2 = f(h_{T_2}, (f/a)_2) ; \text{ where } f/a = 0$$

$$(P_{rT})_{18} = (P_{rT})_2 (P_{T_{18}} / P_{T_2})$$

$$h_{T_{18}} = f(P_{rT_{18}}, (f/a)_{18}) ; \text{ where } f/a = 0$$

and

$$W_8 = W_2 - W_{18} - W_{BX} + W_f$$

$$h_{T8} = (W_2 h_{T2} - W_{18} h_{T18} + W_f Q \eta_B) / W_8$$

($W_{BX} h_{T8}$ is
considered negligible)

$$(P_{rT})_8 = f(h_{T8}, f/a)_8$$

2.3.5 Nozzle Gross Thrust Calculation

The calculation procedure in this section applies to both mixed and non-mixed flow nozzles.

2.3.6 Convergent Nozzle

The velocity at the throat for a convergent nozzle is a function of the total enthalpy (assuming the throat is choked).

$$C_8 = f(h_{T8}, f/a)_8$$

and the static pressure is a function of the static enthalpy

$$h_8 = h_{T8} - \frac{(C_8)^2}{2gJ}$$

$$T_8 = f(h, f/a)_8$$

$$P_{r8} = f(h, f/a)_8$$

$$P_{T8}/P_8 = (P_{rT})_8/P_8$$

P_{T8} is obtained from the tabulated engine input data as $f(P.S., \text{alt.}, M)$ or it is calculated by the procedure described on Page 40.

$$P_8 = P_{T8} / (P_{T8}/P_8)$$

The area of the throat is

$$A_8^* = \left(\frac{WRT}{P_8} \right)_8$$

and the thrust is

$$F_g = \frac{W_8 V_8}{g} + A_8^* (P_8 - P_{amb})$$

2.3.7 Convergent-Divergent Nozzle (fully expanded)

If the exhaust flow is fully expanded, the static pressure of the nozzle exit is equal to ambient, and the exit velocity is a function of the total to static enthalpy.

$$P_{r9} = P_{r8} (P_{amb}/P_8)$$

$$h_9 = f(P_r, f/a)_9$$

$$T_9 = f(h, f/a)_9$$

Since $h_8 = h_9$

$$V_9 = [2gJ(h_{T8} - h_9)]^{1/2}$$

The exit area is

$$A_9 = W_9 R_8 T_9 / P_{amb} V_9$$

and the gross thrust is $F_g = \frac{W_9 V_9}{g} C_{FG}$

2.3.8 Convergent-Divergent Nozzle (not fully expanded)

If the exit area of a convergent-divergent nozzle is less than required for full expansion, the exit static pressure will be higher than ambient. The throat conditions are known; therefore, a guessed exit velocity gives:

$$h_9 = h_{T_8} - V_9^2/2gJ$$

$$T_9 = f(h, f/a)_9$$

$$P_{r9} = f(h, f/a)_9$$

$$P_9 = \frac{P_{r9}}{P_{r8}}$$

$$W_9 = \frac{P_9}{R(T_9)} \quad A_9 V_9 = (\rho AV)_9 = \left(\frac{PAV}{RT}\right)_9$$

An iteration on V_9 to make $W_9 = W_8$ will result in the exit conditions for a given area.

The gross thrust is: $F_g = \left(\frac{WV}{g} + PA\right)_9 C_S - P_{amb} A_9$

2.3.9 Nozzle Pressure Ratio Calculation

The exhaust nozzle pressure ratio can be calculated if thrust, fuel flow and airflow are known. The gross thrust is calculated as follows:

$$F_g = (F_{net} + F_{ram})/C_{FG}$$

$$F_{ram} = \frac{W_2 V_\infty}{g}$$

and the nozzle exit conditions are calculated by assuming that the flow is fully expanded.

$$W_8 = W_2 - W_{BX} + W_f$$

$$h_{T8} = h_{T2} + (Q \eta_B W_f / W_8)$$

$$T_{T8} = f(h_T, f/a)_8$$

$$V_9 = F_g(g)/W_8$$

$$h_9 = h_{T8} - V_9^2 / 2g$$

$$P_{r9} = f(h, f/a)_8$$

$$(P_{rT})_8 = f(h_T, f/a)_8$$

Since $P_9 = P_{amb}$

$$P_{T8} / P_{amb} = (P_{rT})_8 / P_{r9}$$

The pressure ratio calculation will be in error, an amount relative to the value of the thrust coefficient (C_F), because this is usually unknown if pressure ratios and exhaust areas are not given.

SECTION III

LIBRARY MAP CONFIGURATIONS

The purpose of the library of inlet and nozzle/aftbody maps is to provide a readily-available source of input data that can be utilized by the interactive PIPSI computer program. The input data are converted to data tables and stored as permanent files on computer disk storage for computerized retrieval. When interactive calculations are to be performed, the desired library computer files representing the inlet and nozzle/aftbody data along with the uninstalled engine data, are attached externally to the PIPSI program prior to execution of the program

The input data are stored in the form of tables of standardized format representing maps of inlet and nozzle/aftbody performance characteristics. The format of the inlet characteristics is shown in Figure 4. The format of the nozzle/aftbody drag and internal performance (C_{FG}) characteristics is shown in Figure 5.

The data for all the configurations are contained in Volume IV.

3.1 INLET CONFIGURATIONS

The matrix of inlet configurations for which performance characteristics are available is shown in Figure 16. Performance characteristics are available for a total of 18 separate inlet configurations. These configurations include a variety of inlet types: chin, pitot, two-dimensional and axisymmetric external compression, and two-dimensional and axisymmetric mixed compression. The design Mach number range covered by the configurations is 0.5 to 3.5.

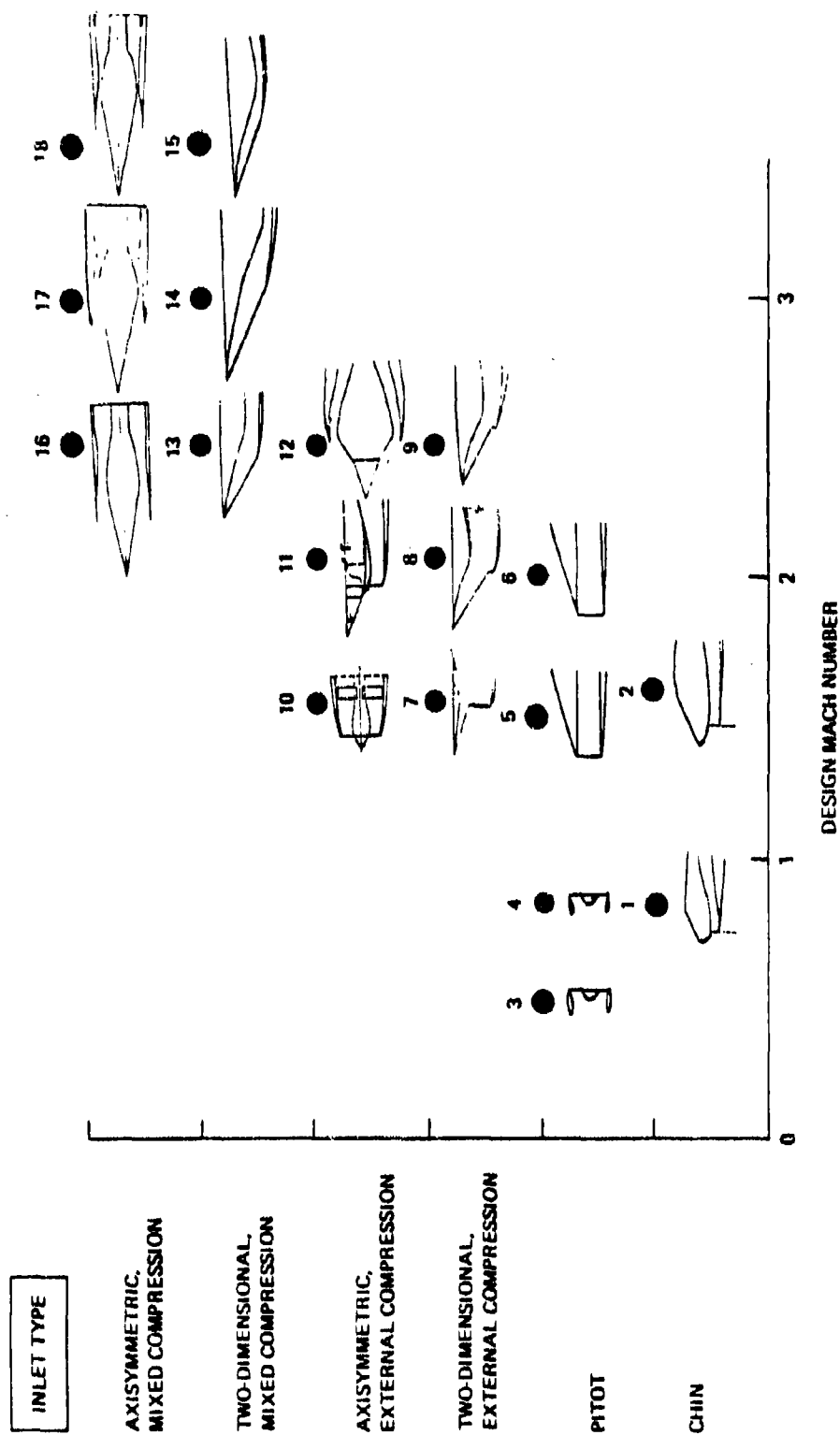


Figure 16. Matrix of Inlet Maps

The inlet configurations that are represented by the library of performance characteristics have been selected by considering the following factors:

- (1) At each design Mach number, the configuration must be typical of an inlet that could reasonably be used at that Mach number. Design Mach number affects such design features as variable geometry, number of compression ramps, boundary layer bleed system design, and mixed vs. external compression scheme. The way typical inlet design features vary as design Mach number is increased is illustrated in Figure 17. In general, the trend is toward more inlet complexity and more variable geometry as design Mach number is increased, assuming a high level of total pressure recovery is to be maintained. The configurations contained in the library of inlets are shown in Figure 17 by their configuration numbers, as defined in Figure 16.

3.2 NOZZLE/AFTBODY MAP CONFIGURATIONS

The nozzle/aftbody configurations include: axisymmetric convergent-divergent nozzles, (single and twin), two-dimensional convergent-divergent nozzles (single and twin), axisymmetric plug nozzles (single and twin), and two-dimensional wedge nozzles (single and twin). The nozzle/aftbody files that are available are shown in Figure 18. These files and the configurations that are represented in the library of inlet and nozzle/aftbody maps are described in detail in Volume IV.

- (2) Experimental data are available for several inlet configurations that can be used to provide well-substantiated inlet performance maps. It has been an objective of the program to use experimental data whenever it is available and the configuration is suitable (or typical) for the intended application. Examples of some of the useful sources of data that have been utilized in developing the inlet performance characteristics are:

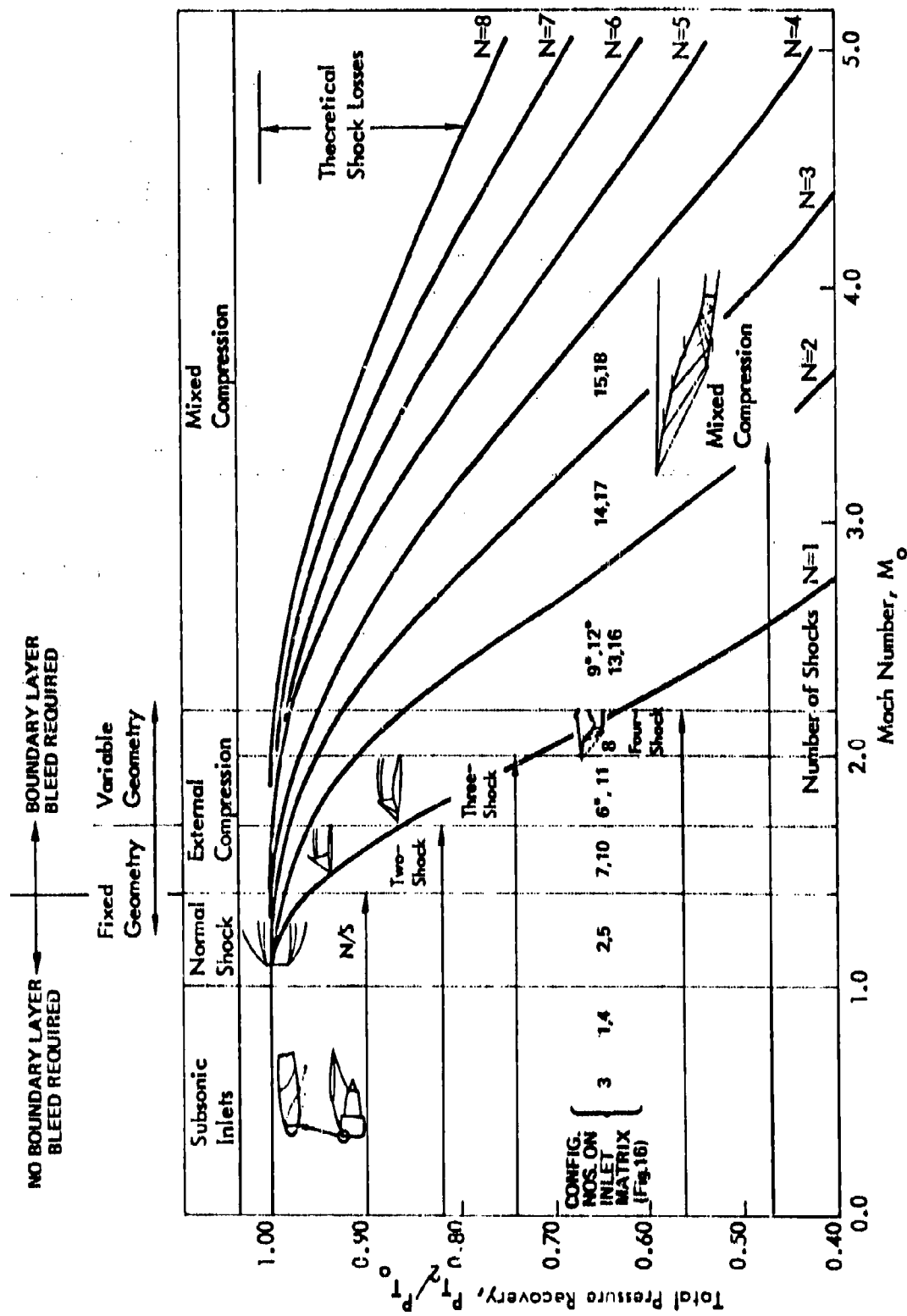


Figure 17. Representative Spectrum of Inlets


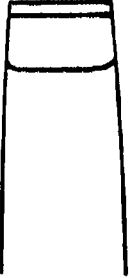
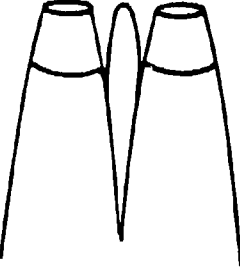
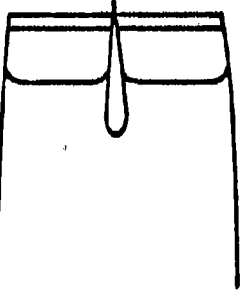

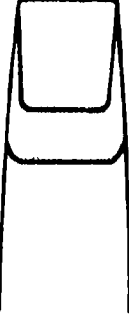
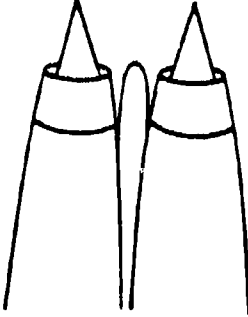
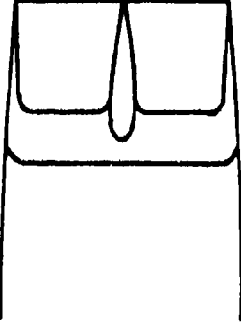
CV MAP	DRAG MAP	AXISYMMETRIC		2-DIMENSIONAL	CV MAP	DRAG MAP
CV1	208N- TTY		CONVERGENT-DIVERGENT		CV2D- CD	DCD2 D1
CV1	CD2R				CV2D- CD	DCD2 D2
CVRP	DRP1		PLUG (WEDGE)		CV2D	SING 2D
CVRP	DRP2				CV2D/ATS	2DM3

Figure 18. Nozzle/Aftbody Files

Tailor-Mate tests (Reference 4), F-15 inlet tests (Reference 5), Boeing LWF tests (Reference 6), XB-70 inlet tests (Reference 7), NAR F-100 inlet tests (Reference 8), and Boeing subsonic inlet tests (Reference 9).

- (3) Several sets of inlet performance characteristics were available from the previously-completed Air Force Contract F33615-72-C-1580 (Reference 1). These data were used in the present contract for Configurations 6, 10, 7, 9, 13 and 14, largely unchanged, except for some revisions in the data table formats.
- (4) Inlet data maps are available at Boeing for configurations 8 and 11. These data are in the PIPSI format and are directly usable in the present contract, because they represent typical inlet configurations for the required design Mach numbers.

A summary chart is presented in Figure 19 which shows the inlet configuration numbers (indexed to Figure 16), a brief description of the inlet, and the source of the data and/or methods used to obtain the inlet performance characteristics. In addition to the information shown in Figure 19, each of the inlets is described in detail in Volume IV.

Inlet number	INLET CONFIGURATIONS AND SOURCES OF DATA USED TO DEVELOP THE INLET MAPS
1	A-7 type inlet; developed from published A-7 data and engineering analysis
2	F-8 type inlet; developed from published F-8 inlet data and analysis
3	Subsonic inlet type; based on data and methods from Boeing subsonic inlet (i.e. 707, 727 etc)
4	Subsonic inlet type; based on data and methods used to develop Boeing 747-type inlets
5	Normal shock inlet; based on data from Rockwell tests of F100 airplane inlet
6	Normal shock-type inlet; based on data from Rockwell F-100 inlet, Boeing LWF inlet tests, and GD LWF inlet data
7	Fixed-Geometry, 2-shock inlet; based on data from Boeing LWF inlet tests
8	Four-shock, variable ramp inlet; theoretical design based on analysis, optimized for $M_o = 2.0$
9	Four-shock, variable ramp inlet; based on data from NR inlet tests of IPS model
10	Fixed-geometry, single cone inlet; based on analytical design for a $M_o = 1.6$ VTOL
11	3-shock, half-round inlet with variable-diameter centerbody; analytical design for a supersonic Navy VTOL configuration
12	3-shock, half-round inlet with variable second cone angle; GD tailor-made tests
13	Mixed-compression; analytical design documented in AFFDL-TR-72-147-vol IV
14	Mixed compression; based on XB-70 type configuration and data
15	Mixed compression; based on NASA AMES configuration and tests of a mach 3.5, 2-D inlet
16	Mixed compression axisymmetric; based on a Boeing analytical study of an AST inlet for NASA AMES
17	Mixed compression axisymmetric; based on data from NASA AMES tests of $M_{\infty} = 3.0$ inlet
18	Mixed compression axisymmetric; based on results of Boeing analytical studies for a NASA AMES mach 3.5 inlet

Figure 19 . Sources of Data for Matrix of Inlet Maps

SECTION IV

DERIVATIVE PROGRAM (DERIVP)

The purpose of the derivative procedure is to provide a first order analytical method to determine the effects on inlet and nozzle performance of configuration differences from the nearest configuration represented in the library of stored maps (which are built-up for specific configurations). The derivative procedure employs analytical and experimental data in determining the changes in the stored performance maps that result from geometric changes in the inlet and nozzle/aftbody configurations.

The derivative parameters are discussed in Subsection 4.1, the inlet derivative procedure is discussed in Subsection 4.2, and the nozzle/aftbody derivative procedure is discussed in Subsection 4.3.

4.1 DERIVATIVE PARAMETERS

The first step in the development of the derivative procedure was the selection of the derivative parameters. The derivative parameters are those parameters that will be perturbed to produce a new set of performance characteristics from an existing (or "baseline") set of maps.

The criteria used to select the derivative parameters were:

- (1) Variations in the parameter must have a significant effect on the content of the maps used to describe inlet or nozzle/aftbody performance. The derivative procedure should be used as part of an overall conceptual analysis procedure for calculating first-order propulsion system installation effects. The derivative

parameters selected for the present procedure are those which have been clearly identified by test or analysis as having "first-order" effects on installed performance. The derivative procedure should not be used for detailed design studies since the procedure may not be sensitive to the effects of small variations in some design variables.

- (2) To the maximum extent possible, an attempt was made to define the derivative parameters in terms of geometric variables that can be easily related to the airplane configuration. This was done to help in evaluating the effects of configuration changes on installed performance.
- (3) Derivative parameters had to represent trends that were strong enough to be clearly evident in spite of the scatter in test data obtained from typical inlet and nozzle tests.

Table I presents a list of the derivative parameters that have been selected for use in the derivative procedures. The definition of each of these parameters is included. Tables III & IV present the derivative parameters and the performance map variables that they affect, either directly or indirectly.

TABLE II
DERIVATIVE PARAMETERS AND THEIR DEFINITIONS

1. Aspect Ratio
(AR)
 - Applicable to two-dimensional inlets only
 - Defined as inlet width divided by inlet lip height (relative to tip position).

2. Sideplate Cutback
(SPC)
 - Applicable to two-dimensional inlets only
 - Defined as the percent of a full sideplate area that is removed to define a partial sideplate.

The upper edge of a full sideplate extends from the ramp tip to the cowl lip.

3. First Ramp or Cone Angle
 - Applicable to two-dimensional and axisymmetric inlets
 - Defined as surface ramp angle, in degrees, relative to horizontal reference line for two-dimensional inlets
 - Defined as cone surface angle, in degrees, relative to inlet centerline for axisymmetric inlets (cone half-angle)

TABLE II (Continued)

4. Design Mach Number (M_0 Design)	<ul style="list-style-type: none"> - Applicable to all inlets - Defined as the maximum Mach number at which the inlet is designed to operate
5. Cowl Lip Bluntness	<ul style="list-style-type: none"> - Applicable to all inlets - Defined as the inlet lip surface radius divided by the lip height.
6. Takeoff Door Area	<ul style="list-style-type: none"> - Applicable to all inlets - Defined as the total door area for the takeoff auxiliary air system divided by the inlet capture area
7. External Cowl Angle	<ul style="list-style-type: none"> - Applicable to all inlets - Defined as external cowl surface angle, in degrees, relative to inlet horizontal reference line
8. Exit Nozzle Type for Bleed	<ul style="list-style-type: none"> - Applicable to two-dimensional and axisymmetric inlets - Defines whether bleed exit nozzle is convergent or convergent-divergent
9. Exit Nozzle Angle for Bleed	<ul style="list-style-type: none"> - Applicable to two-dimensional and axisymmetric inlets - Defined as bleed exit nozzle angle, in degrees, relative to inlet horizontal reference line
10. Exit Flap Aspect Ratio for Bleed (AR_F)	<ul style="list-style-type: none"> - Applicable to two-dimensional and axisymmetric inlets - Defined as flap width divided by flap length
11. Exit Flap Area for Bleed (A_F/A_C)	<ul style="list-style-type: none"> - Applicable to two-dimensional and axisymmetric inlets - Defined as flap area divided by inlet capture area

TABLE II (Continued)

12. Exit Nozzle Type for Bypass	- Applicable to all inlets - defines whether bypass exit nozzle is convergent or convergent-divergent
13. Exit Nozzle Angle for Bypass	- Applicable to all inlets - Defined as bypass exit nozzle angle, in degrees, relative to inlet horizontal reference line
14. Exit Flap Aspect Ratio for Bypass (AR _F)	- Applicable to all inlets - Defined as flap width divided by flap length
15. Exit Flap Area for Bypass (A _F /A _C)	- Applicable to all inlets - Defined as flap area divided by inlet capture area
16. Subsonic Diffuser Area Ratio (A ₂ /A ₁)	- Applicable to all inlets - Defined as exit area (compressor face) divided by entrance area (throat)
17. Subsonic Diffuser Total Wall Angle	- Applicable to all inlets - Defined as the total equivalent wall divergence angle, from entrance to exit
18. Subsonic Diffuser Loss Coefficient (c)	- Applicable to all inlets - Defined by the equation $\frac{P_{T2}}{P_{T1}} = 1 - c \left(1 - \frac{1}{(1 + .2M^2)^{3.5}} \right)$
19. Throat to Capture Area Ratio (A _T /A _C)	- Applicable to Pitot inlets <u>only</u> - Defined as the fixed throat area divided by the inlet capture area
20. Nozzle/Aftbody Area Distribution	- Applicable to all nozzle/aftbodies. Defined by the cross-sectional area distribution as a function of station from A ₁₀ (ref. area) to A ₉ (nozzle exit area). Characterized by the parameter IMS _T

TABLE II (Concluded)

21. Radial Tail Orientation Position	- Applicable to all nozzle/aftbodies with tails. Defined by the angular orientation of the tail relative to the vertical position.
22. Fore-and-aft Tail Location	- Applicable to all nozzle/aftbodies with tails. Defined by the location of the aft point of the tail/aftbody junction relative to the aftbody length ($X_{A10} - X_{A9}$)
23. Base Area	- Applicable to all nozzle/aftbodies with base area. Defined by the ratio of the base area, A_{BASE} to the aftbody reference area, A_{10}
24. Plug Half Angle	- Applicable to round plug nozzles. Defined as the half-angle of the plug centerbody measured relative to the plug axial centerline.
25. Ramp Half Angle	- Applicable to two-dimensional wedge nozzles. Defined by the wedge half-angle relative to the wedge centerline.
26. Aspect Ratio (W_g/H_g)	- Applicable to two-dimensional nozzles, both C-D and wedge types. Defined by the ratio of nozzle width to height at the nozzle exit station.
27. Divergence Half-Angle (θ_{DIV})	- Applicable to convergent-divergent round and 2-D nozzles. Defined as the angle of the diverging section nozzle wall relative to the axial centerline of the nozzle.

TABLE III INLET DERIVATIVE PROCEDURE CROSS-REFERENCE

DERIVATIVE PARAMETER		PROGRAM STEP						
		1	2	3	4	5	6	7
		A_{O2}/A_C	A_{O2LC}/A_C	A_O/A_C	P_{T2}/P_{T0}	C_D SPILL	C_{DBLC}	C_{DBYP}
1	ASPECT RATIO (FOR 2-D INLETS)	●	●	●	●	●	●	●
2	SIDEPLATE CUTBACK (FOR 2-D INLETS)	●	●	●	●	●	●	●
3	FIRST RAMP (CONE) ANGLE	●	●	●	●	●	●	●
4	DESIGN MACH NUMBER	●	●	●	●	●	●	●
5	COWL LIP BLUNTNES	●		●	●			●
6	TAKEOFF DOOR AREA	●		●	●			●
7	EXTERNAL COWL ANGLE					●		
8	EXIT NOZZLE TYPE FOR BLEED						●	
9	EXIT NOZZLE ANGLE FOR BLEED						●	
10	EXIT FLAP ASPECT RATIO FOR BLEED						●	
11	EXIT FLAP AREA FOR BLEED						●	
12	EXIT NOZZLE TYPE FOR BYPASS							●
13	EXIT NOZZLE ANGLE FOR BYPASS							●
14	EXIT FLAP ASPECT RATIO FOR BYPASS							●
15	EXIT FLAP AREA FOR BYPASS							●
16	SUBSONIC DIFFUSER AREA RATIO	●		●	●			●
17	SUBSONIC DIFFUSER TOTAL WALL ANGLE	●		●	●			●
18	SUBSONIC DIFFUSER LOSS COEFFICIENT	●		●	●			●
19	THROAT/CAPTURE AREA RATIO (FOR PITOT INLETS)	●		●				

TABLE IV NOZZLE/AFTBODY DERIVATIVE PROCEDURE REFERENCE LIST

DERIVATIVE PARAMETER	PROGRAM STEP	
	NOZZLE/AFTBODY DRAG CALCULATION	GROSS THRUST COEFFICIENT CALCULATION
AFT-END CLOSURE (INCLUDES EFFECT OF ASPECT RATIO, BOAT- TAIL ANGLE, TWIN NOZZLE SPACING	●	
RADIAL TAIL ORIENTATION	●	
FORE- AND -AFT TAIL LOCATION	●	
BASE AREA	●	
DIVERGENCE HALF- ANGLE (FOR AXI- SYMMETRIC AND 2-D C-D NOZZLES		●
AXISYMMETRIC PLUG HALF-ANGLE		●
ASPECT RATIO (FOR 2-D C-D AND 2-D WEDGE NOZZLES)		●
WEDGE HALF-ANGLE (FOR 2-D WEDGE NOZZLES)		●

4.2 DERIVATIVE PROCEDURE FOR INLETS

The use of inlet performance maps in mission analysis for preliminary design has simplified the task and provided for consistent, rapid results. The existing files of inlet performance maps do not cover all cases, however, and where the existing maps do not match the application, various approaches have been used to generate new maps. The user might modify the performance maps by hand to reflect changes, but no standard procedure is available, and the process would not be conducive to rapid response. Further, there would likely be a lack of consistency in map changes among many users. A common approach has been to use the maps as they exist and accept the possibility of reasonable errors.

A rapid process which would produce modified performance maps that reflect the variables of the installation being considered, would allow maximum utilization of the advantages of the map installation analysis. The concept of a derivative processor fits this requirement. It will produce a new set of performance maps, reflecting the effects of the new installation.

4.2.1 Concept

Since the primary application of the derivative procedure is preliminary design, the user will not have highly detailed information on the inlet design or operating schedules. The starting information will be the existing performance maps, and the derivative parameter values associated with those maps. All results will be anchored in the baseline map file. Thus, level of technology, complexity, and design philosophy are removed as variables in this process. Those variables are reflected in the map files available as baselines. Each map file then represents a class of inlets which reflect the sophistication, level of technology, design philosophy, and design trades present in the baseline inlet. Variation in these parameters is accomplished through selection of the baseline map file. It is important to note that the inlet data for the same design

generated by the derivative processor from dissimilar inlets in the data base will not have unique characteristics. Each derivative inlet will reflect the design of the baseline inlet.

4.2.2 Description

The derivative procedure is structured as an analytical technique as much as possible. Physically based analyses are used to relate parameter changes to the various performance map changes. The effects on all maps and map variables are included. The analyses and governing assumptions provide a procedure that is first order accurate or better. The approach is structured so that all map effects are included in seven consecutive steps that require no iteration between the various steps. In general for each step, those effects which relate to modified geometry are determined first at the existing design Mach number. Then the effect of design Mach number change is determined.

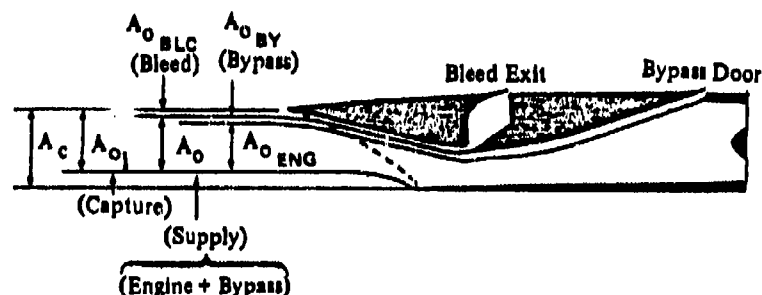
Three types of inlets are included:

1. Two-dimensional
2. Axisymmetric
3. Pitot

The two-dimensional and axisymmetric inlets are treated similarly, though a coneflow solution is required for axisymmetric inlets while wedge flow is used for two-dimensional inlets. These inlets are assumed to have a design Mach number greater than one. The pitot inlet is treated differently because it may have a design Mach number of any value, and the derivative procedure must handle a change from subsonic to supersonic and vice versa. As a result, no simple Mach number scaling is used. For two-dimensional and axisymmetric inlets, Mach number scaling is employed if the design Mach number is changed. This Mach number scaling is accomplished as follows:

If $M_o \leq 1.0$, $M_{o \text{ new}} = M_{o \text{ old}}$	} FOR BOTH MIXED AND EXTERNAL COMPRESSION INLETS
If $M_{o \text{ start old}} > M_{o \text{ design old}}$, $M_{o \text{ new}} = 1.0 + (M_{o \text{ old}} - 1.0) \frac{(M_{o \text{ design new}} - 1.0)}{(M_{o \text{ design old}} - 1.0)}$	
If $M_{o \text{ start old}} < M_{o \text{ design old}}$, $M_{o \text{ start new}} = M_{o \text{ start old}}$	} MIXED COMPRESSION INLETS
for $1.0 \leq M_o \leq M_{o \text{ start}}$, (EXTERNAL COMPRESSION MODE) $M_{o \text{ new}} = M_{o \text{ old}}$	
for $M_{o \text{ new}} > M_{o \text{ start}}$, (MIXED COMPRESSION MODE) $M_{o \text{ new}} = M_{o \text{ start}} + (M_{o \text{ old}} - M_{o \text{ start}}) \frac{(M_{o \text{ design new}} - M_{o \text{ start}})}{(M_{o \text{ design old}} - M_{o \text{ start}})}$	

The starting Mach number is unchanged for mixed compression inlets. The range of starting Mach number is relatively small, and does not vary directly with design Mach number. The assumption of fixed starting Mach number is at least first-order accurate. The terminology for the various inlet flows is illustrated below.



4.2.2.1 Step 1. New Inlet Capture

The first thing done is to establish the matched capture for the existing inlet:

$$(A_{o1}/A_c)_{2CT} = (A_o/A_c)_{2C} + (A_{oBLC}/A_c)_{6B}$$

The remainder of this step will deal with this matched capture. For pitot inlets the existing capture is multiplied by the ratio, new-to-old, of throat-to-capture area ratio. Then if the new design Mach number is less than the old, the table is simply truncated. If the new design Mach number is greater than the old, the matched capture is extended past the previous maximum Mach number using the relation

$$(A_{o1}/A_c)_{M_{o\text{ new}}} = (A_{o1}/A_c)_{M_{o\text{ max old}}} \times \frac{(A/A^*)_{M_{o\text{ new}}}}{(A/A^*)_{M_{o\text{ max old}}}} \frac{(P_{T2}/P_{T1})_{M_{o\text{ new}} \text{ NORMAL SHOCK}}}{(P_{T2}/P_{T1})_{M_{o\text{ max old}} \text{ NORMAL SHOCK}}}$$

which assumes a fixed throat area and throat Mach number represented by the previous highest Mach Number.

For two-dimensional inlets, the Petersen-Tamplin analysis (Reference 10) is used, for $M_o > 1.0$, to determine the effects of geometry changes with the existing design Mach number. This analysis, for single ramp inlets, includes the effect of aspect ratio, ramp angle, and side plate shape, and includes side spillage effects. It is assumed that ramp scheduling will be similar enough between the old and new geometries that the variation in capture will be represented by the relative variations in capture for single ramp inlets. To dimensionalize the inlet it is assumed that the ramp tip shock (old and new) is on the lip at the existing design Mach number. For this existing Mach number range, the maximum capture is determined from the analysis for the old and new geometry:

$$\left(\frac{A_{o1}}{A_c}\right)_{2CT_{new}} = \left(\frac{A_{o1}}{A_c}\right)_{2CT_{old}} \frac{\left(\frac{A_{o1}}{A_c}\right)_P - T_{new}}{\left(\frac{A_{o1}}{A_c}\right)_P - T_{old}}$$

For axisymmetric inlets, at $M_o > 1.0$, a cone flow solution is used for the old and new initial cone angle for Mach numbers up to the old design Mach number. The cone tip shock is assumed to be on lip at the old design Mach number. A translation schedule is determined ($f(M_o)$) for the old cone angle such that the maximum capture is the matched capture determined previously. The new cone angle uses the same translation schedule to determine the new capture.

For all three types of inlets, at $M_o \leq 1.0$, the effects on capture of cowl lip bluntness, takeoff door area, and subsonic diffuser modifications are determined. For cowl lip bluntness and takeoff door area the ratio of inlet airflows is equal to the ratio of effective throat areas. For the subsonic diffuser the compressor face Mach number is assumed fixed so that diffuser recovery affects capture directly ($M_{Th} < 1.0$).

Then for two-dimensional or axisymmetric inlets if the design Mach number is changed, the inlet capture is adjusted. If the design Mach number is increased the design (minimum) throat area goes down (and vice versa). Since geometric variation is limited, the maximum throat size will be changed accordingly. It is assumed that the inlet mass flow ratio at the design Mach number is the same (new and old) while at Mach 1.0

$$\left(\frac{A_{o1}}{A_c}\right)_{new} = \left(\frac{A_{o1}}{A_c}\right)_{old} \times \frac{(M_o \text{ design})_{old}}{(M_o \text{ design})_{new}}$$

This relationship has been shown to be generally valid for several axisymmetric inlets (References 11, 12, 13), but may be conservative for two-dimensional inlets.

4.2.2.2 Step 2. New Inlet Bleed

Pitot inlets are assumed generally to have no bleed, since present examples are unbled. However, in anticipation of a pitot inlet with bleed, the bleed rate tables are simply passed from the old file to the new file. No other approach would be well-founded since system characteristics are as yet undefined.

Two-dimensional and axisymmetric inlets have the effect of design change on bleed rates determined similarly, except that two-dimensional inlets can have a wetted area ratio change with fixed initial ramp angle, due to changes in aspect ratio and/or sideplate area, that axisymmetric inlets do not have. For two-dimensional inlets the bleed rates are multiplied by the ratio (new-to-old) of wetted areas.

The inlet design point, (specified in terms of design Mach number and geometric variables) is assumed to be the critical sizing point for the bleed system. It may be that some off-design condition caused a modification in the system, but that will be reflected in the design point bleed for the existing inlet. There are two criteria which may be generally used to determine the relative amount of boundary layer control: (1) the adverse gradient the boundary layer must traverse and (2) the Reynolds number. The adverse gradient is the dominant effect. Oblique shock reflection results indicate that the allowable pressure ratio divided by the upstream Mach number is a reasonable measure of the likelihood of separation (Reference 14) in the range of interest. Using this as a basis, and assuming a fixed downstream Mach number (throat or compressor face) and neglecting the secondary effects of recovery, the following expression may be derived (remembering that it is the surface pressure gradient the boundary layer must undergo):

$$\left[\left(\frac{A_{o \text{ BLC}}}{A_c} \right)_{\text{new}} \right] M_{o \text{ new}} = \left[\left(\frac{A_{o \text{ BLC}}}{A_o} \right)_{\text{old}} \right] M_{o \text{ old}} \cdot \left[\frac{\left(\frac{P_{\text{surface}}}{P_T} \right)_{M_{\text{surface}} @ M_{o \text{ design old}}} \cdot (M_{\text{surface}})_{M_{o \text{ design old}}}}{\left(\frac{P_{\text{surface}}}{P_T} \right)_{M_{\text{surface}} @ M_{o \text{ design new}}} \cdot (M_{\text{surface}})_{M_{o \text{ design new}}}} \right]$$

This expression works reasonably well when applied to existing inlets. Note that the pressure gradient term is affected by initial ramp or cone angle and design Mach number. The surface condition is obtained from simple wedge flow for two-dimensional inlets, and from cone flow for axisymmetric inlets. The results improve if this expression is multiplied (on the right-hand side) by

$$\left[\frac{\left(\frac{Re/ft/P_{T_o}}{M_{o \text{ design new}}} \right)}{\left(\frac{Re/ft/P_{T_o}}{M_{o \text{ design old}}} \right)} \right]^{1/7}$$

where the $Re/ft/P_{T_o}$ values come from Chart 25 of Reference 15, using the $T = 100^\circ\text{F}$ curve. This last step accounts for the Reynolds number change with Mach number.

It was determined that the expression discussed above provided excellent prediction of forward bleed in mixed compression inlets. This is quite reasonable since it implies that the bleed rate will go up or down with pressure ratio divided by initial surface Mach number to provide a constant throat entry condition.

It was found on further examination that terminal shock bleed (throat bleed for mixed compression or total bleed for external compression) scaled as

$$\left(\frac{A_{o \text{ BLC}}}{A_c} \right)_{\text{new}} = \left(\frac{A_{o \text{ BLC}}}{A_c} \right)_{\text{old}} \cdot \frac{(A/A^*)_{M_{\text{surface new}}}}{(A/A^*)_{M_{\text{surface old}}}} \cdot \left[\frac{\left(\frac{Re/ft/P_{T_o}}{M_{o \text{ design new}}} \right)}{\left(\frac{Re/ft/P_{T_o}}{M_{o \text{ design old}}} \right)} \right]^{1/7}$$

The bleed rate split for mixed compression inlets was based on the mixed compression inlet design guidelines of Reference 16, where it is assumed that forward bleed equals throat blockage, and throat bleed is 2/3 of throat blockage. This translates to

$$(A_{o_BLC}/A_c)_{\text{forward}} = \frac{A_{o_BLC}/A_c}{1.67}$$

and, as demonstrated in the Appendix, this bleed splitting provides excellent results.

It is assumed that for all inlets the variation in bleed rate with inlet supply is a variation in terminal shock bleed alone.

4.2.2.3 Step 3. New Engine Supply

Engine capture is inlet supply minus inlet bleed. Since inlet capture and inlet bleed have been determined for the new inlet in an independent manner, the resultant inlet supply does not simply scale by a shift. In fact non-linear scaling of inlet supply may well result.

$$(A_o/A_c)_{\text{new}}^{2A} = \left[(A_o/A_c)_{\text{old}}^{2A} + (A_{o_BLC}/A_c)_{\text{old}}^{6A} \right] \cdot \left[\frac{(A_{o1}/A_c)_{\text{new}}}{(A_{o1}/A_c)_{\text{old}}} \right] - (A_{o_BLC}/A_c)_{\text{new}}^{6AT}$$

An equivalency of supply, new-to-old, as a function of M_o is determined in this step so that all old tables with supply axes may be rescaled to new supply values.

4.2.2.4 Step 4. New Inlet Recovery

In this step the matched recovery will be modified, and the recovery variation with supply will simply be shifted by the same amount as the matched recovery.

For all Mach numbers less than or equal to 1.0 the ratio of new to old recovery is determined for cowl lip bluntness, takeoff door area, and subsonic diffuser changes. The existing recovery in this Mach number range is multiplied by these recovery ratios (new-to-old) to determine the new recovery. For pitot inlets this correction is applied at all existing Mach numbers.

New effective terminal shock Mach numbers are determined for two-dimensional and axisymmetric inlets at Mach numbers greater than 1.0 and less than or equal to the starting Mach number (external compression). The new values are calculated from the existing terminal shock Mach number and new and old inlet capture (prior to design Mach number change). The recovery difference for a normal shock at the old and new effective terminal shock Mach numbers is determined. The matched recovery is incremented by one-half this amount, since it is assumed ramp scheduling, or centerbody translation scheduling could be used to control this Mach number.

For two-dimensional and axisymmetric inlets at all Mach numbers greater than 1.0 the increment in initial ramp or cone shock recovery is determined for altered initial ramp or cone angle. Wedge flow is used for two-dimensional inlets and a cone flow solution for axisymmetric inlets. The matched recovery is incremented by one-half of the difference, assuming that altered inlet operation can be used to mitigate this effect.

For these same inlets and for this Mach number range the effects on recovery of subsonic diffuser geometry changes are determined for new and old geometries and the existing recovery is multiplied by the ratio new-to-old subsonic diffuser recoveries.

For two-dimensional and axisymmetric inlets, if the design Mach number is changed it is assumed that the loss coefficient $\frac{\Delta P_T / P_{T_0}}{q_0} = f(M_0)$ is still valid. Therefore the new recovery is simply

$$\left(\frac{P_{T2}}{P_{T0}}\right)_{\text{new}} = 1.0 - \left\{ \left[1.0 - \left(\frac{P_{T2}}{P_{T0}}\right)_{\text{old}} \right] \cdot \left(\frac{M_{0 \text{ new}}}{M_{0 \text{ old}}}\right)^2 \right\}$$

using Mach number equivalence. This is probably optimistic for external compression inlets with large design Mach number shifts, but has otherwise proven quite accurate (see the Appendix).

For pitot inlets if the design Mach number is reduced, the existing curve is simply truncated. If the design Mach number is increased the curve is extended by multiplying the recovery of the previous maximum Mach number by the ratio of the normal shock recovery at M_0 divided by the normal shock recovery at the previous maximum Mach number.

The recovery as a function of mass flow curves are simply shifted by the difference in matched recoveries at equivalent Mach numbers. For pitot inlets this involves duplicating the previous maximum Mach number curve and shifting it so that the matched point agrees with the new M_0 matched supply and recovery, or simply deleting some curves if design Mach number is decreased.

The buzz and distortion limit tables are assumed to be physically keyed to recovery, so at the same shift from the matched recovery as in the old inlet, at equivalent Mach numbers, a new inlet supply is determined and the new buzz and distortion limit tables result.

4.2.2.5 Step 5. New Spillage Drag

An inlet capture equivalence is determined

$$\left(\frac{A_0}{A_c}\right)_{\text{old \& new}} = \left(\frac{A_0}{A_c}\right)_{2A_{\text{old \& new}}} + \left(\frac{A_0}{A_c}\right)_{6A_{\text{old \& new}}}$$

using the point-to-point equivalence in Table 2A. This allows simple rescaling of all inlet capture axes, old-to-new.

Next an absolute drag level is established by adding the reference drag levels to the power sensitive drags.

$$C_{D_{JT}} = C_{D_J} + C_{D_{JA}}$$

The drag calculation for two-dimensional inlets is done with the Petersen-Tamplin analysis, which includes the effect of side spillage. The drag analyses in this program are based on momentum equations.

The drag calculation for axisymmetric inlets utilizes a cone flow solution, and the drag calculation procedures are equivalent to those in Petersen-Tamplin, except for side spillage, which has no axisymmetric counterpart.

The drag calculations for pitot inlets are equivalent to the subsonic and detached shock calculation procedures for two-dimensional and axisymmetric inlets, except that no external compression surface exists. Momentum balance equations are used with the upstream condition being freestream or behind a normal shock at freestream Mach number.

In general

$$C_{D_{new}} = C_{D_{old}} \cdot \left(\frac{C_{D_{calculated\ new}}}{C_{D_{calculated\ old}}} \right)$$

the new drag is determined as the old drag times the ratio (new-to-old) of calculated drags. The exception is for two-dimensional and axisymmetric inlets between Mach 1.0 and the starting Mach number where the ramp or cone tip shock is not detached. For those cases

$$C_{D_{new}} = C_{D_{max}} \cdot \left[\frac{C_{D_{max}} \frac{A_{o1}}{A_e}}{C_{D_{max}} \frac{A_{o1}}{A_e}} \right] + \left[(C_{D_{old}} - C_{D_{max}}) \cdot \left(\frac{\Delta C_{D_{calculate new N.S.}}}{\Delta C_{D_{calculate old N.S.}}} \right) \right]$$

the maximum capture drag is determined by multiplying by the ratio of calculated maximum capture drags, but the drag at reduced capture is determined incrementally from the maximum capture drag. This is because the drag increment is due to normal shock spillage, a different mechanism than the maximum capture drag, and the relative contributions in the old and new inlet may not be the same.

For two-dimensional inlets an equivalent single ramp angle as a function of M_0 is determined from the existing tip location to match the maximum inlet capture as a function of M_0 . The drag is calculated using these equivalent ramp angles.

For axisymmetric inlets the actual cone angle is used and the tip is translated to match the maximum capture. The drag is calculated using these translation schedules.

The effect of cowl external angle on spillage drag is included as a multiplier. The ratio of K_{ADD} has been determined empirically (References 1, 10) as a function of cowl external angle, and the updated drags are multiplied by the ratio of K_{ADD} values to determine the final drag.

Then for the specified reference mass flow in 3B, Table 3A is the 3B intercepts in 3T. Table 3 is 3T - 3A.

4.2.2.6 Step 6. New Bleed Drag

The new drag is determined from the old at equivalent M_0 and $A_{o_{BLC}}/A_c$, making use of the point to point equivalency between Table 6A_{OLD} and Table 6A_{NEW}.

$$(C_{D_{BLC}})_{\text{new}} = (C_{D_{BLC}})_{\text{old}} \cdot \frac{(C_{D_{BLC}})_{\text{new calculate}}}{(C_{D_{BLC}})_{\text{old calculate}}}$$

The PITAP (Reference 1) plenum pressure data are used, with the high pressure and low pressure bleed mass flow splits as defined in Step 2 for $M_0 > M_{0 \text{ START}}$. For all other Mach numbers the high pressure curve is used. The calculated drag coefficients are determined from the flap drag and momentum drag procedures (Reference 1).

$$C_{D_{\text{CALC}}} = C_{D_{\text{FLAP}}} + C_{D_{\text{MOM}}}$$

4.2.2.7 Step 7. New Bypass Drag

This step is very similar to Step 6. The new bypass drag is determined from the old at equivalent M_0 and $A_{0_{\text{BYP}}}/A_C$ as

$$(C_{D_{\text{BYP}}})_{\text{new}} = (C_{D_{\text{BYP}}})_{\text{old}} \cdot \left[\frac{(C_{D_{\text{BYP}}})_{\text{calculate new}}}{(C_{D_{\text{BYP}}})_{\text{calculate old}}} \right]$$

using the flap and momentum drag procedures as above. The nozzle plenum pressure is the matched inlet recovery multiplied by the PITAP plenum pressure multiplier, which is a function of bypass flow (Reference 1).

4.3 NOZZLE/AFTBODY DERIVATIVE PROCEDURE

The nozzle/aftbody derivative procedure consists of two parts: (a) nozzle/aftbody drag ($C_{D_{AB}}$) calculation procedure and (b) nozzle internal performance (C_{FG}^{AB}) calculation procedure. Each of these calculation procedures is discussed separately in the subsections which follow.

The purpose of the nozzle/aftbody drag calculation derivative procedure is to provide a rapid first-order computerized calculation method for obtaining the incremental changes in drag due to changes in nozzle and afterbody geometric variables and nozzle static pressure ratio. The basic premise in the development of the nozzle/aftbody drag derivative procedure is that a set of baseline nozzle/aftbody configurations and their estimated (or measured) drag characteristics are available in PIPSI format. The format of the nozzle/aftbody drag maps is illustrated in Figure 20.

The derivative procedure provides a means for calculating the changes in drag that are caused by changes in certain geometric parameters. These geometric parameters are defined by the list of derivative parameters in Section 4.1. The nozzle/aftbody derivative parameters are summarized below.

- | | |
|------------------------------|-----------------------------------------------------------------------------------------------------|
| 1. Aft end area distribution | Includes the effects of rectangular nozzle aspect ratio, nozzle boattail angle, twin nozzle spacing |
| 2. Tail position | Includes the effects of radial tail orientation and longitudinal tail location |
| 3. Base area | |

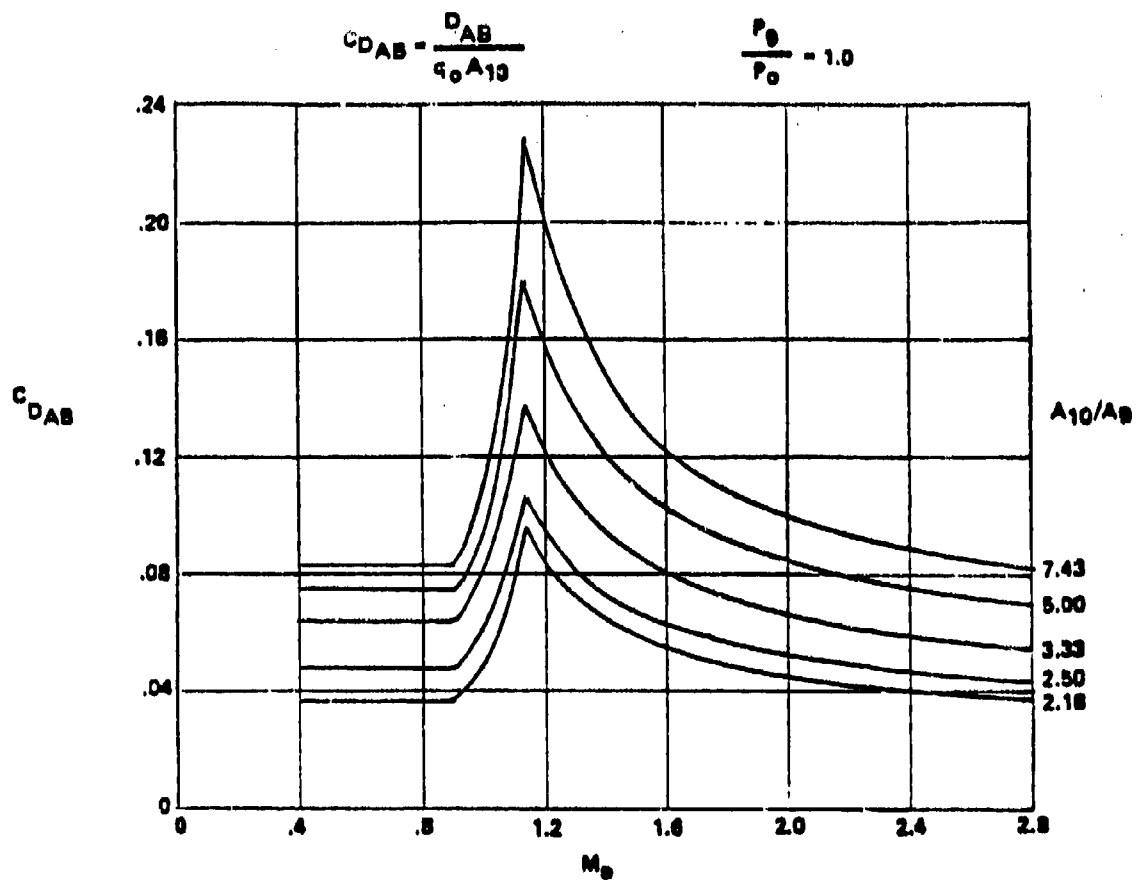


Figure 20. Nozzle/Aftbody Drag Map for Twin Round Nozzles

4.3.1 Drag Due to Aft End Area Distribution

The approach used to calculate the effects of changes in parameters which affect the aft-end area distribution is the truncated integral mean shape IMS_T method documented in References 17 and 18. This calculation procedure is summarized in Figure 21. The calculation of the IMS_T parameter requires that the nozzle/aftbody area distribution be determined as a function of several different nozzle positions ranging from minimum nozzle exit area (A_9) position to maximum nozzle exit area. A typical area distribution such as that required by the IMS_T procedure is shown in Figure 22. The calculated IMS_T parameter for a particular area distribution is used as input to data correlations of nozzle/aftbody drag as a function of IMS_T parameter and free-stream Mach number to obtain the nozzle/aftbody drag coefficient, $C_{D_{A10}}$. Examples of the drag data correlations are presented in Figures 23, 24, and 25.

The computer program is structured to have built-in drag correlation tables such as the data shown in Figures 23, 24, and 25. At the present time, only a limited amount of data has been found to provide the table look-up data required for all configurations. Until such time as better data are available, the same data will be used for 2-D wedge nozzles and 2-D C-D nozzles. Similarly, the only data correlations available for round plug nozzles are for twin round plug nozzles. These data correlations will also be used for single round plug nozzles until better data correlations are available. Twin round C-D nozzle drag correlations will likewise be used for single round C-D nozzles. The basic drag correlations are for a fully-expanded nozzle ($P_9/P_0 = 1.0$). The effects of nozzle exit static pressure ratio (other than 1.0) on drag are calculated using a drag correlation developed during the Exhaust System Interaction Program (Reference 18). This correlation is:

$$C_{D_{A10-A9}} = C_{D_{A10-A9}} \Big|_{@ P_9/P_0 = 1.0} + \left[4.5 e^{-M_0^2} \left(1 - \frac{P_9}{P_0}\right) \cdot \left(1.1 \frac{A_9}{A_8} - 1.0\right) \cdot \left(\frac{A_9}{A_{10}}\right)^{3/2} IMS_T \right]$$

$$\Delta C_D = \left(C_{D_{A10-A9}} \Big|_{@ P_9/P_0 = 1.0} \right) - \left(C_{D_{A10-A9}} \right)$$

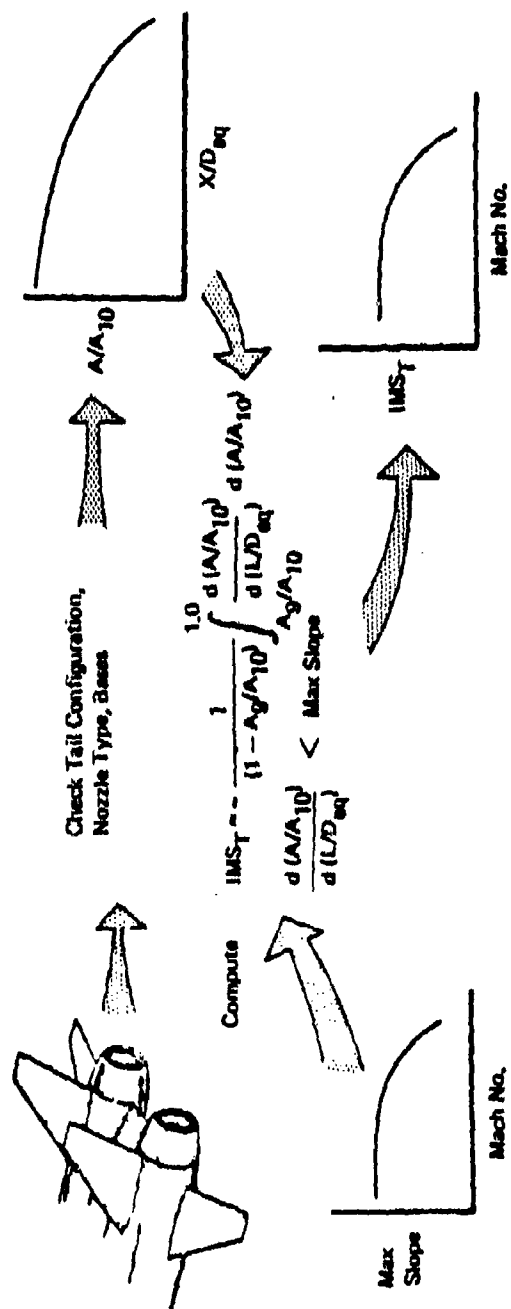


Figure 21. IMS_T Calculation Procedure

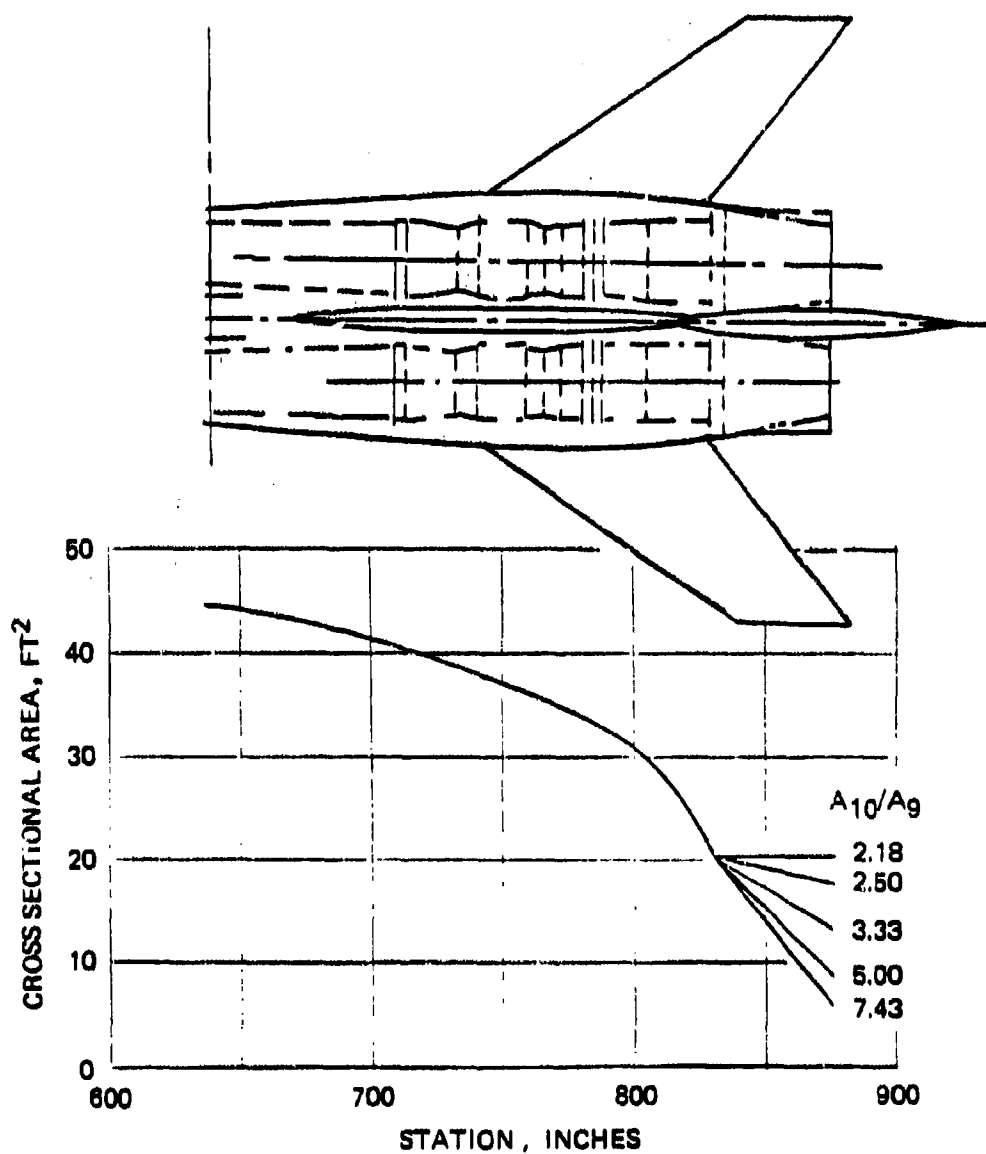


Figure 22. Nozzle/Aftbody Area Distribution for a Twin Round Nozzle Configuration

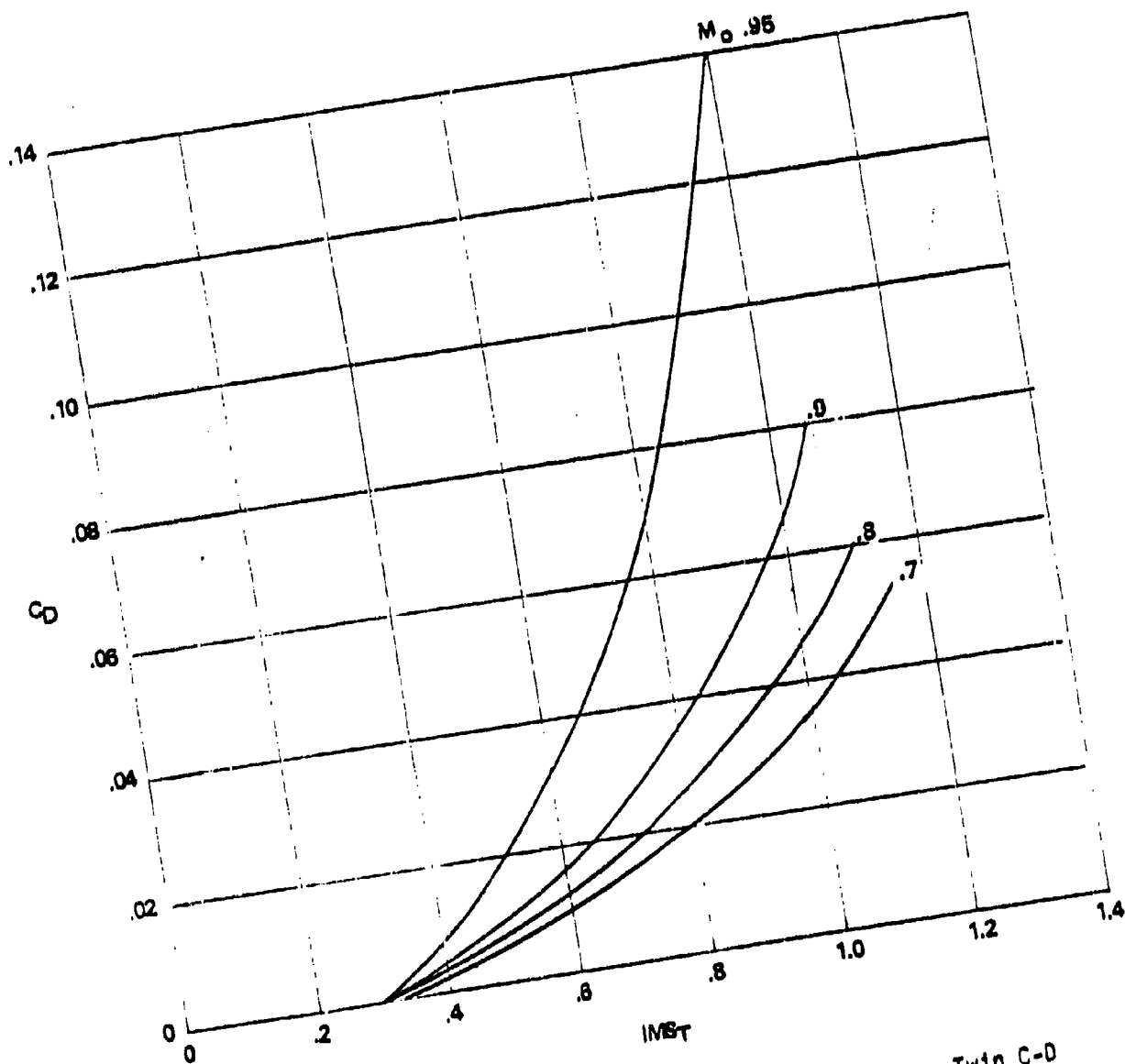


Figure 23. Nozzle/Aftbody Drag Correlations for a Twin C-D Axisymmetric Nozzle Configuration

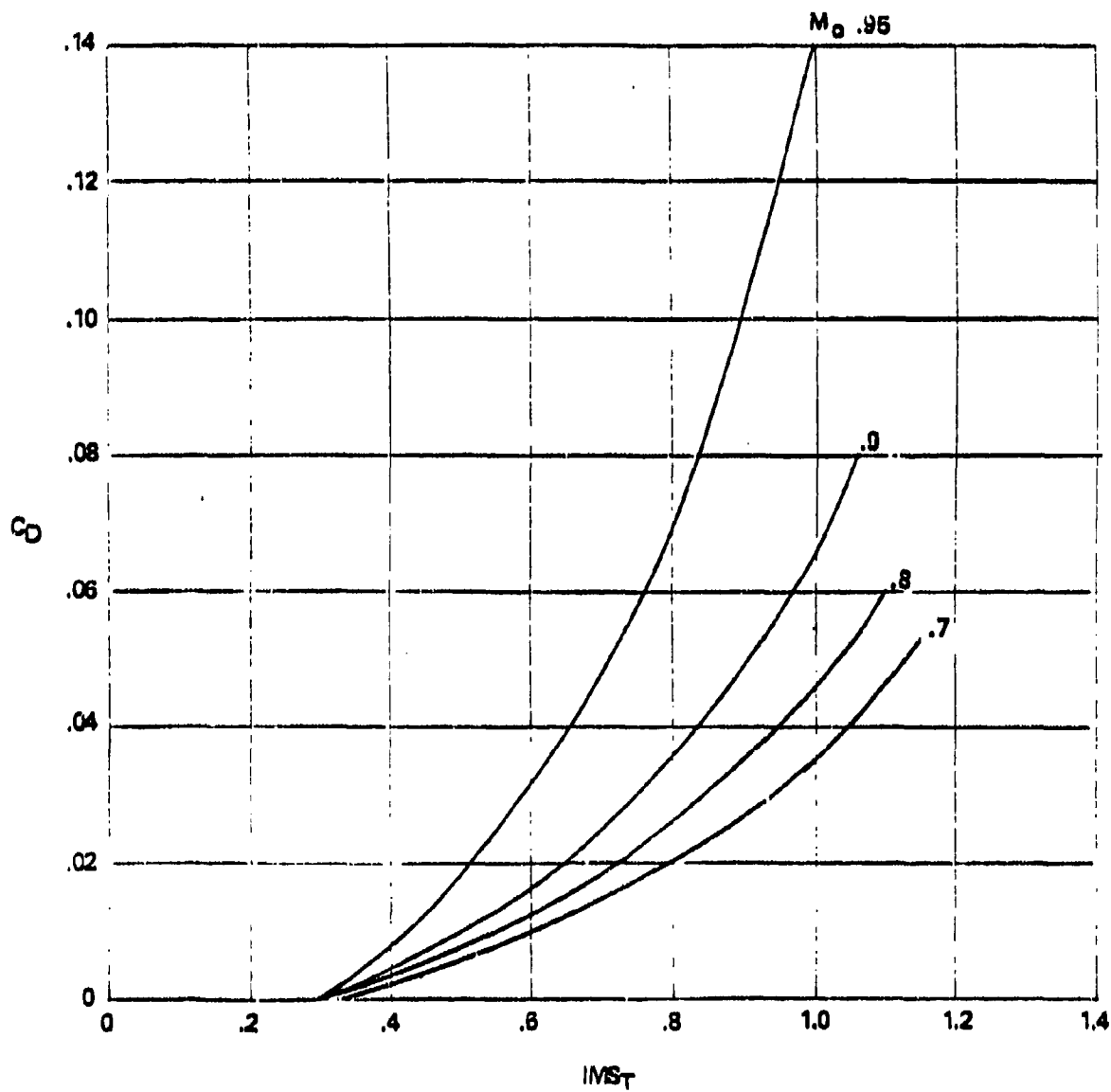


Figure 23. Nozzle/Aftbody Drag Correlations for a Twin C-D Axisymmetric Nozzle Configuration

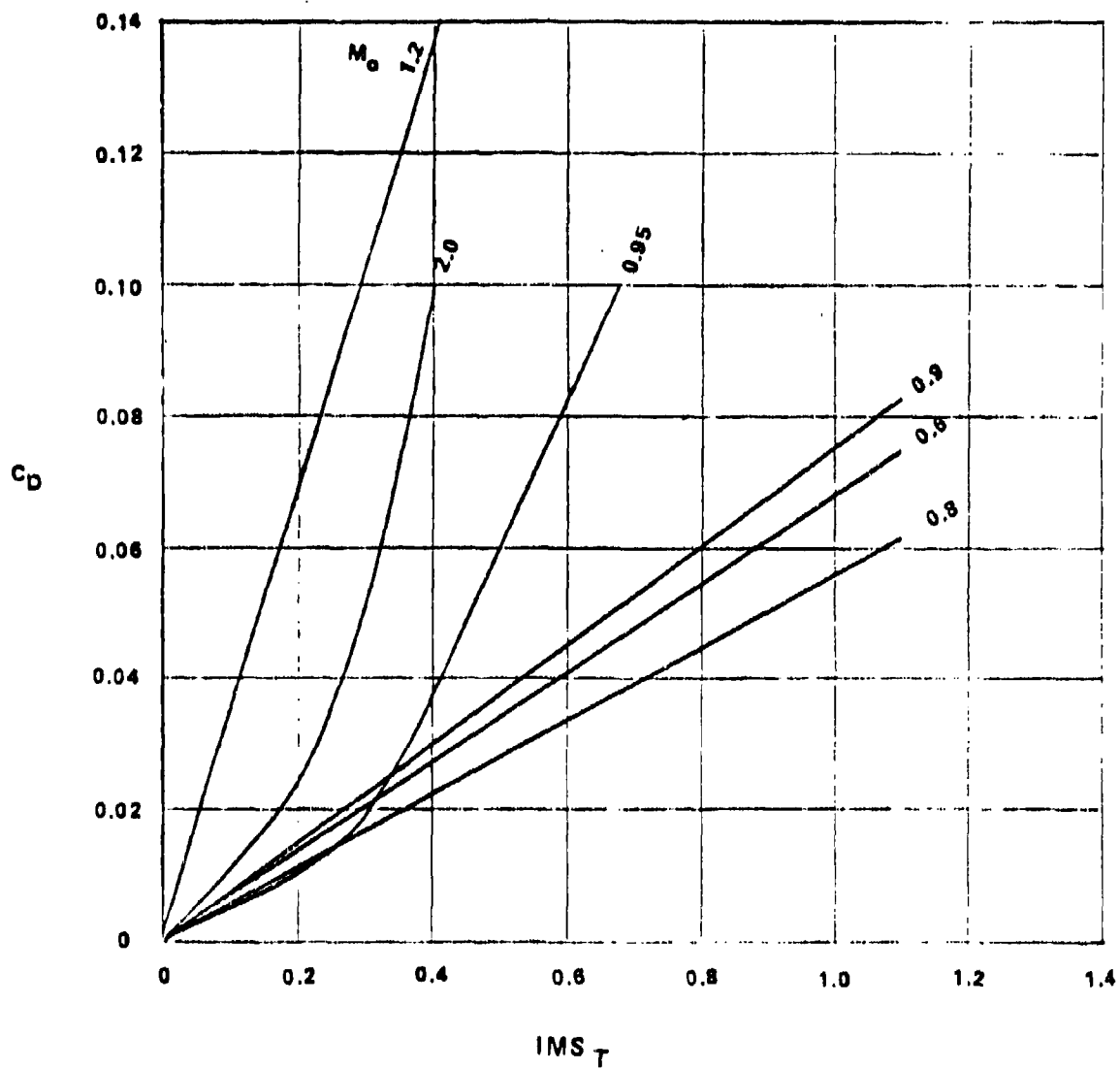


Figure 24. Nozzle/Aftbody Drag Correlations for Twin and Single 2-D Wedge Nozzle Configurations

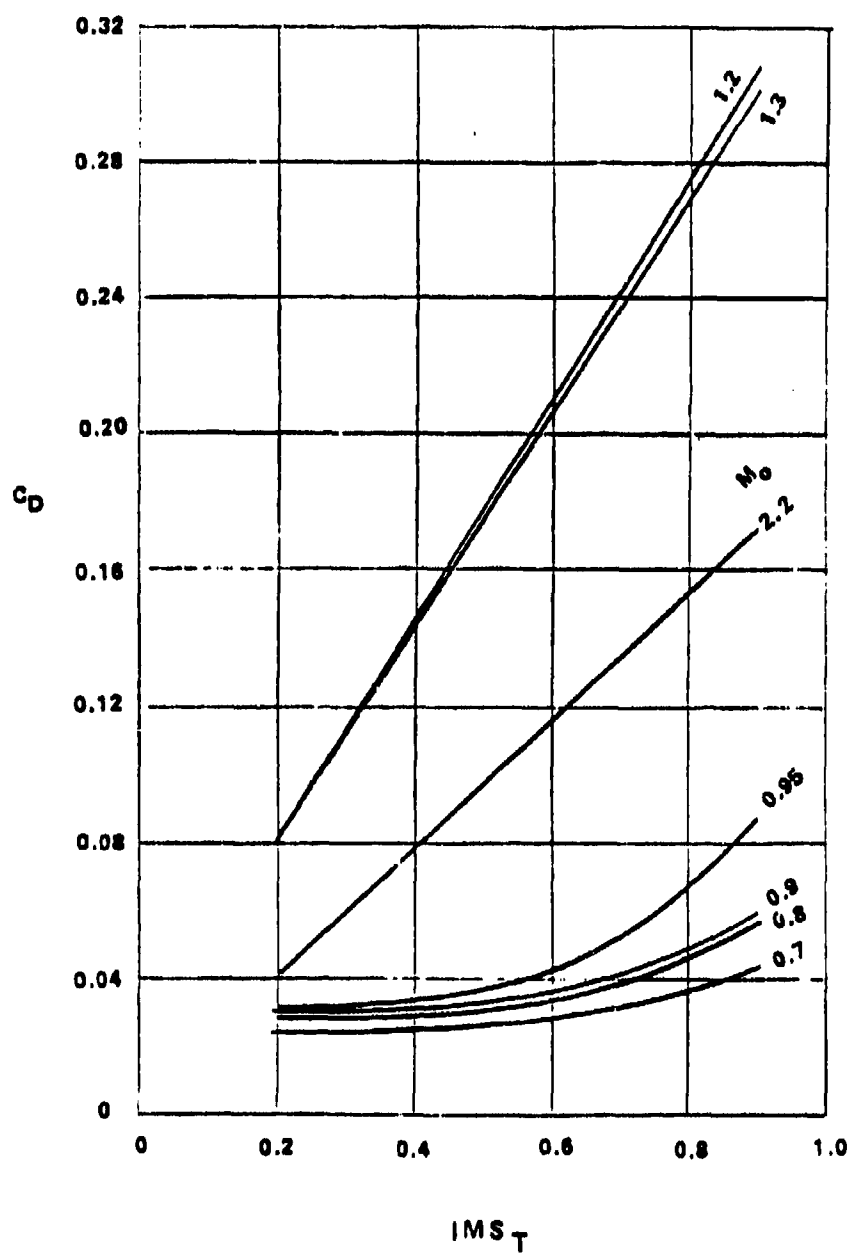


Figure 25. Pressure Drag Coefficient for Twin-Jet Axisymmetric Plug Nozzles

All the parameters required to calculate the above relation are readily available except A_9/A_8 . To obtain A_9/A_8 values, the user of the derivative procedure must input a variation of A_9/A_8 as a function of M_0 or the program will default to a typical area variation schedule. The typical area variation schedule built into the program is shown in Figure 26. Using the above equation, incremental changes in drag due to pressure ratio effects will be calculated and stored as tables that can be used as input for the PIPSI program. A flow chart that illustrates the steps in the above part of the drag calculation procedure is shown in Figure 27.

4.3.2 Drag Due to Tail Effects and Base Area

After the calculation of drag due to aft-end closure effects (previously described) drag increments are added to account for the radial orientation of tails, longitudinal location of tails and base drag. The program is structured to contain a table of incremental drag corrections (ΔC_{D_R}) as a function of free-stream Mach number, M_0 , and radial tail orientation angle, θ_R . However, due to the lack of experimental data to show the effect on drag of radial tail orientation, it has not been possible to construct a satisfactory correction table. Therefore, the table structure was coded to contain $\Delta C_{D_R} = 0$ for all Mach numbers and tail angles. When adequate data are available to construct a satisfactory table of corrections, the data can be entered in the computer program code. The format of the table is shown in Figure 28.

An incremental drag correction to account for the effects of fore-and-aft movement of the tail surfaces on aftbody drag has been developed from analysis of the data contained in Reference 19. These data were for single engine installations. Figure 29 shows the variation of $\Delta C_{D_{DAP}}$ as a function of the tail fore and aft location for a nozzle static pressure ratio, $P_9/P_0 = 1.0$. The computer program is structured to contain the incremental tail location drag data shown in Figure 29. If better data become available, the computer code can be changed to incorporate the data tables.

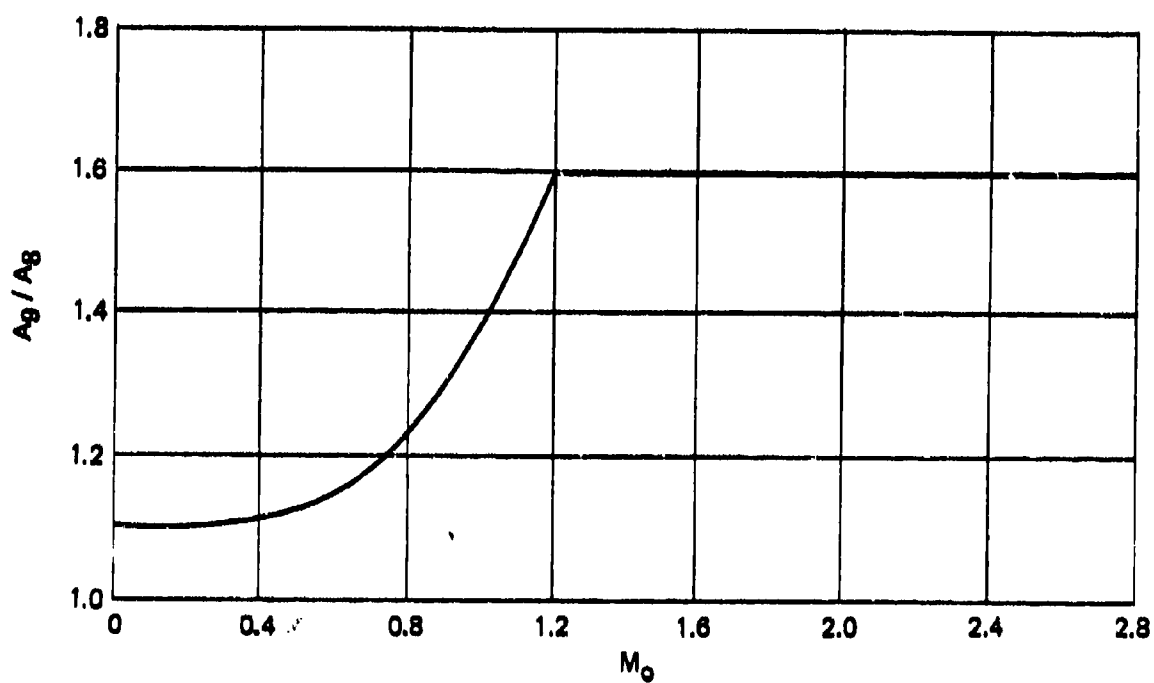


Figure 26. Default Nozzle Area Ratio Schedule

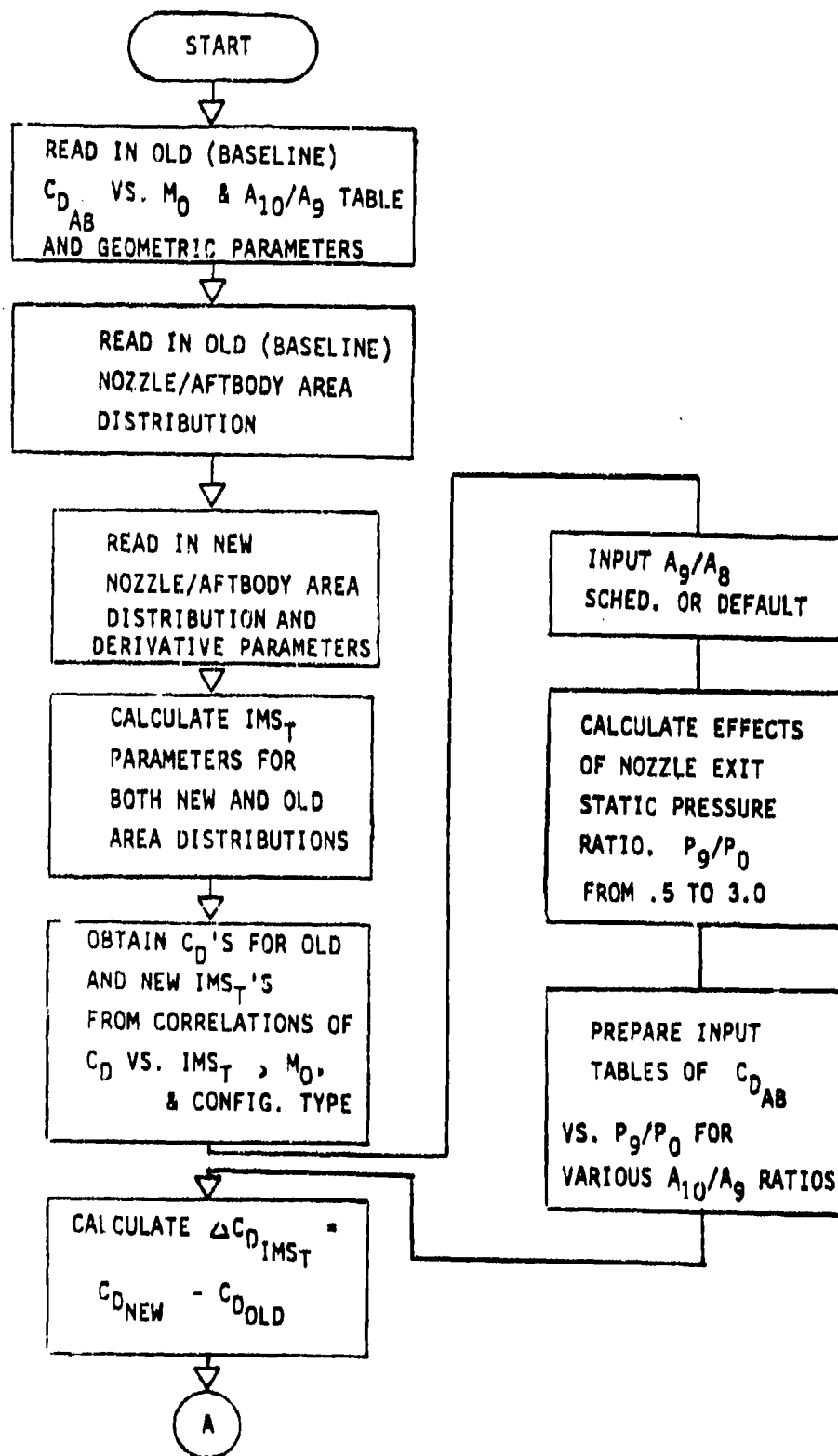
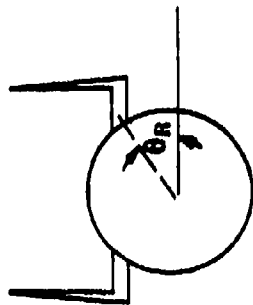


Figure 27. Nozzle/Aftbody Drag Derivative Procedure



NOTE: TO ILLUSTRATE DATA TABLE FORMAT ONLY

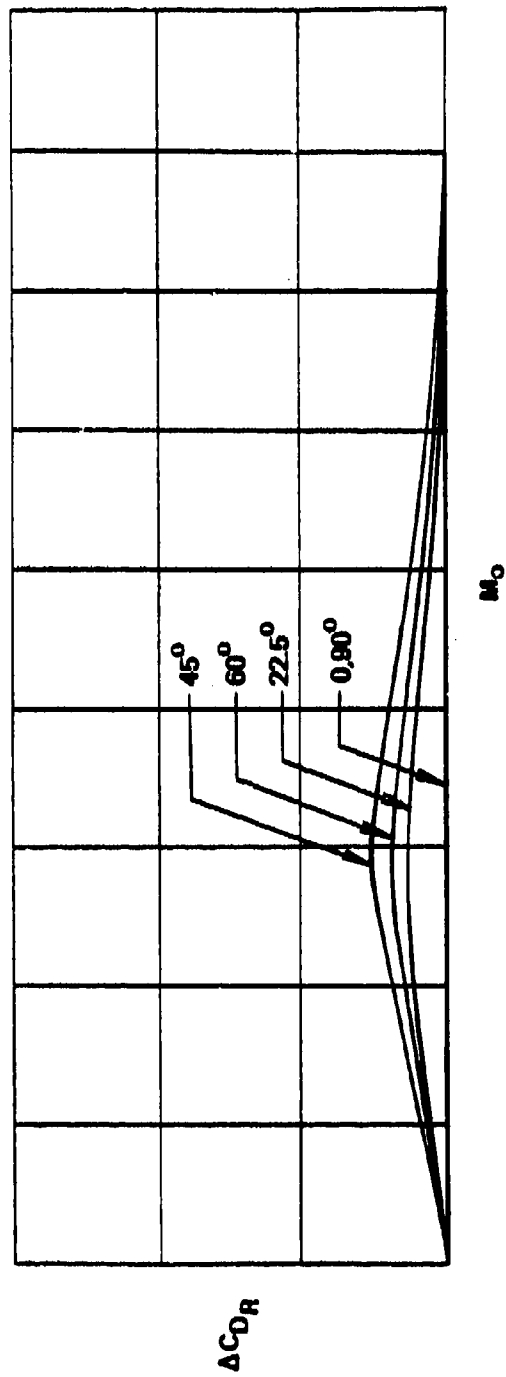


Figure 28. Correction for Radial Orientation of Tail

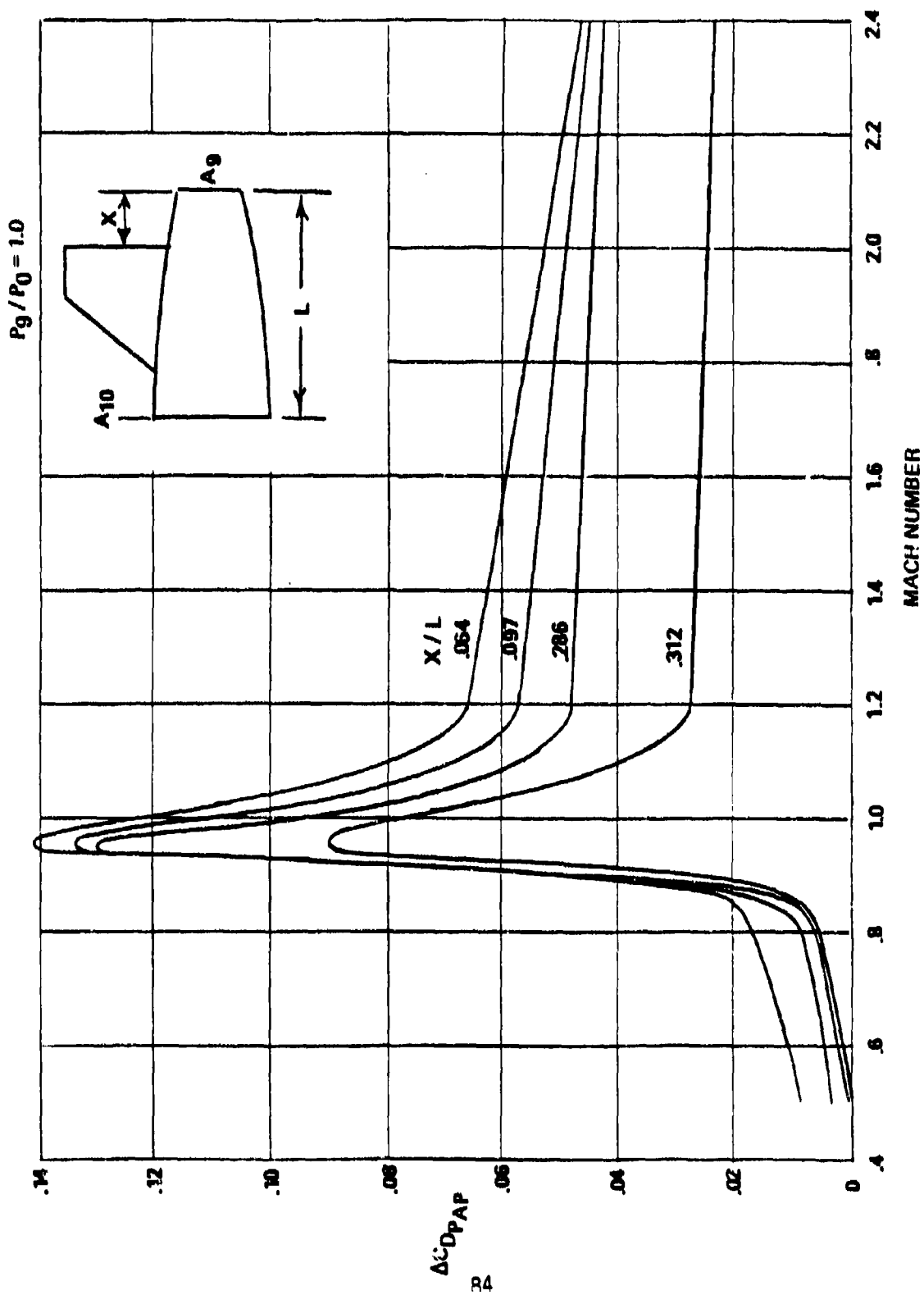


Figure 29. Incremental Drag Coefficient Due to Tail
Fore-and-Aft Location

The first-order effects of base area on drag are calculated by using input tables of base pressure coefficient as a function of free-stream Mach number, M_0 , and nozzle type (either axisymmetric or two-dimensional). The base pressure coefficient in the program is shown in Figure 30. Using the base pressure coefficient, C_{p_B} , and the base area ratios, the incremental base drag coefficient is calculated by the following relation:

$$\Delta C_{DB} = C_{p_B} \cdot [(A_{base}/A_{10})_{new} - (A_{base}/A_{10})_{old}]$$

A flow chart showing the main steps involved in the calculation of radial and longitudinal tail effects and base pressure drag increments is presented in Figure 31.

The total of the incremental changes in drag due to geometry are added and the resultant drag increment applied to the input drag map to obtain the new nozzle/aftbody drag map.

4.3.3 Nozzle Gross Thrust Coefficient Derivative Procedure

The calculation methods employed to determine the effects on nozzle gross thrust coefficient (C_F) of changes in nozzle geometric variables depend greatly on the type of nozzle being used. Separate calculation flow paths were constructed to handle each of the following nozzle types:

- (1) Axisymmetric Convergent-Divergent
- (2) Axisymmetric Plug
- (3) Two-Dimensional Convergent-Divergent
- (4) Two-Dimensional Plug (Wedge)

For all the above nozzle types, the approach used in developing the derivative procedure was to utilize as much as possible the data from experimental results, with theoretical calculations used where there were data voids or where it was necessary to calculate geometric relationships for typical trends of nozzle variations.

Doattail Angle = 0°
No Jet
No Fins

Ref: WADC T.N. 57-28

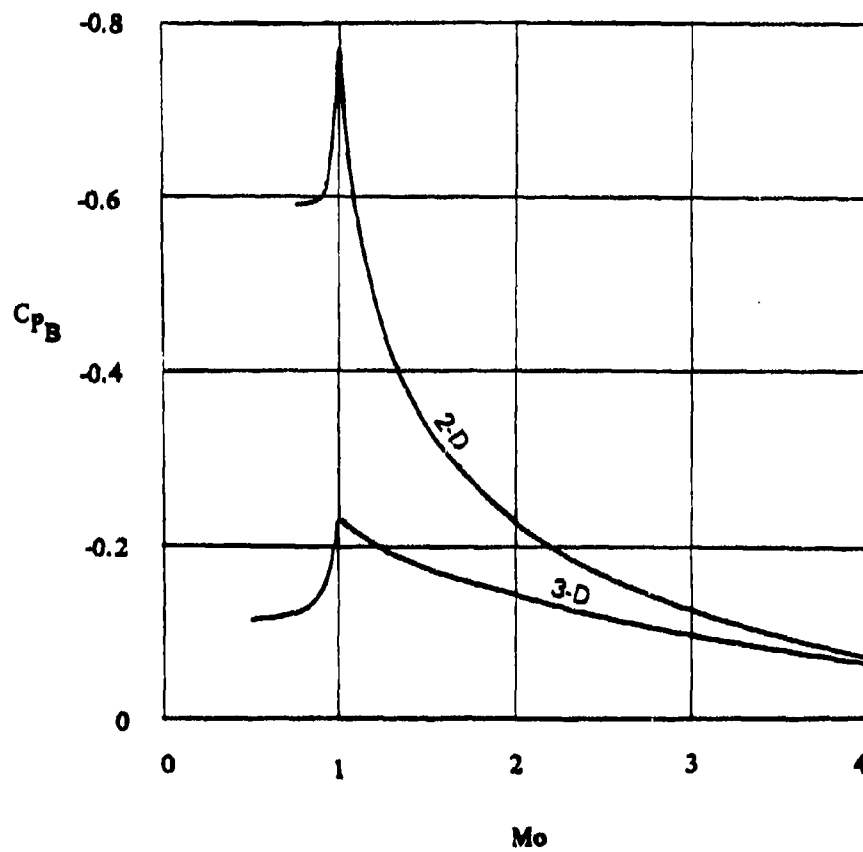


Figure 30. Base Pressure Coefficient

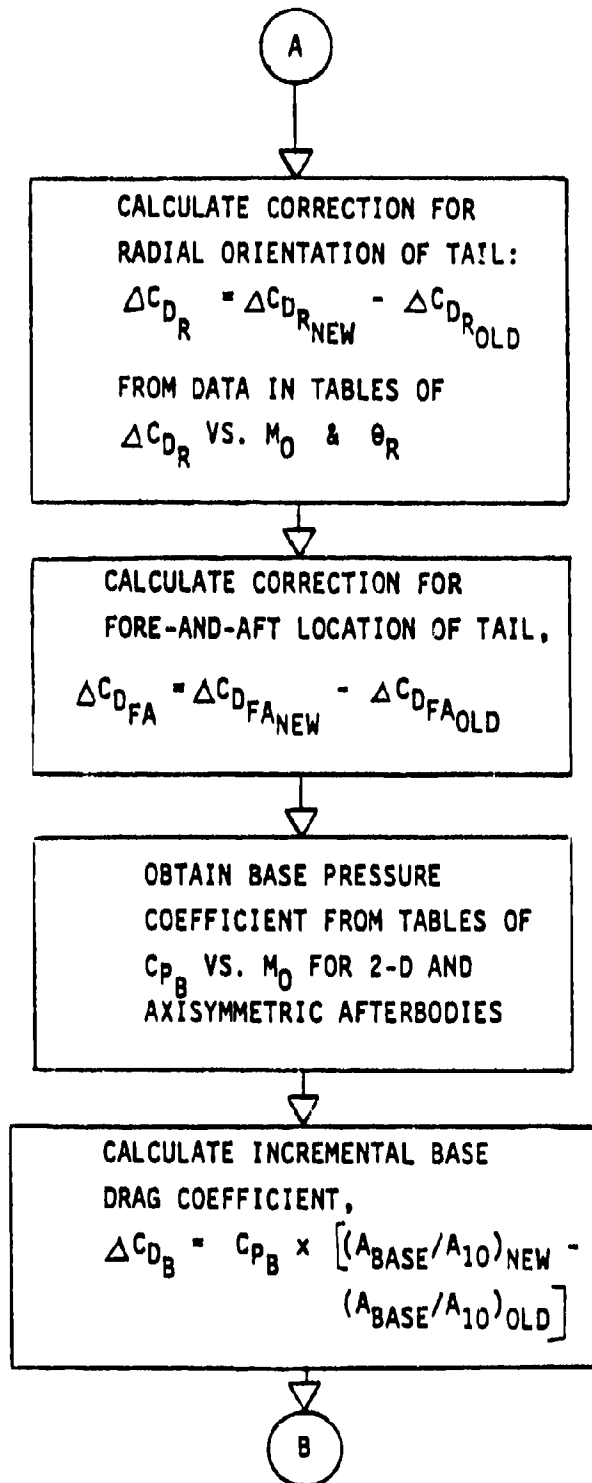


Figure 31. Flow Chart for Tail Effects and Base Drag Increments

The derivative parameters for each nozzle type are summarized in table V:

TABLE V
DERIVATIVE PARAMETERS FOR NOZZLE C_{FG} CALCULATION

<u>NOZZLE TYPE</u>	<u>DERIVATIVE PARAMETERS</u>	
AXI C-D	θ_{DIV}	DIVERGENCE HALF-ANGLE
AXI PLUG	θ_p	PLUG HALF-ANGLE
2-D C-D	W_g/H_g θ_{DIV}	ASPECT RATIO DIVERGENCE HALF-ANGLE
2-D WEDGE	W_g/H_g θ_N	ASPECT RATIO RAMP (WEDGE) HALF-ANGLE

The user of the derivative procedure has the options available to calculate the effect on the input C_F map of any of the derivative parameters shown in the right hand column of Table V. The methods and data used to calculate the effects of variations in each of the derivative parameters are described in the sections which follow.

4.3.4 Effect of Divergence Half-Angle on C_{FG} for a Round C-D Nozzle

The input map format for round C-D nozzles used by the PIPSI program is illustrated in Figure 32. This map provides C_{FG} as a function of nozzle pressure ratio, P_{T8}/P_0 , for various nozzle expansion ratios, A_9/A_8 . To provide a method whereby the effect of θ_{DIV} could be related to area ratio, a typical round C-D nozzle θ_{DIV} variation as a function of A_9/A_8 was examined. Based on the results of this examination the simplified variation shown in Figure 33 was adopted for programming into the procedure. With a knowledge of A_9/A_8 and

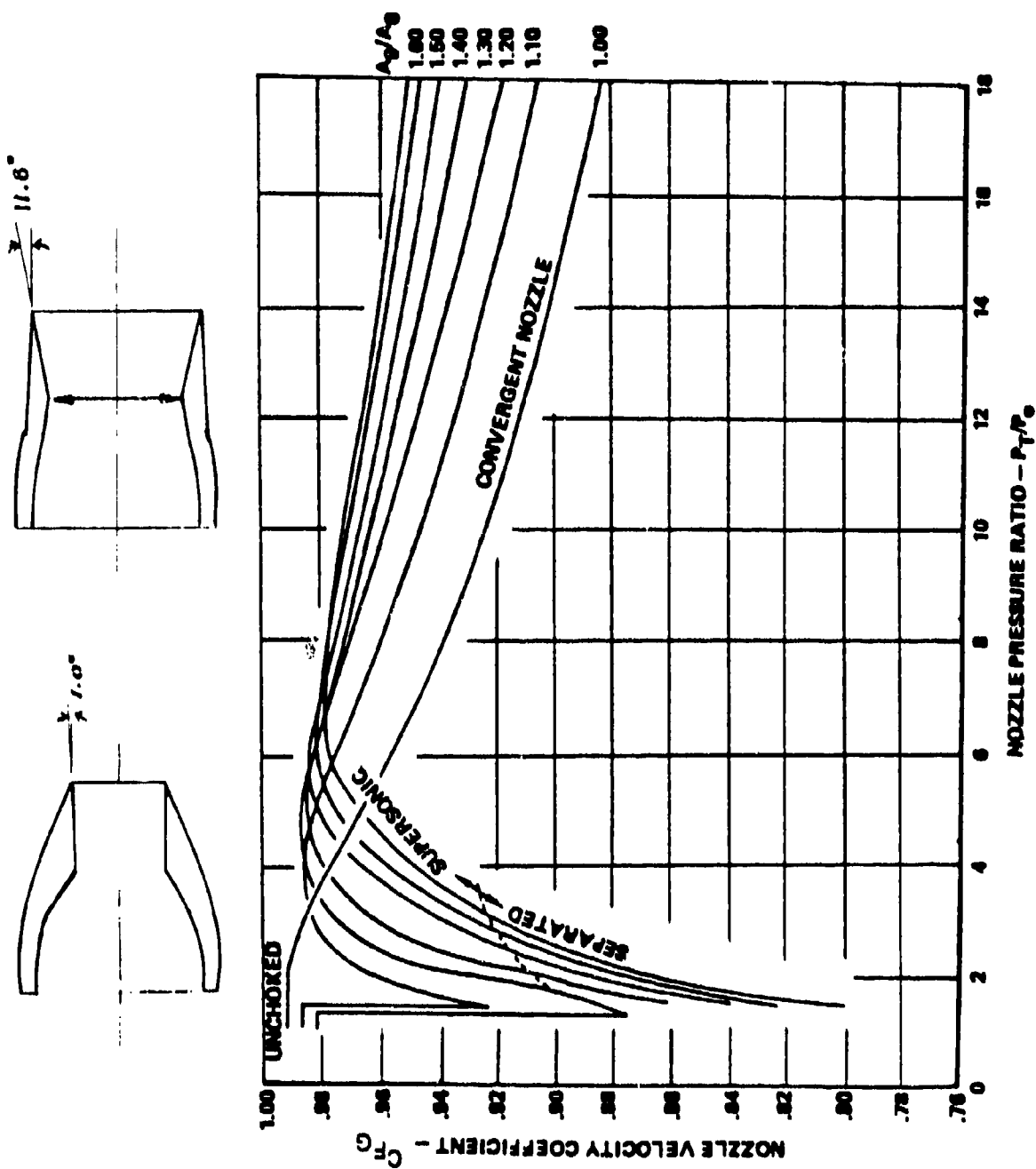


Figure 32. Gross Thrust Coefficient for a Round C-D Nozzle

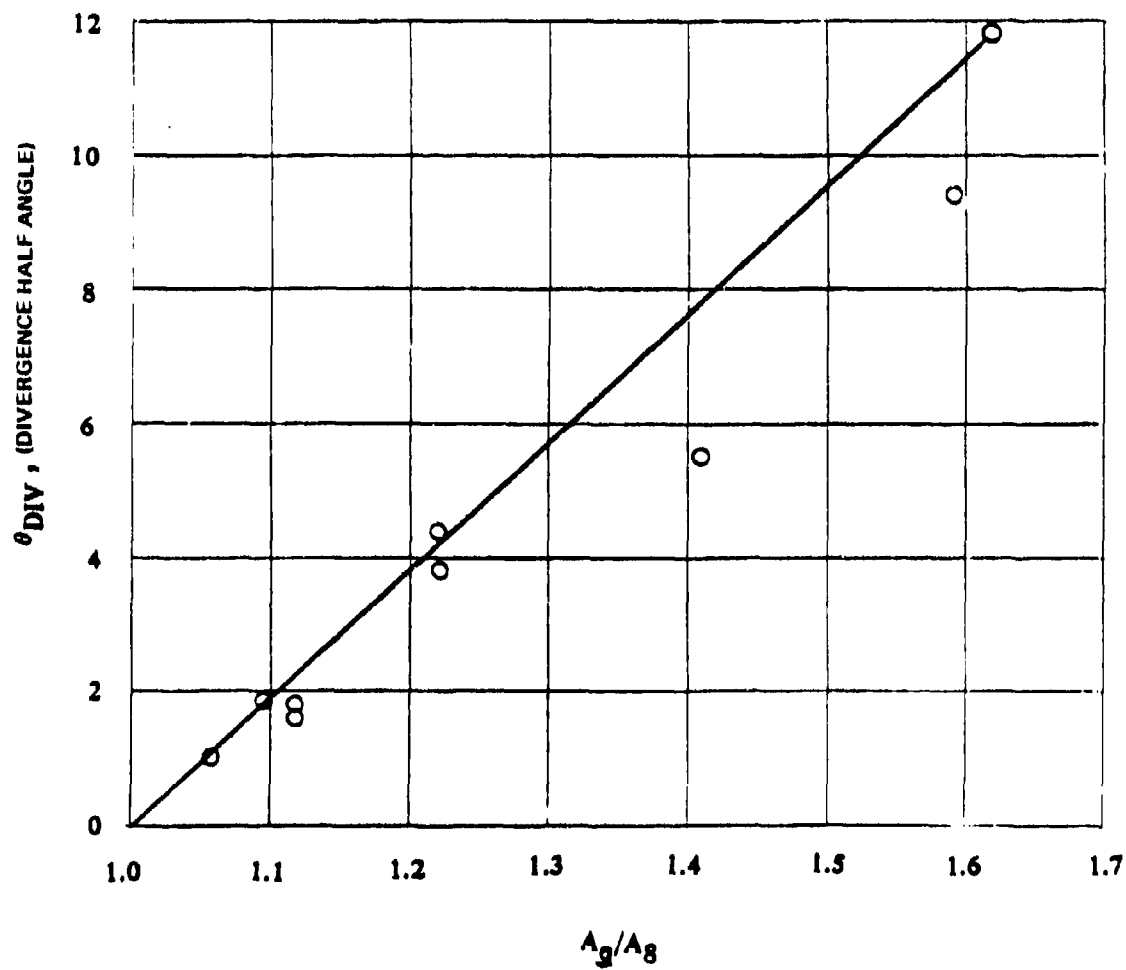


Figure 33. Divergence Angle/Area Ratio Relationship for a Round C-D Nozzle

θ_{DIV} , it is possible to determine the angularity loss, using the angularity loss coefficient data from Reference 1. These experimental data are shown in Figure 34.

4.3.5 Effect of Plug Half-Angle on C_{FG} for a Round Plug Nozzle

The input map format for an axisymmetric plug nozzle is shown in Figure 35. This format provides nozzle gross thrust coefficient, C_{FG} , as a function of nozzle pressure ratio P_{TB}/P_0 for various area ratios, A_9/A_8 . To obtain the relationship of A_9/A_8 and plug half angle, a two-dimensional table look-up set of data was prepared that represents the geometric relationships between lip angle, α plug half angle, θ_p , and area ratio, A_9/A_8 , for a typical plug nozzle configuration. These data, presented in Figure 36, is programmed into the code to provide inputs necessary to calculate the parameter $(\alpha - \theta_p)$. The parameter $(\alpha - \theta_p)$ is then used to enter Figure 37 to obtain the plug nozzle performance loss. Figure 37 documented in Reference 1, is based on experimental data.

4.3.6 Effect of Aspect Ratio and Divergence Half-Angle on C_{FG} for a Two-Dimensional Convergent-Divergent Nozzle

The methods used in developing the computer code for the 2-D C-D nozzle internal performance calculations are based primarily on the experimental data gathered during the AFAPL Installed Turbine Engine Survivability Criteria contract documented in Reference 20. These tests provided data on a variety of 2-D nozzles of various aspect ratios and divergence angles.

The input map format for the 2-D C-D nozzle C_{FG} is shown in Figure 38. This format provides nozzle C_{FG} as a function of pressure ratio and nozzle jet area. Two jet area schedules are provided, minimum jet area and maximum jet area, corresponding to the experimental configurations tested. An optimum schedule of area ratio is used for each of the

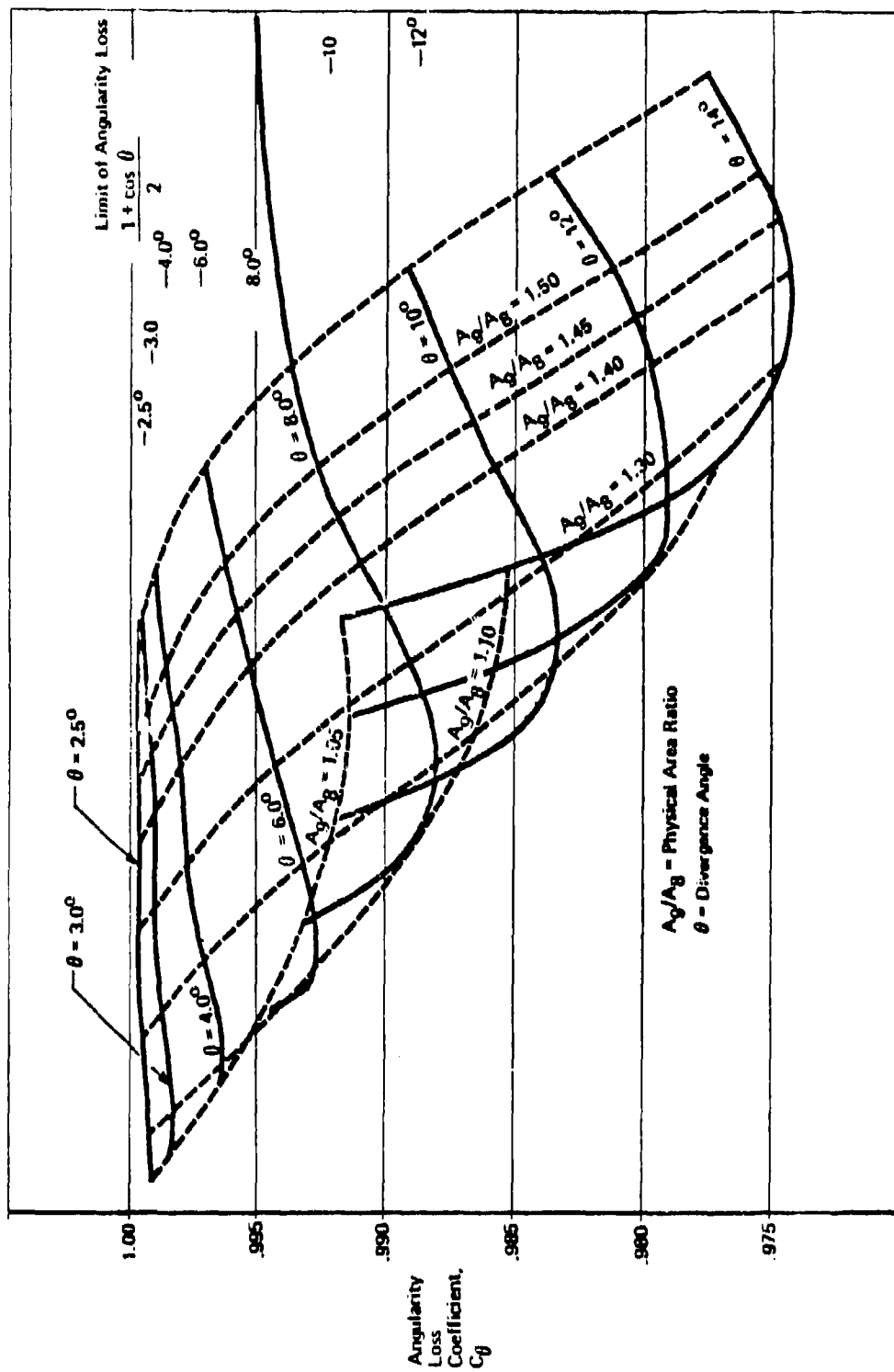


Figure 34. Angularity Loss Coefficient for Convergent-Divergent Nozzles

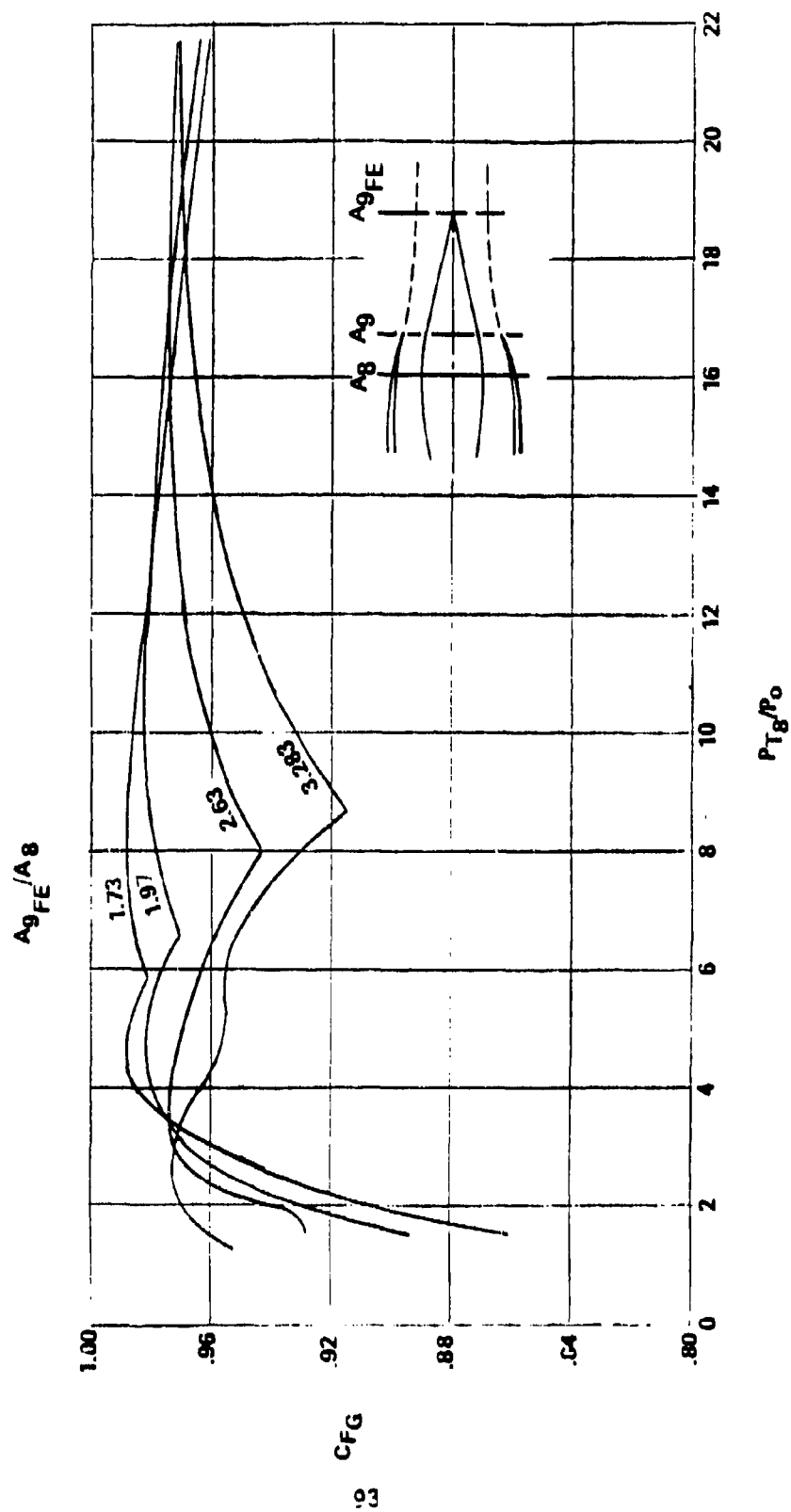


Figure 35. Gross Thrust Coefficient for Axisymmetric Plug Nozzles

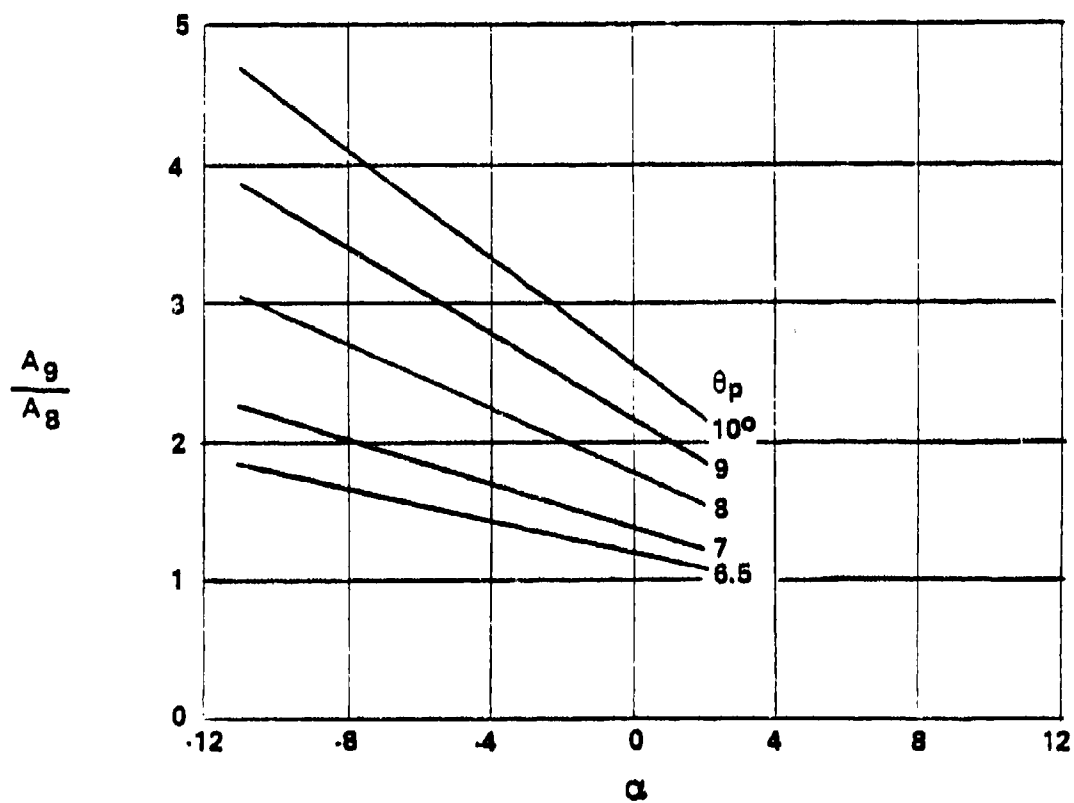


Figure 36. Internal Area Variation for a Round Plug Nozzle

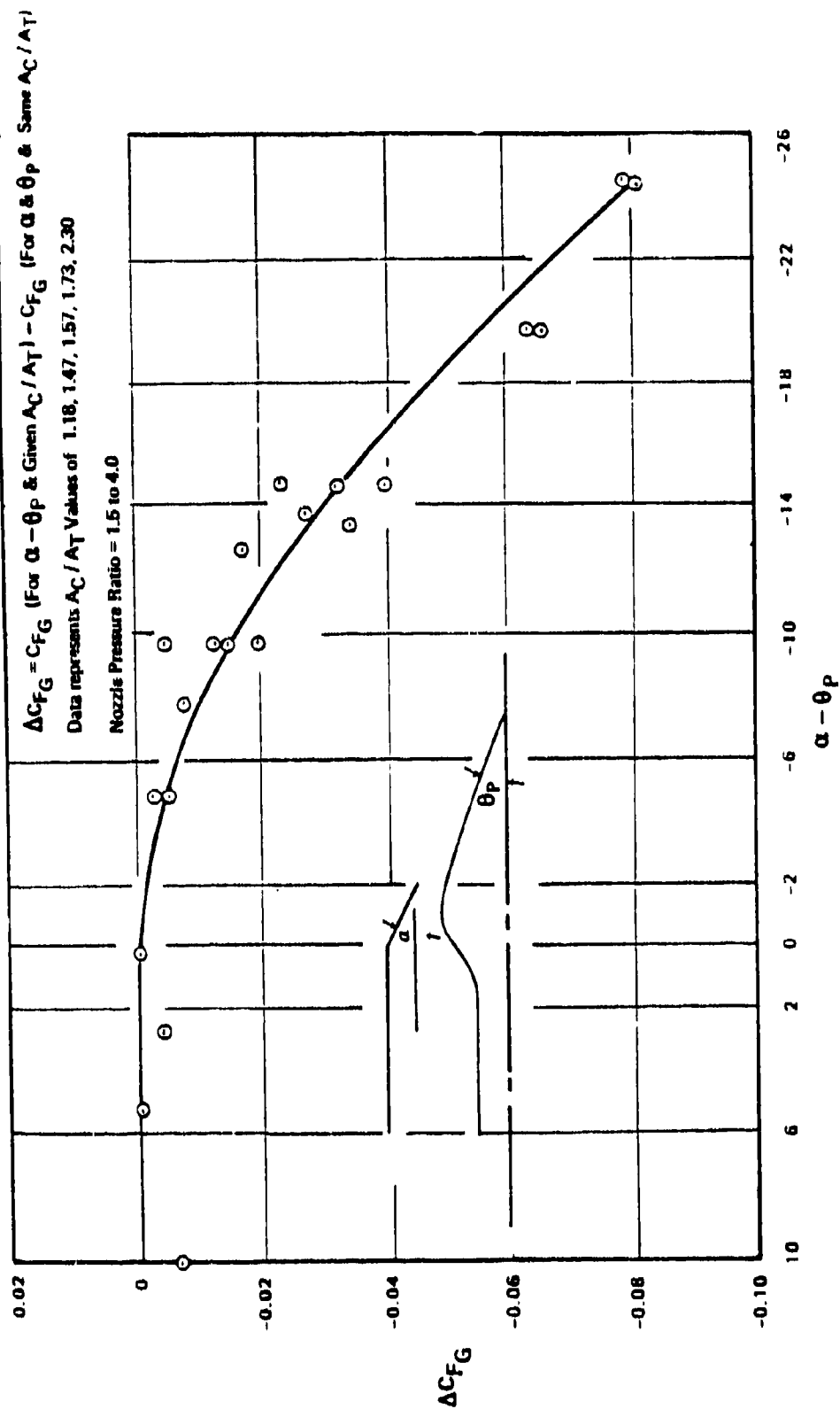


Figure 37. Performance Loss Due to Difference Between Cowl Angle and Plug Angle

jet area settings. This area ratio schedule is presented in Figure 39. The area ratio schedule is truncated at a maximum area ratio of 1.60, corresponding to the maximum area ratio used in the tests. A divergence angle schedule was also obtained from the test configurations, as shown in Figure 40. With the geometric relationships provided by the previous A_9/A_8 and θ_{DIV} schedules, the necessary input parameters are available to obtain $C_{F_G^{PEAK}}$ as a function of A_9/A_8 and θ_{DIV} from the correlation of experimental data presented in Figure 41. The $C_{F_G^{PEAK}}$ values for old and new configurations provide the data needed to obtain the ΔC_{F_G} resulting from the geometric change in θ_{DIV} .

The experimental data from Reference 20 were also used to obtain the effect of nozzle aspect ratio. These data, presented in Figure 42, provide a correction factor, $C_{F_G}/C_{F_G, AR=1}$ as a function of $\log AR$ for minimum and maximum jet area settings.

4.3.7 Effect of Aspect Ratio and Wedge Half-Angle on C_{F_G} of a 2-D Wedge Nozzle

The format for 2-D wedge nozzle PIPSI input data maps is shown in Figure 43. This format provides C_{F_G} as a function of nozzle pressure ratio P_{T8}/P_0 , for two nozzle area ratio schedules, one for non-afterburning operation and one for maximum afterburning operation. These schedules assume that variable area nozzle geometry is available such that the nozzle area ratio can be scheduled to operate at the optimum value until the geometric limits of nozzle travel are reached.

The experimental data from Reference 20 were used to provide the correction factors for 2-D wedge nozzle aspect ratio and wedge angle. The data used in the computer program were prepared as correction factors relative to the baseline values of a wedge angle, θ_p , of 10° and an aspect ratio, AR , of 1.0. The resulting correction factors are presented in Figures 44 and 45.

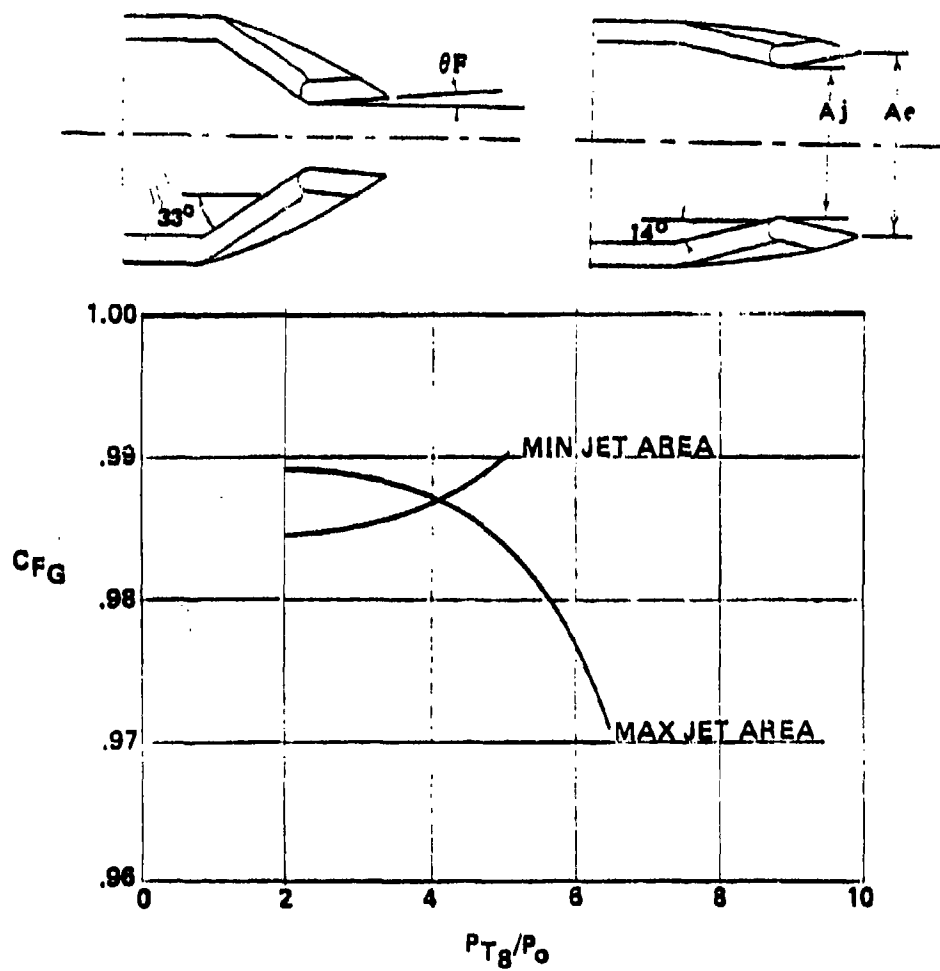


Figure 38. Gross Thrust Coefficient for a 2-D/C-D Nozzle

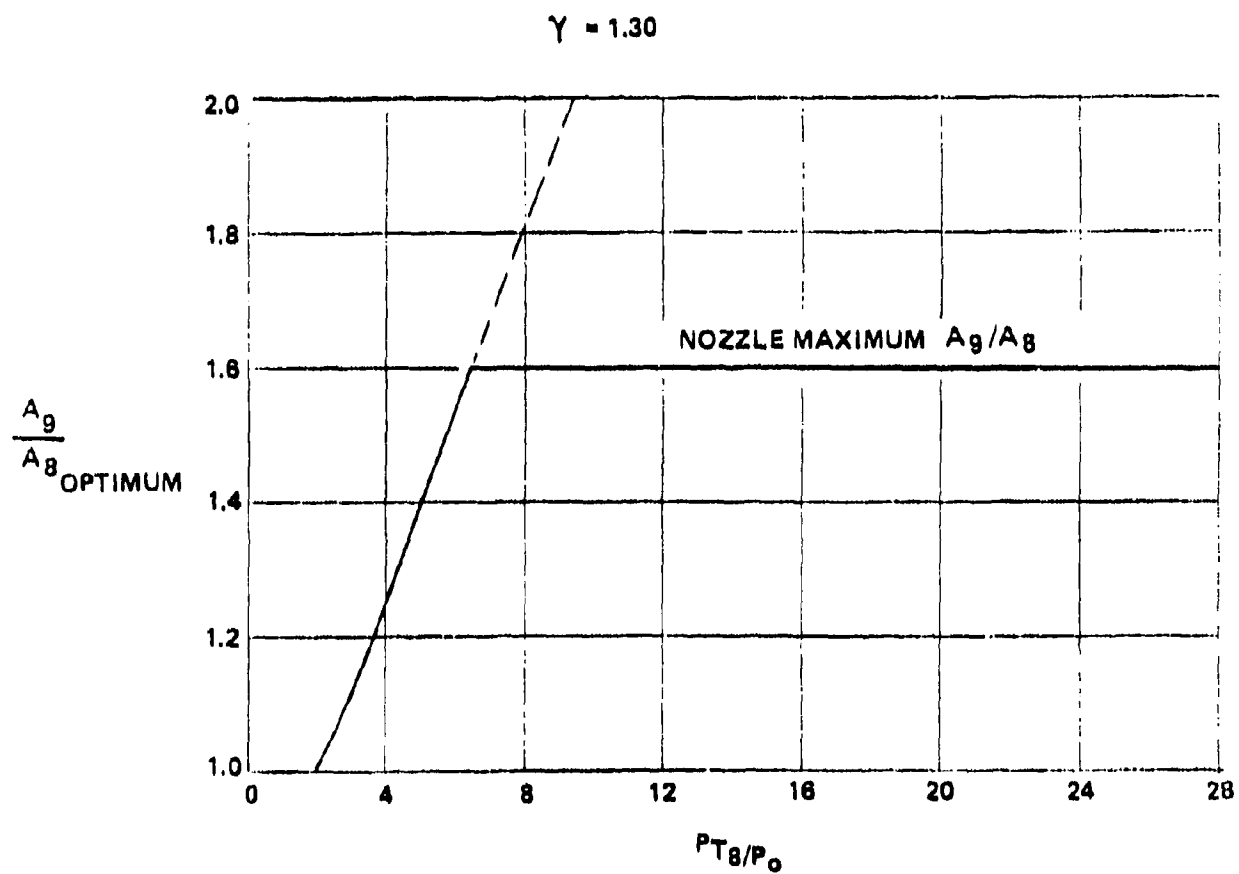


Figure 39. Optimum Area Ratio for a 2-D/C-D Nozzle

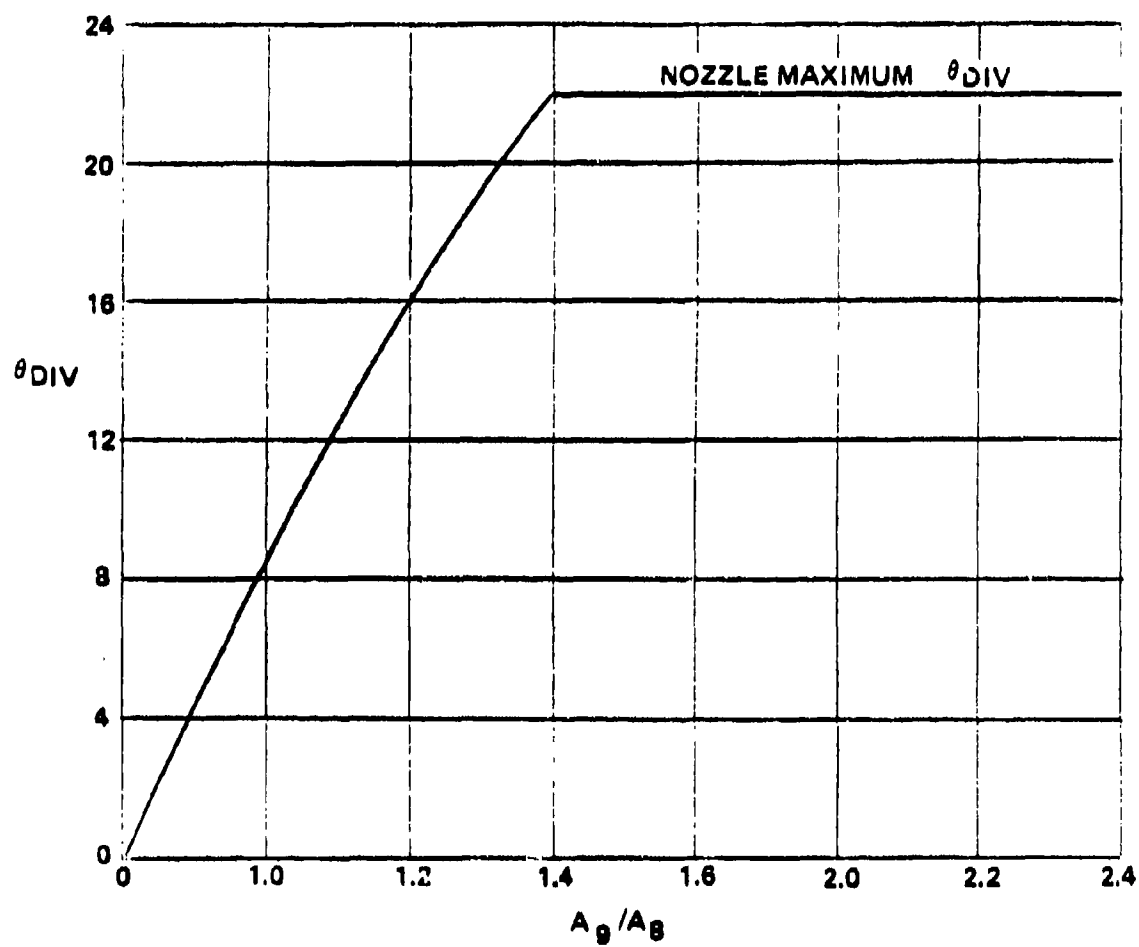


Figure 40. Optimum Divergence Angle as a Function of 2-D/C-D Nozzle Area Ratio

VALID FOR BOTH MIN. AND MAX. JET AREA

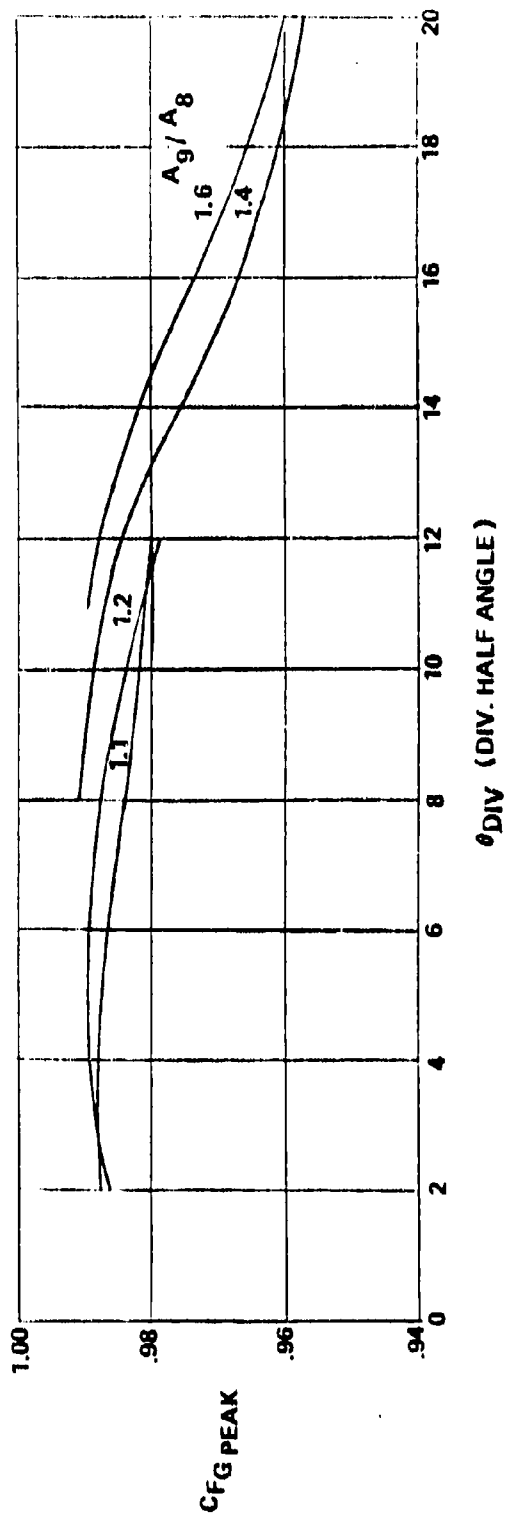


Figure 41. Effect of Divergence Angle on C_{FG} for a 2-D/C-D Nozzle

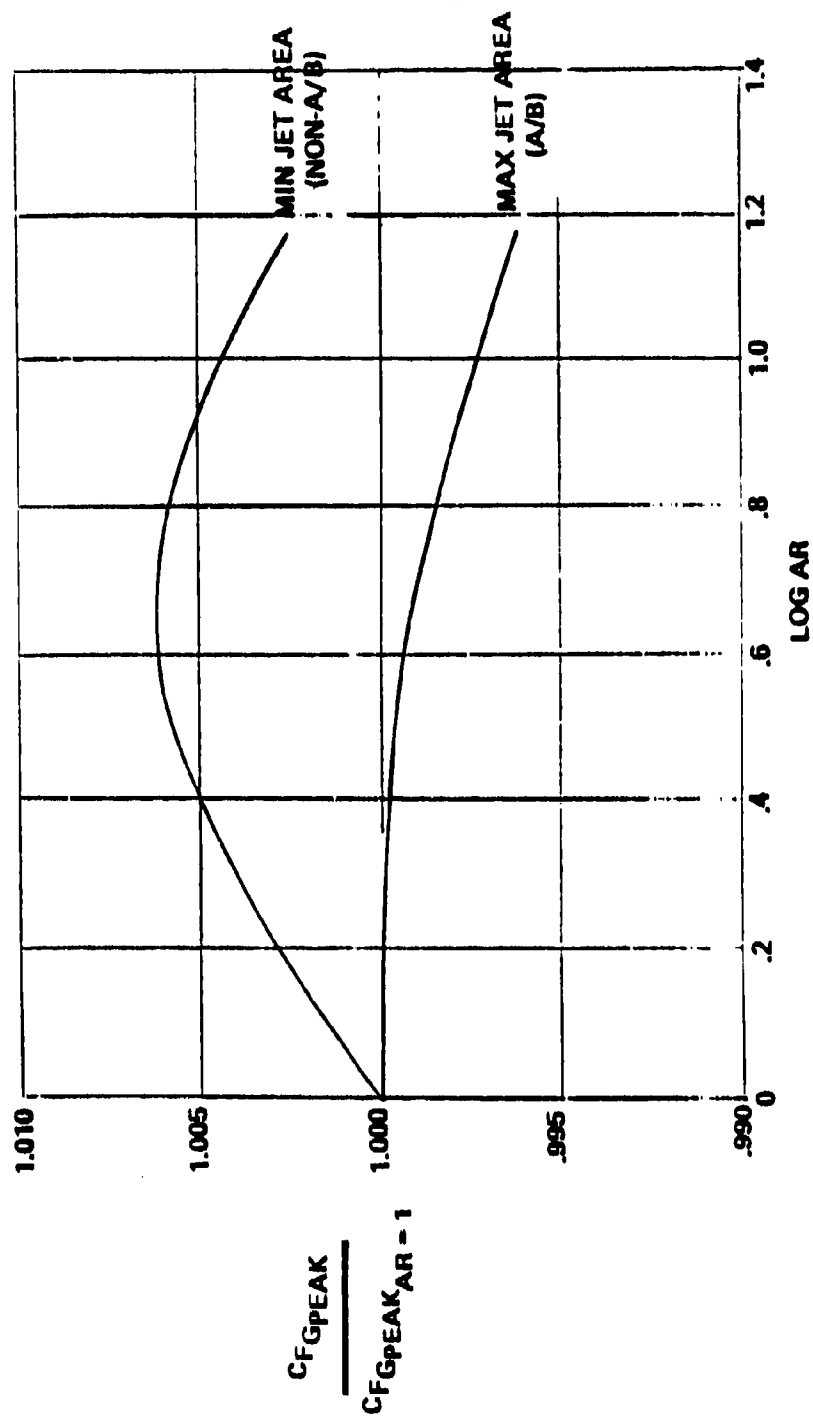


Figure 42. Effect of Aspect Ratio on 2-D/C-D Nozzle Performance

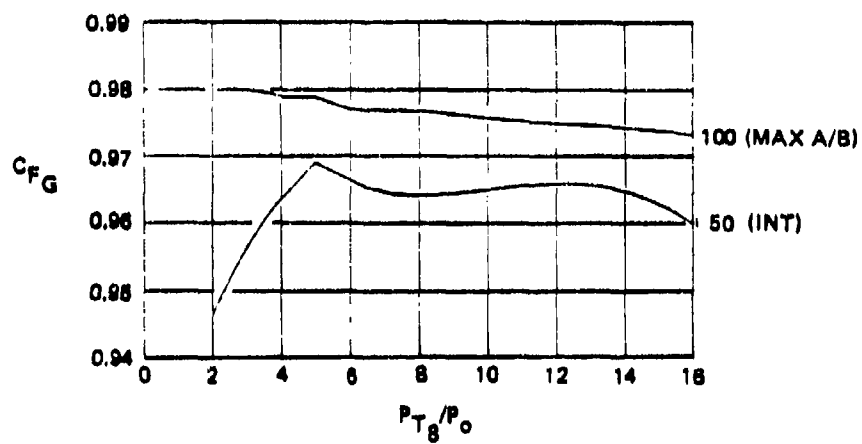
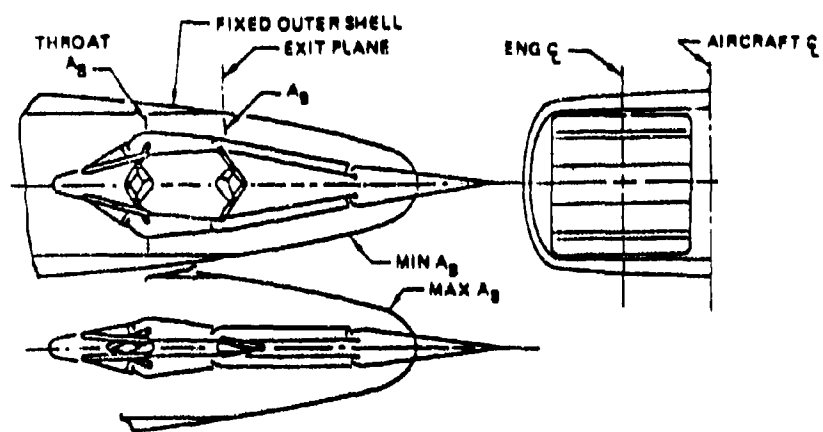


Figure 43. Gross Thrust Coefficient for a 2-D Wedge Nozzle

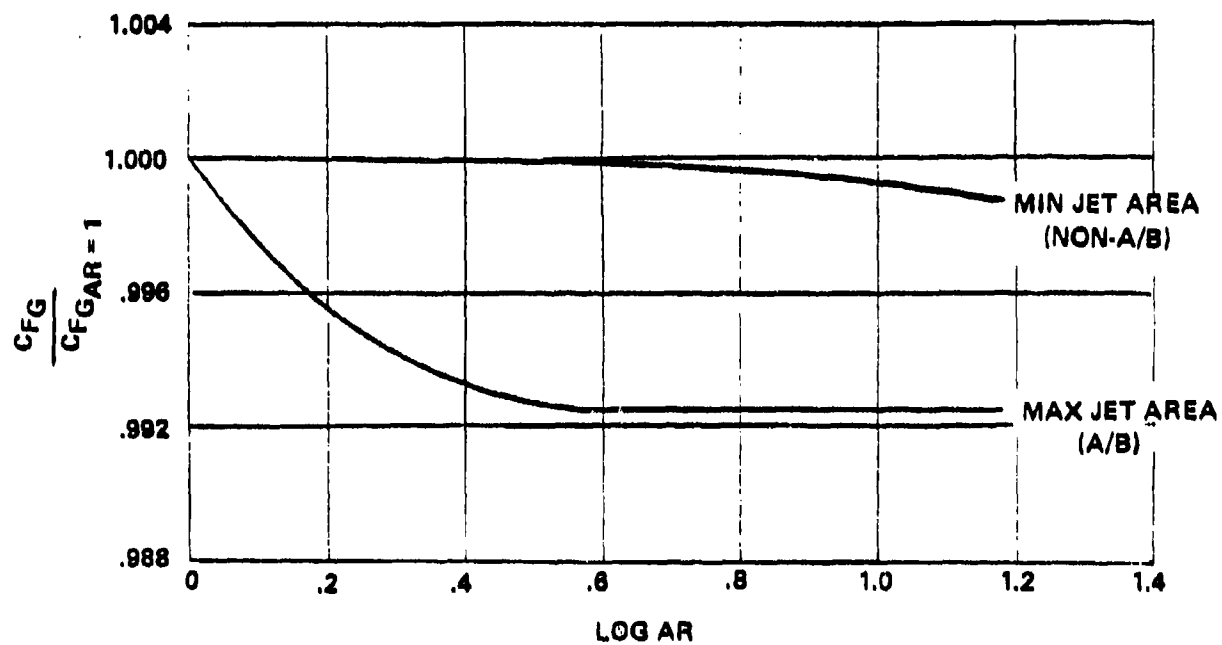


Figure 44. Effect of Aspect Ratio on 2-D Plug Nozzle Performance

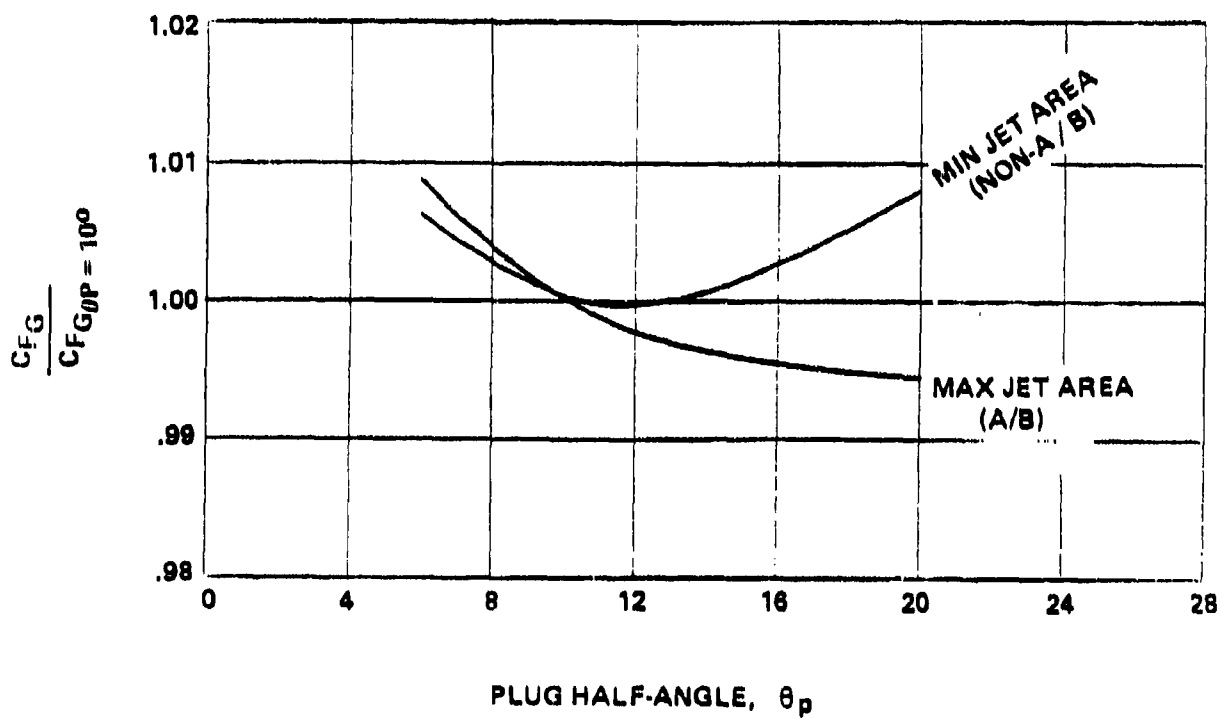


Figure 45. Effect of Plug Angle on 2-D Plug Nozzle Performance

APPENDIX

CHECK OF SOME DERIVATIVE PROCEDURE METHODS

This appendix will show results for a limited number of inlets, using the inlet derivative procedure methods for bleed rates, and inlet design point recovery with varied inlet design Mach number. The attempt will be made to transform from one known inlet to the parameters of another known inlet.

Two groups of inlets are considered. The first consists of three mixed compression, two-dimensional inlets, defined in the following table. All values are given for the design Mach number.

Design Mach No.	2.50	2.60	3.0
Recovery	0.905	0.916	0.885
Bleed Rate	0.07	0.07	0.105
Initial Ramp Angle	7.00	5.00	7.00
Aspect Ratio	1.0	0.91	1.0
Side Plate Cutback	0.0	0.0	0.0
Ramp Surface Mach No.	2.179	2.381	2.65
Reference	1	26	7

Since there is very little difference in aspect ratio, its effect will be neglected in the following. Bleed rate calculations will be made for these inlets, then recovery calculations will be considered.

Two bleed predictions methods will be used. The first will use the equation

$$\left(\frac{A_{0BLC}}{A_c}\right)_{new} = \left(\frac{A_{0BLC}}{A_c}\right)_{old} \cdot \left[\frac{\left(\frac{P}{P_T}\right)_{M_{S_{old}}} \cdot (M_S)_{old}}{\left(\frac{P}{P_T}\right)_{M_{S_{new}}} \cdot (M_S)_{new}} \right] \cdot \left[\frac{(Re)_{M_{O_{design\ new}}}}{(Re)_{M_{O_{design\ old}}}} \right]^{1/7}$$

The second will use this same equation for the low pressure bleed, where

$$\left(\frac{A_o}{A_c}\right)_{LP} = \left(\frac{A_o}{A_c}\right)_{old} \cdot \frac{1}{1.67} \quad , \quad \left(\frac{A_o}{A_c}\right)_{HP} = \left(\frac{A_o}{A_c}\right)_{old} - \left(\frac{A_o}{A_c}\right)_{LP}$$

and it will use

$$\left(\frac{A_o}{A_c}\right)_{new} = \left(\frac{A_o}{A_c}\right)_{old} \cdot \left[\frac{(A/A^*)_{M_{surface\ old}} \cdot (M_{surface\ old})}{(A/A^*)_{M_{surface\ new}} \cdot (M_{surface\ new})} \right] \cdot \left[\frac{(Re/P_{T_o})_{M_o\ design\ new}}{(Re/P_{T_o})_{M_o\ design\ old}} \right]$$

for the high pressure bleed.

For the Mach 2.5 inlet transformed to the Mach 2.6 inlet design variables, the following results were obtained:

$$\text{Mach 2.5} \quad \frac{A_o}{A_c} = 0.07$$

$$\text{Mach 2.6 Method 1} \quad \frac{A_o}{A_c} = 0.087$$

$$\text{Method 2} \quad \frac{A_o}{A_c} = 0.085 \text{ (vs. 0.07)}$$

For the Mach 2.5 to Mach 3.0 design variables

$$\text{Method 1} \quad \frac{A_o}{A_c} = 0.116$$

$$\text{Method 2} \quad \frac{A_o}{A_c} = 0.111 \text{ (vs. 0.105)}$$

For the Mach 2.6 to Mach 3.0 design variables

$$\text{Method 1} \quad \frac{A_o}{A_c} = 0.092$$

$$\text{Method 2} \quad \frac{A_o \text{ BLC}}{A_c} = 0.90 \quad (\text{vs. } 0.105)$$

These results do not seem initially to be consistent. If one were to say that they are due to differences in maneuverability, with higher bleed rate equating to higher maneuverability, then we would rate the inlets with the Mach 2.6 as least maneuverable, the Mach 2.5 as most maneuverable, and the Mach 3.0 inlet between. This was done by comparing bleed rates at a Mach 3.0 design for each inlet. Examining the references it was found that the Mach 2.5 inlet was for a fighter-bomber, the Mach 2.6 inlet for a commercial SST, and the Mach 3.0 inlet for a bomber. The maneuverability characteristics would indeed rank the inlets as listed from the prediction.

It is likely that high maneuverability brings lowered recovery to achieve stable operation. Knowing the ranking above, it would be expected that for a Mach 3.0 design, the Mach 2.6 base would have highest recovery, the Mach 2.5 lowest recovery, and the Mach 3.0 between them.

The recovery calculation assumes that the inlet loss coefficient, $\frac{\Delta P_T/P_{T_o}}{q_o} = f(M_o)$ is valid. Thus when design Mach number changes, q_o changes. The equation is

$$\frac{P_{T_2}}{P_{T_o \text{ new}}} = 1 - \left[\left(1 - \frac{P_{T_2}}{P_{T_o \text{ old}}} \right) \cdot \left(\frac{M_{o \text{ new}}}{M_{o \text{ old}}} \right)^2 \right]$$

For the Mach 2.5 to Mach 2.6 design

$$\frac{P_{T_2}}{P_{T_o \text{ new}}} = 0.897 \quad (\text{vs. } 0.916)$$

For the Mach 2.5 to Mach 3.0 design

$$\frac{P_{T_2}}{P_{T_o \text{ new}}} = 0.863 \quad (\text{vs. } 0.885)$$

For the Mach 2.6 to Mach 3.0 design

$$\frac{P_{T_2}}{P_{T_0 \text{ new}}} = 0.888 \text{ (vs. 0.885)}$$

These predictions of recovery would, in fact, order the inlets in the same manner as previously ranked. The result of these comparisons is that the bleed and recovery analyses show the correct trends. It also illustrates the effect and importance of the selection of the baseline inlet map file. Further demonstration of the methods requires evaluation among a family of inlets with similar designs and applications.

The second group of inlets consists of four mixed compression, axisymmetric inlets, all designed for supersonic cruise application. The following table provides information at the design Mach number.

Design Mach No.	2.35	2.65(A)	2.65(B)	3.5
Recovery	.93	.927	.907	.837
Bleed Rate	.0553	.0662	.07	.134
Initial Cone Angle	10.30	11.20	9.00	10.00
Cone Surface Mach No.	2.174	2.326	2.439	3.125
Reference	13	11	11, 27	12

The two bleed rate prediction methods used previously are used again.

For the Mach 2.35 to the Mach 2.65(A) design

$$\begin{array}{ll} \text{Method 1} & \frac{A_{o \text{ BLC}}}{A_{c \text{ new}}} = 0.0643 \text{ (- 2.8\%)} \\ \text{Method 2} & \frac{A_{o \text{ BLC}}}{A_{c \text{ new}}} = 0.0635 \text{ (- 4.1\%)} \end{array}$$

For the Mach 2.35 to the Mach 2.65(B) design

$$\text{Method 1} \quad \frac{A_{o \text{ BLC}}}{A_{c \text{ new}}} = 0.0732 \text{ (+4.6\%)}$$

$$\text{Method 2} \quad \frac{A_{o \text{ BLC}}}{A_{c \text{ new}}} = 0.0715 \text{ (+2.1\%)}$$

For the Mach 2.35 to the Mach 3.5 design

$$\text{Method 1} \quad \frac{A_{o \text{ BLC}}}{A_{c \text{ new}}} = 0.153 \text{ (+14.0\%)}$$

$$\text{Method 2} \quad \frac{A_{o \text{ BLC}}}{A_{c \text{ new}}} = 0.141 \text{ (+5.4\%)}$$

For the Mach 2.65(A) to the Mach 3.5 design

$$\text{Method 1} \quad \frac{A_{o \text{ BLC}}}{A_{c \text{ new}}} = 0.157 \text{ (+17.4\%)}$$

$$\text{Method 2} \quad \frac{A_{o \text{ BLC}}}{A_{c \text{ new}}} = 0.147 \text{ (+9.8\%)}$$

For the Mach 2.65(B) to the Mach 3.5 design

$$\text{Method 1} \quad \frac{A_{o \text{ BLC}}}{A_{c \text{ new}}} = 0.146 \text{ (+9.05\%)}$$

$$\text{Method 2} \quad \frac{A_{o \text{ BLC}}}{A_{c \text{ new}}} = 0.138 \text{ (+2.95\%)}$$

These comparisons show that Method 2 produces less than 10% error in bleed rate for all these design modifications, when compared to the actual inlet. Generally the error is considerably smaller than that. Method 2 is used in the derivative procedure for mixed compression inlets. These results are better than first order accurate.

The recovery calculation is as described previously in this Appendix.

For the Mach 2.35 to Mach 2.65(A) design

$$\frac{P_{T_2}}{P_{T_0 \text{ new}}} = 0.911 \text{ } (-1.7\%)$$

For the Mach 2.35 to Mach 2.65(B) design

$$\frac{P_{T_2}}{P_{T_0 \text{ new}}} = 0.911 \text{ } (+0.44\%)$$

For the Mach 2.35 to Mach 3.5 design

$$\frac{P_{T_2}}{P_{T_0 \text{ new}}} = 0.845 \text{ } (+0.92\%)$$

For the Mach 2.65(A) to Mach 3.5 design

$$\frac{P_{T_2}}{P_{T_0 \text{ new}}} = 0.873 \text{ } (+4.26\%)$$

For the Mach 2.65(B) to Mach 3.5 design

$$\frac{P_{T_2}}{P_{T_0 \text{ new}}} = 0.838 \text{ } (+0.09\%)$$

These results show excellent agreement, certainly better than first order accurate.

REFERENCES

1. Ball, W. H., Propulsion System Installation Corrections, AFFDL-TR-72-147-Volumes I-IV, Air Force Flight Dynamics Laboratory, December 1972.
2. Ball, W. H., and Atkins, R. A., Performance of Installed Propulsion Systems-Interactive (PIPSI) Users Manual, Document D180-22824-2, The Boeing Company, Seattle, Washington, 15 May 1978.
3. Hickcox, T. E., Atkins, R. A., Jr., and Ball, W. H., Derivative Procedure Users Manual, D180-22824-3, The Boeing Company, Seattle, Washington, 15 May 1978.
4. Cawthon, J. A., et al, Supersonic Inlet Design and Airframe-Inlet Integration Program (Project TailorMate), Volume III, Composite Inlet Investigation, AFFDL-TR-71-124, Vol. III, Air Force Flight Dynamics Laboratory, WPAFB, Ohio, May 1973.
5. Rejeske, J. V., and Porter, J. L., Inlet/Aircraft Drag Investigation, AFFDL-TR-74-34, Air Force Flight Dynamics Laboratory, WPAFB, Ohio, April 1974.
6. Gould, D. K., and Eastman, D. W., Methods Used to Determine Aerodynamic Drag and Installed Propulsion Thrust for the Boeing Lightweight Fighter, D199-10003-1, The Boeing Company, 1972.
7. Randall, L. M., The XB-70A Air Induction System, AIAA Paper No. 66-634, AIAA Second Propulsion Joint Specialist Conference, Colorado Springs, Colorado, 13-17 June 1966.
8. Randall, L. M., et al, Experimental Investigation to Determine the Effect of Several Design Variables on the Performance of the F-100 Duct Inlet, NA-53-26, North American Aviation, Inc., 7 January 1953.

9. Bates, D. L., and Welling, S. W., Engine Inlet Pressure Survey - 747 Airplane, Boeing Report No. D6-30622, The Boeing Company, Seattle, Washington, 17 November 1969.
10. Petersen, Martine W., and Tamplin, Gordon C., Experimental Review of Transonic Spillage Drag of Rectangular Inlets, Air Force Report No. APL-TR-66-30, May 1966.
11. Syberg, J., and Koncsek, J. L., "Transonic and Supersonic Test of the SST Prototype Air Intake", FAA-SS-72-50, April 15, 1972.
12. Syberg, J., and Koncsek, J. L., "Experimental Evaluation of a Mach 3.5 Axisymmetric Inlet", NASA CR-2563, Prepared by Boeing Commercial Airplane Company for NASA Ames Research Center, July 1975.
13. Syberg, J., "Analytic Design of AST Inlet", Boeing Company Document D180-20551-1, The Boeing Company, Seattle, Washington, March 8, 1977.
14. Paynter, G. C., Shock and Ramp Induced Incipient Separation of a Turbulent Boundary Layer, D6-11847, The Boeing Company, November 3, 1967.
15. Equations, Tables, and Charts for Compressible Flow, NACA Report 1135, 1953.
16. Syberg, J., and Hickcox, Design of a Bleed System for a Mach 3.5 Inlet, NASA CR-2187, January 1973.
17. Exhaust System Interaction Program, Handbook, D162-10467-12, The Boeing Aerospace Company, Seattle, Washington, Contract F33615-70-C-1450, April 1973.

18. Wynosky, T. A., and Spurrell, R. M., Final Progress Report, Exhaust System Interaction Program, PWA-4745, Contract No. F33615-70-C-1450, 5 June 1973, Pratt and Whitney Aircraft, East Hartford, Connecticut.
19. Berrier, B. L., Effect of Nonlifting Empennage Surfaces on Single-Engine Afterbody/Nozzle Drag at Mach Numbers from 0.5 to 2.2, NASA TN D-8326, 1977.
20. Paul, S. A., Installed Turbine Engine Survivability Criteria (ITESC Program) Pratt & Whitney Aircraft Group Report FR-8824, 31 August 1977.
21. Landgraf, C. W., "Performance Comparison-Blow-in-Door and Fixed Lip Inlets", Coordination Sheet No. ME-747P-3302, March 14, 1972, The Boeing Company 747 Propulsion Staff.
22. Ross, P. A., and Ball, W. H., "Propulsion System Development for Lightweight Fighter-Inlet Design and Performance, D180-14475-1TN, The Boeing Company, August 1, 1974.
23. Johnson, R. H., et al, Propulsion System Integration and Test Program (Steady State) Summary: Part I, Integration Technique and Test Activities, AFAPL-TR-69-36, Part I, AFAPL, June 1969.
24. Anderson, W. E., and Wong, N. D., "A Two-Dimensional, Mixed-Compression Inlet System Designed to Self-Restart at a Mach Number of 3.5", Journal of Aircraft, Vol. 7, No. 5, Sept-Oct 1970.
25. Smeltzer, D. B., and Sorensen, N. E., "Investigation of a Nearly Isentropic Mixed-Compression Axisymmetric Inlet System at mach Numbers 0.6 to 3.2, NASA TN D-4557, NASA Ames Research Center, Moffett Field, CA, May 1968.

26. Ball, W. H., "Design Studies of a Supersonic Transport Propulsion System with Dual-Inlet/Engine Pods", D6A11445-1, The Boeing Company, Seattle, Washington, October 1970.
27. Koncsek, J. L., and Syberg, J., "Transonic and Supersonic Test of a Mach 2.65 Mixed-Compression Axisymmetric Intake", NASA CR-1977, March 1972.
28. Weirich, R. L., "A Summary of the Angle-of-Attack Performance Characteristics at Supersonic and Subsonic Mach Numbers of Several Air Induction Systems which are Applicable to Fighter-Type Aircraft, Langley Working Paper No. LWP-481, NASA Langley Research Center, 1963.
29. Keenan, J. H. and Kaye, J., "Gas Tables", John Wiley and Sons, New York, 1954.